SYNTHESIS AND PROPERTIES OF WELL-DEFINED POLYMER-GRAFTED NANOPARTICLES

(SÍNTESIS Y PROPIEDADES DE NANOPARTICULAS CON CADENAS DE POLÍMERO INJERTADAS)

Trabajo de Fin de Grado – Grado de Ingeniería en Tecnologías Industriales

Alumno: Marco Mouriz

Tutores: Berna Serrano, Amaia Llorente

Escuela Politécnica Superior, Universidad Carlos III de Madrid

Curso 2014-2015

Abstract

The addition of inorganic nanoparticles (mainly metals and metals oxides) to polymers causes changes in their properties and applications of both the nanoparticles and polymers.

This thesis presents the design and synthesis of hybrid materials made out of alumina commercial nanoparticles (Aldrich, ϕ= 50 nm, provided by fabricant) with polysulfone chains (Aldrich, Mn= 16.000 g/mol and Mw= 32.000) grafted to alumina surface. These materials are commonly known by hairy nanoparticles (HNP) and are a kind of polymer brush. The polysulfone chains are grafted to the surface of the core nanoparticle by one ending. Two grafting methods are reviewed in this study (designed "Method A" and "Method B"), obtaining different grafting density σ_{graft}, (low density in method A and high density in method B). Variation on σ_{graft} gives different molecular structures from the layer, affecting the dispersion/aggregation of HNP in the matrix and so the properties of the final material.

Once the HNP were synthesized and characterized, they were included in a polysulfone matrix at low load (1-5 % wt), studying the influence of the nanoparticles in the polymeric matrix.

During the study the material was tested from different stages of synthesis to the final composite to evaluate its mechanical and thermal properties by diverse essays as TGA, DSC, F-TIR, DLS, Vickers hardness.

Finally, the structure-behavior relation and its final properties were evaluated to determine its qualities and future applications, in different fields from optical, energetic and sensors to mechanic properties improvement.

This work was developed within Universidad Carlos III de Madrid Department of Materials Science and Engineering and Chemical Engineering's Laboratories.

Keywords: Hybrid materials, grafting, polymers, nanoparticles, composites, alumina, polysulfone

Table of Contents

List of Tables

List of Figures

1. Introduction and objectives

1.1. Composite materials

Composite materials are made from **two or more constituent** materials with significantly different physical and/or chemical properties, that when combined, produce a material with **characteristic differences from the individual components** [1]. The individual components **remain separate** and distinct within the finished structure. The new material may be preferred for many reasons: common examples include materials which are stronger, lighter or less expensive when compared to traditional materials.

Historically, composite materials have companied mankind throughout its existence from wattle and daub for construction dating from Neolithic 6000 or bricks made of mud and straw combined used for the same reasons by Egyptians [1].

1.2. Nanocomposites

A **Nanocomposite** is a heterogeneous material with at least **one characteristic length scale in the nm range** ($x10^{-9}$m). The transition from microparticles to nanoparticles of its components leads to a drastic change in the properties of the material [2].

In mechanical terms, nanocomposites differ from conventional composite materials due to **high aspect ratio** of the reinforcing phase and/or its exceptionally high surface to volume ratio [2], as shown in Figure 1 for most common geometries. Since surface and surface properties are decisive in chemical and chemical interactions, a nanostructured material can have **substantially improved properties than** a material with the same composition and **bigger-dimensional components**.

Therefore, a smaller-dimensional component leads to smaller nanoparticles or thinner fibers or layers and so a higher surface-to-volume ratio (see Figure 1), then enables a better tailoring in the structuration of the nanocomposite, which can lead to better properties [3].

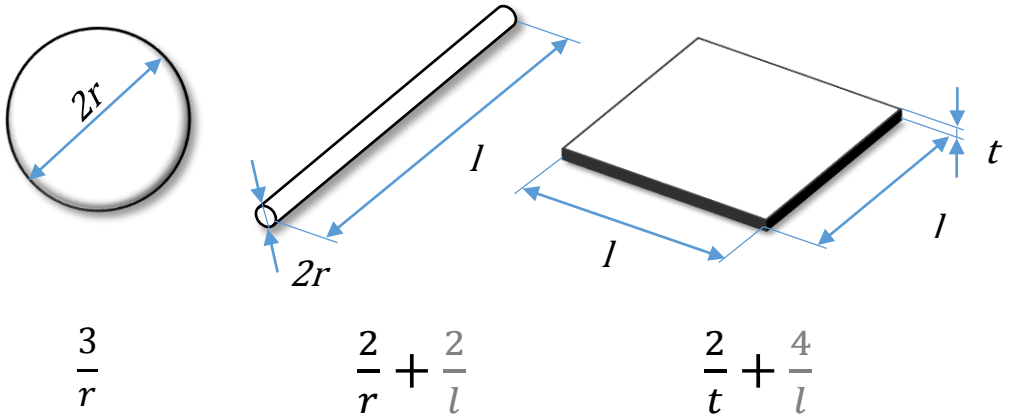

Figure 1. Common surface-to-volume ratios for each geometry

For the fiber and layered material, the surface area/volume is dominated, especially for nanomaterials, by the first term in the equation. The second term (2/l and 4/l) has a very small influence and it is often omitted.

As Kanartzidis said: 'The properties of nanocomposite materials depend not only on the properties of their individual parents, but also on their morphology and interfacial characteristics' [4]. Therefore, this presents new challenges in reaching this control over the distribution in size and dispersion of the nanosize constituents which receive a strong attention.

Nanocomposites exist naturally, for instance in animal bones or shells. They have been manufactured throughout human history scarcely, as for example Blue Mayan, an azure pigment used in paint by Mayans and Aztecs based on different clays, which conserves the tone over more than 4000 years [5][6]. From the mid-1950s nanoscale organo-clays have been used to control flow of polymer solutions (e.g. as paint viscosifiers) or the constitution of gels. However, it has been relatively soon (1970 decade) that their promises of realizing unique combinations of properties unachievable with traditional materials have caused an explosion of research in this area [3]. This surge in the field of nanotechnology has been facilitated by the appearance of the scanning tunneling microscopy and the scanning probe microscopy in the early 1980s.

Nanocomposite technology uncovers a broad new horizon of possibilities as nanocomposite automotive, aerospace and defense structures, polymer nanocomposite foams, nanocomposites for optic applications, conductive nanocomposites for corrosion protection, energy storage and conversion devices, nanofibers for tissue engineering scaffolding, protective armor and biosensing.

1.2.1. Matrix materials. Composition

Regarding the **matrix composition**, nanocomposites can be classified in:

- **Ceramic Matrix Nanocomposite** (CMNC): Ceramic nanocomposites offer improved hardness, strength, toughness and creep resistance over conventional ceramic matrix composites. The utilization of nanocomposites in materials processing leads is forecasted to have a major impact in catalytic, sensor, optical, electroceramic and structural ceramic materials [7]. This has been raised by the discovery of new techniques synthesis and densification of ceramic matrix composites as Spark plasma sintering and strong magnetic field alignment. This composites are used [8].

  Continuous SiC-fiber-reinforced/SiC matrix composites have non-substitutable applications as thermal components in the aerospace (turbine coating parts) and atomic energy industries (enhance the accident tolerance of light water reactors) due to their excellent mechanical, thermal and radiation properties. Furthermore, ceramic matrix composites are used for metal cutting applications and dental restoration [9].

  However, these relatively new composites are still at the development stage and there are several obstacles that need to be resolved.

- **Metal Matrix Nanocomposite** (MMNC): Metal matrices reinforced by nanoparticles are very promising materials suitable for a large number of applications. The nanoparticles can offer opportunities to tailor material properties such as hardness, tensile strength, ductility, density, thermal and electrical conductivity, and wear resistance [10]. Different kinds of metals, mainly Al, Cu and Mg, have been employed for the production of composites reinforced by nanoceramic particles such as carbides, nitrides, oxides as well as carbon nanotubes [11] (For example, carbon nanotubes have been shown to exhibit ultra-high strength and modulus, and have anisotropic electrical conductivity. When included in a matrix, carbon nanotubes could improve the resulting nanocomposite significantly [12]). The main matter of concern for the synthesis of these materials consists in the low wettability of the reinforcement phase by the molten metal, which does not allow the synthesis by conventional casting methods.

  MMNCs are not relevantly extended in commercial applications since their development is still very recent. However, metal matrix nanocomposites display better mechanical properties than bare metal or metal matrix composite materials with bigger particles as reinforcement. This is why they are considered to substitute bigger particle sizes MMCs

and some monolithic alloys in structural and electrical fields. The enhanced wear resistance and the good thermal conductivity combined with the high specific strength make MMNCs attractive materials for aircraft brakes. Moreover, the specific strength and elastic modulus could be exploited in sport industry, for instance for rackets or bicycle frames and other components [11].

- **Polymeric Matrix Nanocomposite** (PMNC): The inclusion of nanofillers in polymeric matrices extend the function and utility of polymers while maintaining their original manufacturing and processing flexibility. In particular, polymer nanocomposites have been successful with regard to overcoming traditionally antagonistic combinations of properties, obtaining very competitive materials regarding other options [13].

  This addition not only can give improved thermal or mechanical properties, but also attribute the polymer new ones which enhance material applications [14]. Particular examples of polymer matrix nanocomposites will be given in next chapter.

1.2.2. Reinforcing materials. Geometry and nanoparticles composition

1.2.2.1. Geometry

Nanocomposites can be classified by their reinforcing material (filler) **shape**:

- Particles nanocomposites or nanoparticles: The reinforcement of a material with nanoparticles improves properties to the resulting composite as well as implements new features in the matrix [15]. Different particles have been used to prepare polymer/inorganic particle nanocomposites, including:

  . Metal (Al, Fe, Au, Ag, etc.)

  . Metal oxide (ZnO, Al_2O_3, $CaCO_3$, TiO_2 etc.)

  . Nonmetal oxide (SiO_2)

  . Other (SiC)

  The nanoparticle material and its distribution within the matrix are chosen depending on the desired thermal, mechanical, and electrical properties of the nanocomposites. For example, Al nanoparticles are often selected due to their high conductivity; calcium carbonate particles are chosen because of the relative low cost of the material and the toughening of the resulting material [16] [17]; and silicon carbide (SiC) nanoparticles are

used because of their high hardness, corrosion resistance, and strength [18]. Nowadays and foreseen nanoparticles reinforcements as well as their applications and improved properties will be exposed in next subchapter. The principal advantage nanoparticles represent facing other geometries is the ease distribution along the matrix and therefore its superior percolation capacity; also the homogeneity and non-directionality gives more uniform properties to the material.

- Fibers nanocomposites or nanofibers: the utilization of nanoscale fibers, also known as nanorods, in polymer composites not only enables the development of uniquely created structures but also provides a means for the development of unique properties and functionalities at levels not possible with conventional fiber reinforced composites, carbon nanotubes (CNT) nanocomposites have attracted the fancy of many scientists worldwide due to their high performance in mechanical, electronic, electrochemical applications [19]. The advances in carbon nanotube nanocomposite started with the discovery of the helical tube geometry of carbon nanotubes by Iijima in 1991 [20].

  The tubes exist as either single-walled carbon nanotubes (SWCNT) or multi-walled carbon nanotubes (MWCNT) where individual tubes are nested concentrically inside one another like tree rings. These unique nanostructures are considered one-dimensional due to their high aspect ratio (length-to-diameter) leading to superior mechanical and electrical properties. The advantage of fibers compared to other geometries is the possibility to orientate the reinforcement in a desired direction, obtaining better properties in that or a different direction.

- Layers nanocomposites or nanoplatelets: the addition of 2D nanofillers in the matrix also confers improved properties to the product. Graphite nanoplatelets [21] down to 2-10 mm thick are being investigated as reinforcement for high strength carbon-carbon composites and for silicates [22] and other polymers [23], as well as using PU-Montmorillonite clay nanoplatelets composite [24], conferring improved physical and mechanical properties.

  A common disadvantage for fiber and layer nanocomposites is the low filler percolation threshold which limits the percentage by weight (mass fraction) of the filler introduced due to its high aspect ratio.

The subject of this study is the polymer based nanocomposites; which are comprised of a **polymeric material as matrix** and a **nanoscale material as filler**.

The addition of metal nanoparticles (including metal oxides and hydroxides) into polymeric matrix results in mechanically, electrically and optically improved resulting materials; which due to their applications in fields as bio-imaging, bio-medicine, bio-technology, catalysis, cross linkers, fuel cells, sensors, as flame retardant, UV shielding, optical, electronic and magnetic, among others, have generated a huge interest.

1.2.2.1. Nanoparticles composition

Hereby will be shown the most employed or promising metal and metal oxides/hydroxides nanoparticles used as nanofillers in polymeric matrices, the fields in which they are or could be applied, and the function or improved properties of the resulting material.

- Silica Nanoparticles:

  Silica nanoparticles are large scale produced by flow methods, SNPs have broad excitation band and size-dependent optical emissions, so they can be used for detection purposes, although, some modifications are necessary in order to improve surface defects and to achieve intense and stable luminescence.

  The Polymethacryloyloxyethyl Phosphorylcholin (poly (MPC)) -grafted silica has the ability to delay the coagulation of blood due to its extremely hydrophilic nature [25]. With Polyethylene Glycol (PEG), silicon nanoparticles were applied in bio-imaging as fluorescent tracers [26], also Poly (acrylic acid) (PAAc) grafted silicon nanoparticles can be used as fluorescent bioimaging material for cells or other biological molecules [27]. poly(N-isopropyl acrylamide) -silica nanocomposites have high pH sensitivity, antibacterial activity and biocompatibility, and are applied in drug release systems, diagnosis and enzyme imaging [28].

- Magnetic Nanoparticles:

  Iron oxide (Fe_3O_4) nanoparticles are widely used in nanotechnology due to their extraordinary magnetic properties, furthermore it is biocompatible, non-toxic and can be produced at low cost.

  With Chitosan iron oxide nanoparticles improve the control of drug release with the change of temperature or pH [29]. With Poly(acrylic acid) is also used in drug delivery aiming at cancer treatment [30].

  Poly(poly(ethylene glycol) monomethacrylate) (PEGMA) grafted magnetic nanoparticles are employed as contrast agent in magnetic resonance

imaging [31]. With Polymethylmethacrylate (PMMA), magnetic nanoparticles (MNPs) form very transparent nanocomposites used in magneto-optical instruments and shielding applications [32]. Poly(glycidylmethacrylate) (PGMA) grafted Fe_3O_4 nanoparticles can be used to construct a range of biosensors [33].

- Titanium Dioxide Nanoparticles:

TiO_2 is the natural oxide of titanium. It has many properties such as high refractive index, UV light absorption and photocatalytic activity.

Modified titanium oxide is used as photocatalyst. Poly methyl methacrylate (PMMA) grafted TiO_2 in nanofibers improves mechanical properties such as the elastic moduli and are used in dental composites, bone cement and implant biomaterials [34]. TiO_2 nanoparticles with Polystyrene present a good wear resistance and a high transmittance [35]. In the same way, with Poly (dimethyl siloxane) (PDMS) is obtained an improvement in mechanical properties. These Titanium dioxide nanocomposites are used as new Light Emitting Diodes (LED) encapsulant materials, acquiring better light extraction efficiency.

- Zinc Oxide Nanoparticles

Nanoparticles of Zinc Oxide are relevant due their high luminous transmittance, chemical stability, antibacterial properties, high catalytic activity and intensive UV and IR absorption.

Different polymers grafted to Zinc Oxide Nanoparticles were examined, like Poly methyl Acrylic Acid (PMAA), Polystyrene (PS) and Polyhydroethyl acrylate (PHEA); obtaining nanocomposites used in functional devices [36], semiconductor devices and for UV-shielding (in for example cosmetics) [37].

- Alumina Nanoparticles

Alumina nanoparticles (ANPs) present outstanding wear resistance, high strength and stiffness. Besides good thermal and mechanical stability with a competitive price compared to other options are found. This is why ANPs attract a big attention throughout the last decades [38].

With Polydimethylsiloxane, ANPs have excellent insulating properties, thus they are used for encapsulating photovoltaic devices and field-effect transistors [39]. Grafting Polystyrene (PS) and Polypropylene to γ-alumina enhances the mechanical properties of the nanocomposites (tensile strength) [40], due to the increase of cross linking agents (increases covalent bonds between polymer chains). Grafting Polysulfone (PSU) chains to alumina nanoparticles leads to an improvement of mechanical properties compared to bare Polysulfone.

- Magnesium Hydroxide Nanoparticles

Magnesium hydroxide ($Mg(OH)_2$) is a metal hydrate, Mg(OH)2 nanoparticles dispersed in Polystyrene can be used as environmental-friendly flame retardant in polymeric materials [41][42].

- Gold Nanoparticles

Gold nanoparticles are extensively employed due to their outstanding properties as nanomaterial filler in fields such as optics, biomedicine, electronics and catalysis.

As Polystyrene coat, the gold nanocomposite is used as catalyst [43]. PEGylated gold (Polyethylene Glycol) can be applied in selective cell targeting [44]. Finally, gold with polymethacrylic acid is used as ultrathin high performance biomimetic molecularly imprinted sensing layers and sensor devices [45].

- Silver Nanoparticles

Silver nanoparticles are synthesized by vapor deposition and ion implantation. They are implemented in several fields due to their optical, diagnosis, antibacterial and conductive properties. Nevertheless, the support of a polymer matrix is desirable.

It helps improving antibacterial properties in cotton fabric with good washing durability [46]. Polystyrene grafted to silver NPs nanocomposite have antibacterial potential against E. coli for instance; furthermore, the resulting material presents thermal and chemical stability against degradation, a higher glass transition temperature and transparency. They are used in clinical paints and as coating material in biomedical applications [47].

- Gadolinium Oxide Nanoparticles

Gadolinium oxide nanoparticles with Polyethylene glycol result in a composite which can be used as contrast agent for Magnetic Resonance Imaging (MRI) [48]. Besides, Poly(ethylene glycol) phosphate grafted Gadolinium oxide (PEG-phosphate grafted GD_2O_3) are employed in cellular/molecular preclinical imaging [49].

- Manganese Oxide Nanoparticles

Manganese Oxide (MnO_2) nanoparticles are used in new generation batteries, in bioimaging as contrast agent and in water treatment. MnO_2 NPs grafter with Polyaniline (PANI) created a high electrical conductivity nanocomposite with very stable coulomb efficiency [50], valuable for the development of new super capacitors. With polyethylenimine (PEI) they can be used for cancer detection and nanocarriers for cancer therapy [51].

- Cerium Oxide Nanoparticles

Cerium oxide (CeO_2, also named ceria) nanoparticles are broadly used as UV protection agent in glass coatings and cosmetics due to its transparency, good optical properties and ultraviolet shielding [52]. Common matrices are PMMA [53] and Phosphonated-Polyethylene Glycol (PPEG) [54].

- Copper Nanoparticles

Copper nanoparticles have a naturally high electrical and thermal conductivity, an elevated surface activity and easy to elaborate. With polyacrylamide grafted Poly (vinyl alcohol) PAM-g-PVA and disposed in thin films, they can be used as sensing materials since the solvent in which the material is immersed varies the resistance [55]. Furthermore, these cupper nanoparticles are used in mechanic, magnetic, electric and chemistry applications.

- Platinum Nanoparticles

Platinum nanoparticles are grafted with polybutyl methacrylate, PS, and Poly (acrylic acid) g-Multiwalled Carbon Nanotubes. The applications of these nanocomposites are in fuel cells, as catalyst in hydrogenation of α, β-unsaturated aldehydes, and as biosensor [56] [57].

- Palladium Nanoparticles

Palladium has excellent properties as catalyst. Palladium nanoparticles with Chitosan grafted to Graphene (CS-GR) have led to the development of glucose biosensors with wide linear range, low detection limit and good reproducibility [58]. In the same way, these PdNPs/CS-GR nanocomposites can be used in other types of biosensors. Polyaniline grafted to Palladium NPs can also have an application in biosensors and electrochemical sensors in micro and nanoelectronic devices [59].

1.2.3. Design of polymer nanocomposites

The properties of polymer nanocomposite (PNCs) are determined, in part, by the chemical composition of the polymer and the type and size of nanoparticles: metallic oxides, graphene, quantum dots, nanorods, clays, fullerenes and metallic nanocrystals. However, the properties of the composite materials can be engineered through judicious selection and chemical and physical modification of nanoparticles and polymer [60].

This section refers almost exclusively to inorganic nanoparticles (metal oxides), because the selected nanofillers are alumina nanoparticles (Al_2O_3). Inorganic

nanoparticle/polymer composites with enhanced mechanical, electrical, dielectric, thermal, and optical performance have been reported [13].

Extensive efforts have been made to improve the compatibility between metal oxide nanoparticles and organic polymers. Unfortunately, the high specific surface area of nanoparticles favors particle-particle attraction and subsequent agglomeration. Simply blending nanoparticles with organic polymers usually results in agglomeration of the nanoparticles within the polymer matrixes and loss of optical transparency due to intense light scattering by the agglomerated nanoparticles.

Nowadays is well known and accepted that the success of polymeric matrix nanocomposites is mainly based in the surface treatment employed on the nanofillers; this can be either to introduce additional functionalities or to design new morphologies and nanostructured materials. Surface engineering can be relatively simple, for instance the grafting of short-chain molecules to nanoparticle surface, designed for better compatibility with the polymeric chain; it also can grow in complexity, with the introduction of one or more new properties including bimodal (or multimodal) grafting of ligands which allow a relatively independent control of enthalpic and entropic interactions between nanoparticle and matrix.

Short-chain molecules grafted to the surface of the nanofiller improve enthalpic compatibility between particle and matrix. However, polymer chains grafted to the surface of the nanoparticle functionalizes it controlling the compatibility with the matrix. For instance, the synthesis of a layer of specially designed grafted polymer on the surface of magnetic nanoparticles can change and modulate the fundamental behavior of surface grafted chains [61].

It is well known nanocomposites prepared by mechanical mixing and/or compression molding totally lost their optical transparency even at low loads (<1%wt) of nanoparticles [62]. The optical transmittance of Al-doped ZnO/epoxy nanocomposites has also been reported to degrade rapidly even with less than 0.2 wt % loading [63]. Therefore, effective techniques are desired to achieve good dispersion of nanoparticles within organic polymer matrices and thereby high optical transparency of the composite materials.

Recent advances reveal routes to exploit both enthalpic and entropic interactions so as to direct the spatial distribution of nanoparticles in the polymer matrix and thereby control the macroscopic performance of the material. A challenge for future studies is to create hierarchically structured composites in which each sublayer contributes a distinct function to yield a mechanically integrated, multifunctional material [64] [65] [66].

1.2.3.1. Dispersion techniques of nanoparticles in the matrix.

The percentage in weight (named mass fraction) of nanoparticles within the reinforcement can remain very low due to the low filler percolation threshold (the flow of the filler through the matrix) and it usually surrounds 0.5-5 %; this phenomena is increased in the case of non-spherical and high aspect ratio fillers (carbon nanotubes or clay nanoplatelets for instance). The spatial distribution of nanoparticles in a polymer matrix is a critical importance issue since it determines the new properties of the resulting composite. It is now well-known that specific nanocomponents dispersion optimizes and controls the properties of the resulting nanocomposites [67].

The dispersion (and interfacial adhesion also) depends on physicochemical properties of the polymer matrices and nanoparticle surface, as well as the techniques and processing conditions during the fabrication off the nanocomposite. It is crucial to have the uniform nanofiller dispersion within the polymer matrix, in particular for the preparation of transparent nanocomposites and mechanical requirements, because larger agglomerates are weak points which will eventually result in an adverse effect on the mechanical properties [68].

The most common method to prevent the formation of aggregates is the surface modification. The basic principle of the surface modification of the nanoparticle is the need to screen the nanoparticles surface reducing van der Waal attraction between them, at the same time of increasing compatibility with the matrix [69][70].

Different approaches of surface modification to stabilize nanoparticles in homopolymer matrices have been reported, including silanization, surfactant absorption, carboxylation among others [71][72], and polymer grafting [73][74][75]76][77][78][79]. Polymer brushes could control both nanoparticle dispersion and improve wettability of the matrix with the polymer chain grafted. Benicewicz et al. [74] suggested that inorganic nanofillers could be stabilized and well dispersed in polymer matrices using bimodal grafts, where both short and long brushes are present on the same particle. The short brushes prevent the particle-particle attraction, whereas the long brushes promote entanglement with the polymer matrix [80], two examples are given in figure 2.

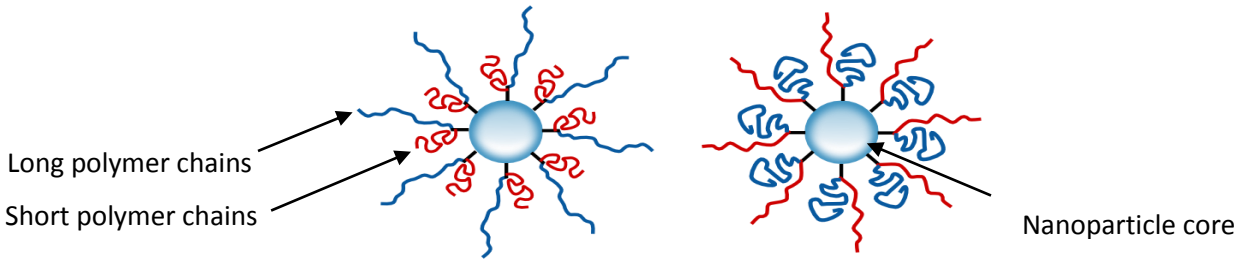

Figure 2. Examples of hairy nanoparticles.

Therefore, depending on the surface properties of the nanofiller, the nanoscale interaction with the host polymer can improve both the mechanical and physical properties of nanocomposites.

1.2.3.2. Grafted chain polymer: "Hairy nanoparticles"

The synthesis of the hybrid nanoparticles with the chemically-bound polymer grafts has been carried out utilizing both "grafting to" and "grafting from" methods and the most of them consist on the formation of a covalent bound between polymer and particle:

- Grafting from: technique also called surface-initiated polymerization, the polymer grows on the surface of nanoparticles. This growing of polymer chains on the surface of nanoparticles is given with the initiator first grafting [81][82][83].

- Grafting to: reaction between functionalized polymer chains and nanoparticles. Over the past several years, a variety of methods have been developed, using controlled radical polymerization (CRP) techniques, to graft polymer chains to nanoparticle surfaces (ATRP or RAFT are an example) obtaining a monodisperse grafting. In "grafting to" methods [84], the polymer is covalently grafted to the surface of the particle by a high performance reaction between a terminal functional group of the polymer and a functionalized surface in the nanoparticle (already existing or introduced). The advances in click chemistry [85] are an example of it. The first allows a high grafting density due to the small length of the momomer, but requires an accurate control of reaction conditions; as the second limits density and uniformity of the grafting due to the esteric requirement of the polymer chain.

Grafted chain polymer in inorganic nanoparticle are effective for the regulation of interparticle distance and their interactions, avoiding formation of aggregates and allowing the tuning of final physical and mechanical properties of the polymer matrix nanocomposite. The nature of the polymer (molecular weight, flexibility, monomer unit, etc.) and graft density determines interaction of the particles with the environment, whereas their physical properties are governed by both the size and shape of the inorganic core and the surrounding polymer layer [85].

The structure of the hairy nanoparticles or polymer brushes is analyzed in terms of the constitution and conformation of polymer chains, which depends on the length of the chain and graft density, in addition to the curvature of the surface. The following figure shows a schematic representation of the varied conformational behaviors of polymer brushes attached to spherical interfaces.

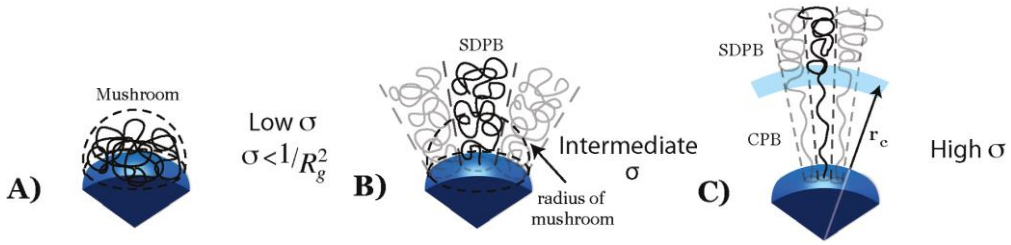

Figure 3. Conformational behaviors of polymer brushes attached to spherical interfaces [85].

Where Rg is the radius of gyration of the grafted polymer chains, and σ is the grafting density. At low grafting density, the Rg does not exceed the interchain spacing and individual chains do not interact with adjacent chains, and thus they assume mushroom-like conformations on the surface (Figure 3 A). Figue 3 B and C present a semidilute polymer brush, SDPB, and higher graft densities a concentrated polymer brush, CPB respectively. If the chains are long enough, then brushes initially in the CPB regime, will transition to the SDPB regime at some distance, r, from the center of the nanoparticle [85].

1.2.3.3. Structure and properties of grafted NP/polymer nanocomposites

Hairy nanoparticles can be dispersed in a polymer miscible for the grafting or similar), avoiding chemical incompatibilities which lead to aggregation. In general, the properties of these materials rely on the grafting; nevertheless, some entropic phenomena may occur, as autophobic dewetting which restricts dispersion in a high molecular weight matrix [86][87][88][89].

The morphological structure of mixtures of polymer matrix with hairy nanoparticles depends on the grafting density, the chain length, the interaction between the grafted chains and between the host (polymer matrix) and grafted chains [90]. On the other hand, changing particle size and length of grafting polymer on the fillers, all can significantly affect polymer nanocomposite properties. Other important properties to consider besides are nanoparticle curvature and the thermodynamic (Flory–Huggins) interaction parameter, χ, between the host and grafted chains [91]. However if the grafted polymer and the polymer matrix are the same, the interaction parameter should be favorable ($\chi<0$).

At very low grafting densities, σ, the morphology of these polymer nanocomposites (PNCs) is largely determined by the attractive enthalpic interactions ($\Delta H<0$) between the nanoparticle cores, mediated by entropic interactions with the grafted polymer chains. The entropic term comes from the fact the matrix polymer chains lose entropy when they are confined between the surfaces of two adjacent particles. Entropic effects that drive the chain interpenetration capacity scale as the inverse of the chain length, whereas enthalpic contributions are proportional to the

chain length. These competing interactions have been shown to be responsible for the anisotropic organization of the nanoparticles within polymer hosts. At high grafting densities, however, even in cases where the host chains (polymer matrix) and the grafted chains have identical chemical structure, the entropic grafted layer/free chain interactions are dominant, leading to miscibility (isotropic dispersion of the nanoparticles within the polymer host) or to microscopic and macroscopic phase separation.

Summarizing, both entropic and enthalpic factors affect the miscibility between the grafted and the surrounding matrices and therefore the morphology. In order to entropically favor wetting and entanglement of the matrix chain for polymer grafted nanoparticles, the degree of polymerization (length) of the graft, N, should to be equal to, or larger than, the degree of polymerization of the matrix chains [91].

1.3. Initial approach

The chosen matrix in this work is Polysulfone (PSU), which has proved outstanding thermal and mechanical properties, along with its biocompatibility and resistance to water and high temperatures [92][93]. This is why it is widely employed in medical devices which require high sterilization temperatures. Polysulfone is highly used in orthodontic devices such as brackets, but represents problems which might reduce its service life, such as erosion induced by mastication.

In order to achieve a higher strength and thus to reduce the undesired erosion, a nanoreinforcement is added. The chosen filler was Aluminum Oxide (Alumina or Al_20_3), a ceramic oxide which has proved to improve mechanical properties as filler in polymeric matrices nanocomposites [94][95][96][97]. It has also shown biocompatible as long as it displays minimal or no tissue reaction and blood compatibility tests are satisfactory [98][99].

Due to the high surface/volume ratio of nanoparticles, particle-particle attraction is favored and so the formation of aggregates (agglomeration). This causes a problem of dispersion resulting in weak points where the alumina forms aggregates, and therefore a heterogeneous material with likely worse mechanical properties.

To solve this problematic, it is desirable to modify chemically the nanoparticles surface (functionalization).

So as to obtain a more uniform dispersion of nanoparticles along the matrix, and to acquire a better attachment of the particles to the matrix, it is desirable to graft Polysulfone chains to the alumina nanoparticles surface (hairy nanoparticles). Then, this polysulfone chains (“hairs” or “brushes”) from the alumina nanoparticle get entangled with the polysulfone matrix, providing a more stable union and a better dispersion.

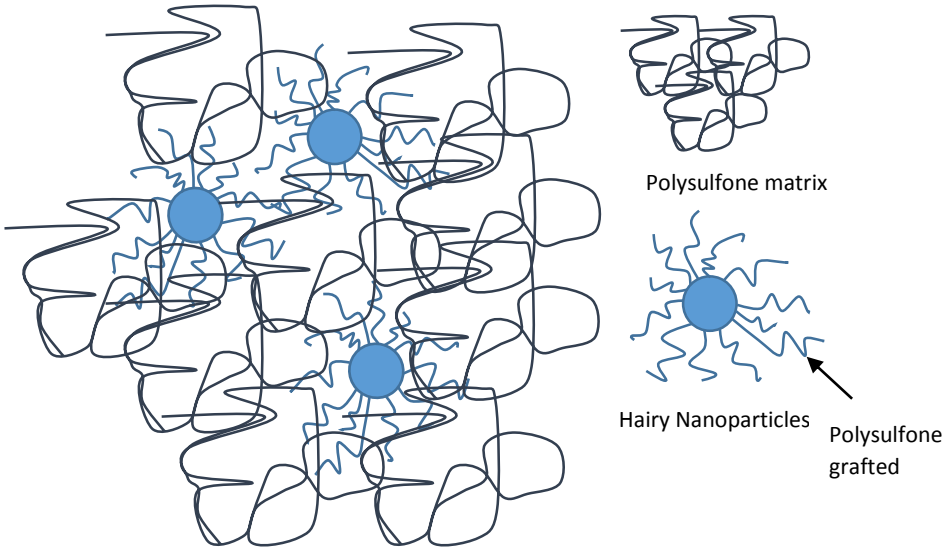

Figure 4. Entanglement of hairy nanoparticles with a polymer matrix.

1.4 Objectives

Starting hypothesis and general objectives

The starting hypothesis of this work is to improve the properties of a polysulfone matrix by introducing alumina nanoparticles previously functionalized with polysulfone chains of the same nature as the polymeric matrix. The goal of this functionalization is to compatibilize nanoparticle and polymeric chain obtaining an optimum dispersion and reaching an effective entanglement between both kinds of chains: matrix and hairs.

Therefore, the general objective of this project is to generate materials with controlled morphologies by surface modification techniques and processing methods.

Specific objectives

Relative to each stage of the nanocomposite synthesis, production and characterization.

1. To functionalize alumina nanoparticles with polysulfone chains by two different methods to generate low graft density and high graft density nanoparticles.
2. To prepare polysulfone grafted to modified alumina nanoparticles with functionalized surface nanocomposite.
3. To study experimentally the nanocomposites to understand the effect of the synthesis parameters: grafting density and alumina composition. To compare morphology with properties.
4. To evaluate the properties of the nanocomposite and its possible applications.

2. Experimental Section

2.1 Characterization Techniques and Methods

Hereby all the characterization techniques employed to define the properties of the final composites and/or any of its synthesis stages will be described, as well as the method employed during the characterizations realized.

2.1.1. Thermogravimetric analysis (TGA)

Thermogravimetric or thermal gravimetric analysis (**TGA**) is a method of thermal analysis in which changes in physical and chemical properties of materials are measured as a function of increasing temperature (with constant heating rate), or as a function of time (with constant temperature and/or constant mass loss). TGA can provide information about physical phenomena, such as second-order phase transitions, including vaporization, sublimation, absorption, adsorption, and desorption. Likewise, TGA can provide information about chemical phenomena including chemisorption, desolvation (especially dehydration), decomposition, and solid-gas reactions (e.g. oxidation or reduction) [100].

TGA is commonly used to determine selected characteristics of materials that exhibit either mass loss or gain due to decomposition, oxidation, or loss of volatile compounds (such as moisture) [101].

The analyzer device employed was a Perkin Elmer PYRIS TGA - STA 6000, which can be seen in Figure 5. This instrument has simultaneous analysis of TG with DTA (Differential Thermal Analysis) mode (ΔT) and DSC (Differential Scanning Calorimetry) (mW) mode for fast enhanced result interpretation. The operating temperature can vary between 15 and 1000 °C, and heating rate goes from 0.1 to 100 °C/min.

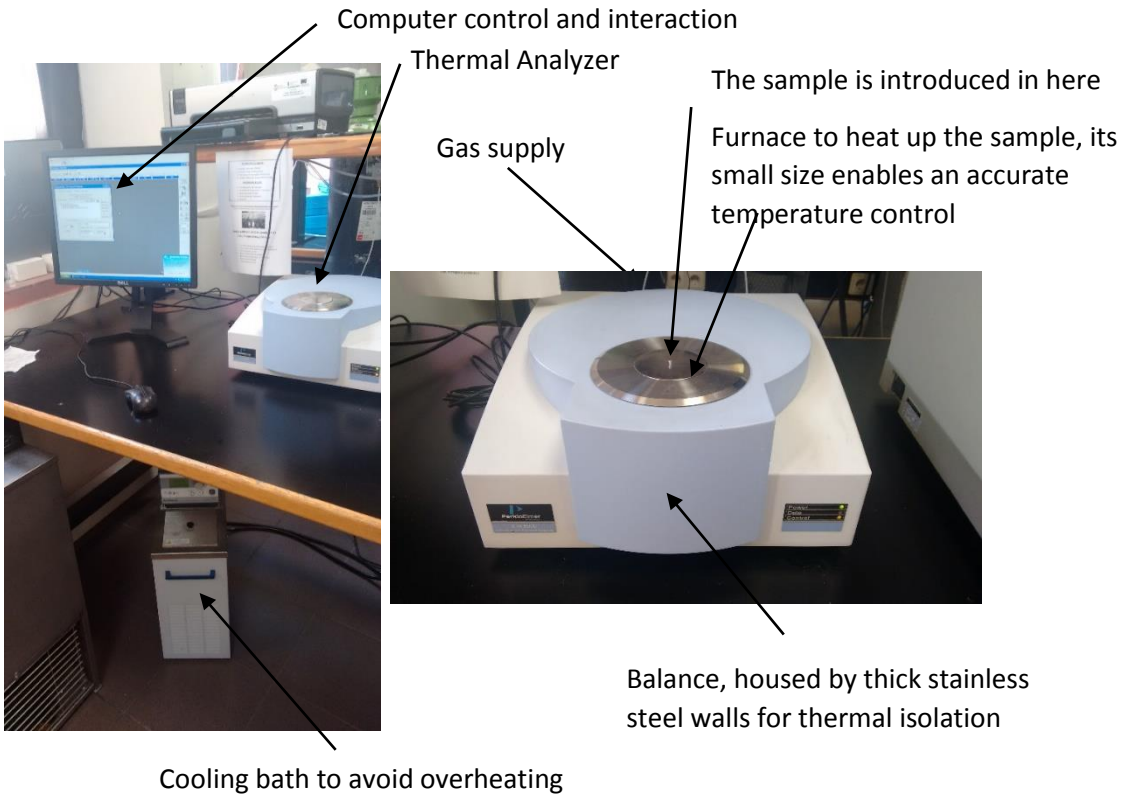

Figure 5. Perkin Elmer TGA – STA 6000 with the set-up employed in this study

The TGA's were carried out using air as supply gas at 40 ml/minute, N_2 as purge; the designed program makes one scan from 50°C to 900°C at a heating rate of 10°C/min (1 hour 25 minutes per analysis) . The used samples of the material to measure had a weight of about 20 mg.

2.1.2. Fourier transformed Infrared spectroscopy (FTIR)

Fourier transformed Infrared spectroscopy FTIR is a technique used to obtain information on the molecular structure, chemical bonding and molecular environment of the measured sample. This is done by obtaining an infrared spectrum of absorption, emission and photoconductivity of a solid, liquid or gas. A FTIR spectrometer collects simultaneously high spectral resolution data over a wide spectral range. This confers a significant advantage over a dispersive spectrometer which measures intensity over a narrow range of wavelengths at a specific time [102] [103].

The raw data still need to be transformed into an exploitable spectrum, it requires some mathematical processes in which the Fourier transform is used, which gives this method its name. The output data obtained is given in absorbance units deppending on the wavelenght scanned (in the employed tests goes from 400 cm^{-1} to 4000 cm^{-1}), the graphical

interpretation of this scan gives a chart with peaks which refers to a bigger absorbance units, due to the presence of a given compound, identifiable by reference charts by its characteristic absorbance [104].

The employed spectrometer was a Perkin Elmer Spectrum GX FT-IR System, as shown in Figure 6.

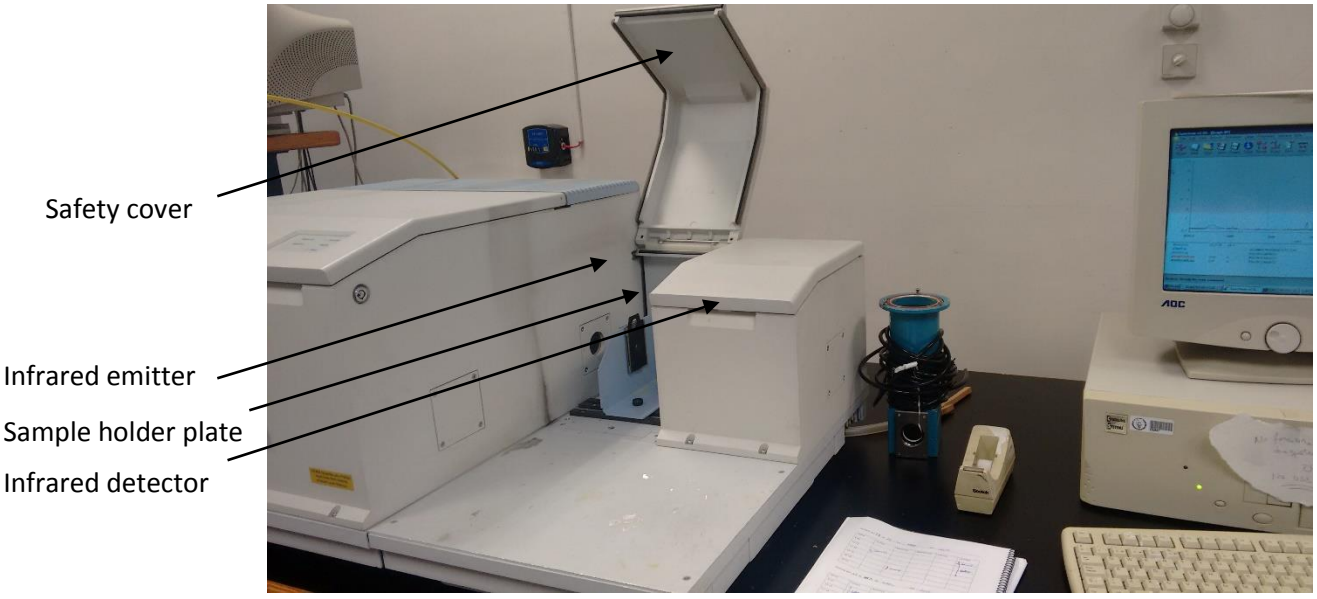

Figure 6. Perkin Elmer Spectrum GX FT-IR System employed for FTIR analysis

Every sample to be analyzed is mixed in a 1/100 weight ratio with KBr powder, pulverized and compressed into a 1.5 cm diameter pellet in a press. The pressure applied was 150 kPa during one minute, then 100 kPa during one minute. After the analysis the obtained spectrums were compared and the compounds responsible of the peaks found in the charts identified.

Figure 7.Pellets preparation process.

2.1.3. Differential Scanning Calorimetry (DSC)

DSC is a thermoanalytic technique employed to measure the difference of heat flow in function of the temperature between a sample and a reference to characterize diverse processes and properties of the material sampled [105].

Generally, the heating program for a DSC analysis is made to heat linearly the carrier of the sample in function of time. The sample must have a well-defined heat capacity in the temperature range which is going to be swept [106].

The basic principle of this technique is the need of an increase or decrease of heat flow in order to keep both sample and reference at the same temperature when the sample experiments a physical transformation, such as a phase transition. This increase or decrease of heat flow depends on the exothermic or endothermic nature of the process.

For instance, when a solid sample melts will require a bigger heat flow to the sample to increase its temperature at the same speed than the temperature of the reference. This is due to the heat absorption produced during an endothermic phase transition. Nevertheless, when the sample experiments exothermic processes, like a crystallization, it will require a reduction on the heat flow due to the extra heat given by this process.

Therefore, by calculating the difference between the heat flow received by the sample and the reference, DSC calorimeters can measure the heat flow absorbed or eliminated during any process. Like this, Differential Scanning Calorimetry can measure diverse characteristic properties from a sample [107]; using this technique is possible to characterize processes like fusion, crystallization and oxidation. It is especially important its capacity to characterize subtler processes as the glass-liquid transition (or glass transition), and then determine the glass transition temperature (Tg). The glass transition for glasses, polymers and other amorphous inorganic compounds, is a pseudotransition given at a temperature (glass transition temperature (Tg)), at which the material diminish its density, hardness and stiffness, and its elongation percentage decreases drastically.This glass transition appears in a DSC chart as an alteration (step) over the baseline of the DSC signal.

DSC is broadly used in quality control for polymer production, since it can determine the purity of the samples and as tool to determine curate for polymers [108].

The employed DSC device is a Mettler Toledo DSC, The calorimeter has two small, low mass furnaces (for sample and reference, prepared in aluminum sample pans) that heat and cool rapidly, providing better resolution and higher sensitivity enabling detection of transitions. The method used carries out two scans from 25^{o}C to 225oC at 10^{o}C/min increase, in a N_2 atmosphere with a 10 ml/min flux, the first scan eliminates the thermal historic from the polymer.

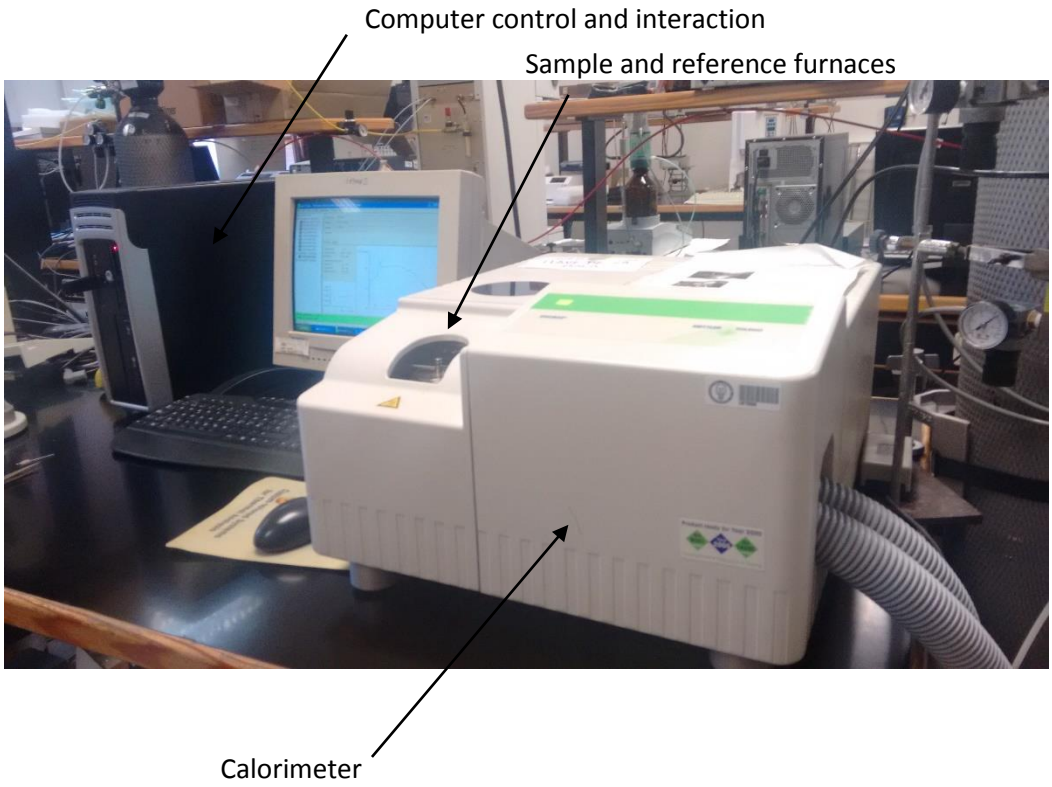

Figure 8. Mettler Toledo DSC with the set-up employed in this study

2.1.4. Dynamic Light Scattering (DLS)

Dynamic Light Scattering (DLS), sometimes referred as photon correlation spectroscopy or Quasi-Electric Light Scattering (QELS) is a physical, non-invasive, well-established technique employed for measuring the size and size distribution of molecules and particles typically in the submicron region to determine the size distribution of small particles in suspension or polymers in solution [109].

A monochromatic light source, in most of cases including this one, a laser, is shot through a polarizer into the sample, contained into a particle cell made of glass or quartz. The scattered light crosses the sample and goes through a second polarizer, where is collected by a photomultiplier and the resulting image is projected onto a screen [109]. In the way through the sample, the hit with the molecules diffract the light in every direction, these light beams interact constructively (light regions) or destructively (dark regions). The repeating of this measurements are analyzed by an autocorrelator, comparing light in every spot over time and then calculating the size of the measured sample [109] [110].

.

DLS is used to characterize size of various particles including proteins, polymers, micelles, carbohydrates, and nanoparticles. If the system is monodisperse, the mean effective diameter of the particles can be determined. This measurement depends on the size of the particle core, the size of surface structures, particle concentration, and the type of ions in the medium. Since DLS essentially measures fluctuations in scattered light intensity due to diffusing particles, the diffusion coefficient of the particles can be determined [111].

Stability studies can be done conveniently using DLS. Periodical DLS measurements of a sample can show whether the particles aggregate over time by seeing whether the hydrodynamic radius of the particle increases. If particles aggregate, there will be a larger population of particles with a larger radius.

The DLS employed in this study was a Malvern DLS Zetasizer Nanoseries presented in Figure 9, which measures wet samples in a range from 0.3 nm to 10 micrometers [112]. 3 ml samples of the measured materials were prepared in a 0.01 % solution/suspension in weight (in Tetrahydrofuran and Dymethylformamide), previously filtered in a 0.45 micrometers silicon filter and introduced in a quartz cell, as shown in Figure 10.

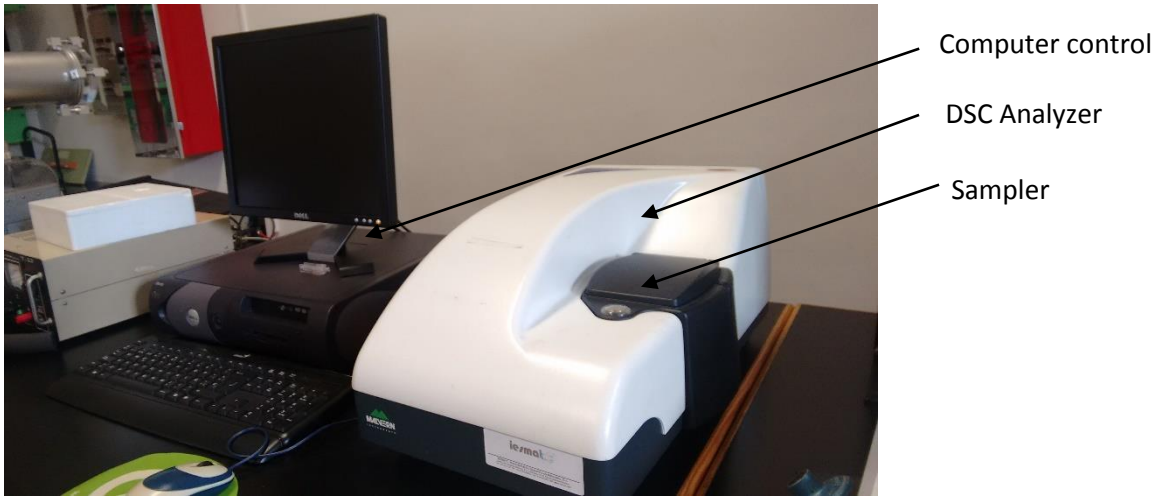

Figure 9. Malvern DLS Zetasizer Nanoseries set-up employed.

Figure 10. Preparation of Alumina suspensions for DLS analysis.

2.1.5. Transmission Electron Microscopy (TEM)

Transmission electron Microscopy (TEM) is a microscope technique where the interaction of the specimen with a beam of electrons which passes through it is captured, magnified and focused by a conjoint of lenses and a fluorescent screen (or detected by sensors) acting as imaging device [113].

The resolution of TEM is significantly higher than traditional light microscopes, TEM is able to measure even as small as a single column of atoms, which is thousands of times smaller than the smallest resolvable object in a light microscope [113]. TEM is a widely employed method in diverse biological and physical fields, TEMs find application in cancer research, virology, materials science as well as pollution, nanotechnology, and semiconductor research [114].

An ultra-thin specimen is irradiated with an electron beam of uniform current density; the electron energy is in the range of 69-150 keV (usually 100 keV) or 200 keV-3 MeV in the case of High Voltage Electron Microscope (HVEM) [115].

Electrons are emitted from an electron gun by thermionic emission from tungsten cathodes. The electron intensity distribution behind the specimen is imaged with a four stages lens system onto a fluorescent screen.

The employed microscope was a JEOL JEM 2100 belonging to the ICTS Centro Nacional de Microscopía affiliated to Universidad Complutense de Madrid, the device has an acceleration voltage of 200 kV and a resolution of 0.25 nm. The samples were prepared in a ultrathin plate as a dilution in acetone for fast evaporation.

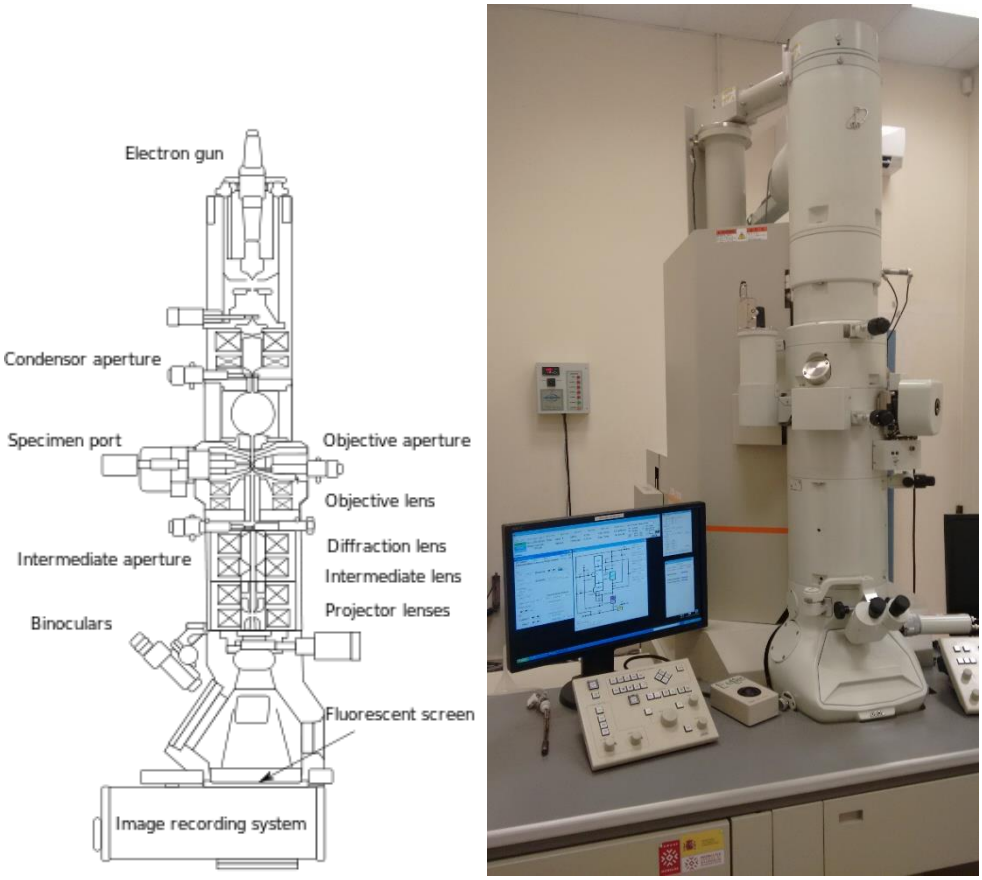

Figure 11. A) TEM scheme and B) TEM employed during measurements.

2.1.6. X-Ray Diffraction (XRD)

X-ray Diffraction (XRD) is a technique employed to identify the atomic and molecular structure of a material, in which the atoms cause a beam of incident X-rays to diffract into many specific directions. By measuring the angles and intensities of these diffracted beams, it can reproduce a three-dimensional picture of the density of electrons within the material. From this electron density, the mean atomic structure, chemical bonds and the disorder can be calculated [116][117].

The technique consist in an incident beam of radiation in different angles so as to generate a X Ray diffraction diagram, the position and intensity of the peaks will be characteristic of every material and crystalline phase. The angular distribution follows Bragg's Law [118]:

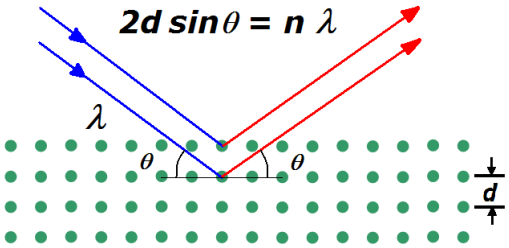

Figure 12. Bragg's Law.

Where n is a natural number, λ the incident wavelength, d the distance between crystalline planes and θ the infraction or Bragg's angle. The successive diffractions of the beam will be recovered in a receptor.

The employed diffractometer was a Philips X'pert X-Ray Diffractometer as shown in figure 12, which employs Cu K radition (λ= 1.541 A) with a 0.02 ° pass and 10 seconds each pass, with an initial angle of 15° and finishing at 90°.

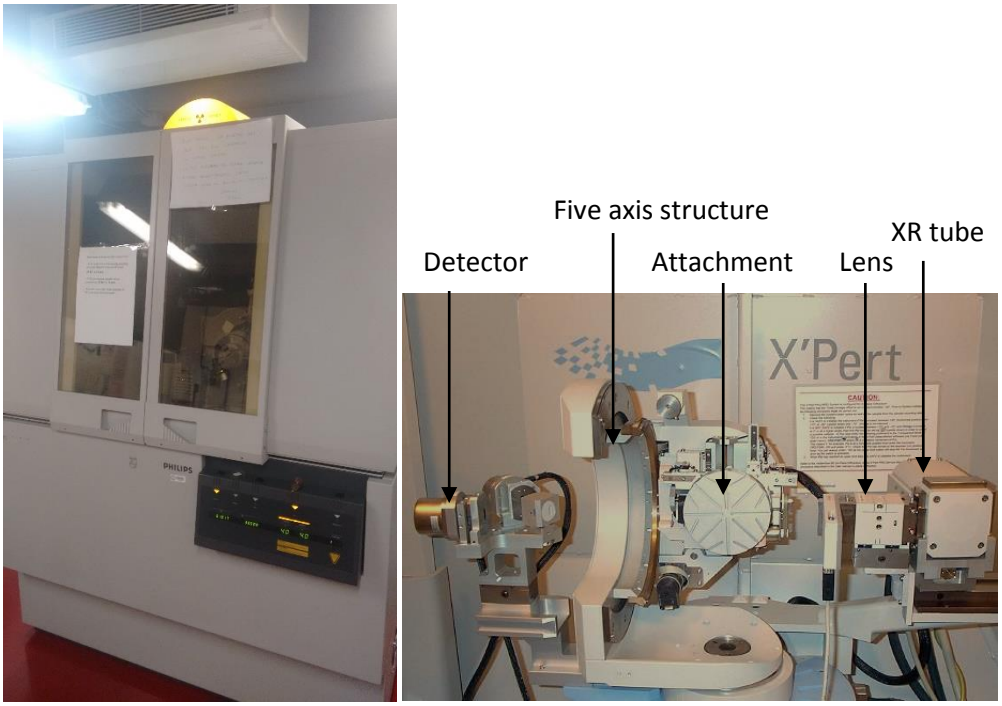

Figure 13. Philips X'pert X-Ray Diffractometer employed.

2.1.4. Microindentation Test (Vickers Hardness)

Indentation hardness tests are used in mechanical engineering to determine the hardness of a material to deformation. The term "microhardness" has been widely employed to describe the hardness testing of materials with low applied loads, where the applied force (test load) goes from 1 to 1000 grams-force (gf), typically 2N (200 gf) and produce indentations of about 50 µm [119]. Microhardness testing can be used to observe changes in hardness on the microscopic scale; therefore a microscope examination is needed to measure the indentation. The two most common methods are Vickers hardness test and Knoop hardness test. Vickers hardness test was employed during the tests.

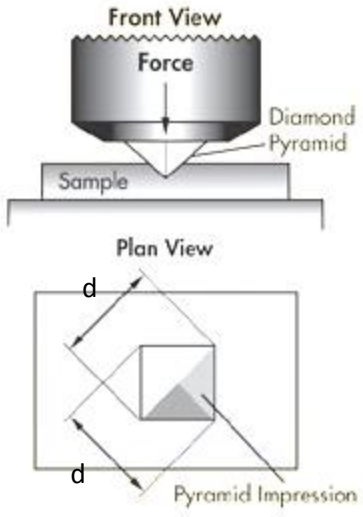

Figure 14. Vickers Hardness Test indenter.

The Vickers Hardness Test or HVT employs a diamond with an apical angle of 136°. HV is calculated following the next formula [119]:

$$A = \frac{d^2}{2\sin(136°/2)} \approx \frac{d^2}{1.8544}$$

$$HV = \frac{F}{A} \approx \frac{1.8544 \cdot F}{d^2}$$

Figure 15. Vickers Hardness formula.

Being F the force in kilograms-force (kgf), and d the average length both the diagonal left by the indenter. Then HV units are kilograms-force per square millimeter (kgf/mm²) and are expressed xxHV, being xx the Vickers Hardness of the material, taking as reference diamond: 10000HV.

Indentation Depth h in mm can also be calculated according to:

$$h = \frac{d}{2\sqrt{2}\tan(\frac{\theta}{2})} \approx \frac{d}{7.0006}$$

Figure 16. Indentation depth formula.

The microhardness tests was done on a Zwick Roell BZ 2.5, which is based in a hardness measurement head with a Vickers Hardness pyramidal diamond mounted on a line. It also equips a measuring light microscope with three different lenses (although only the 20:1 resolution lens was employed), testXpert software calculates Vickers hardness based on indentation after test. Indentation head is interchangeable for other hardness tests.

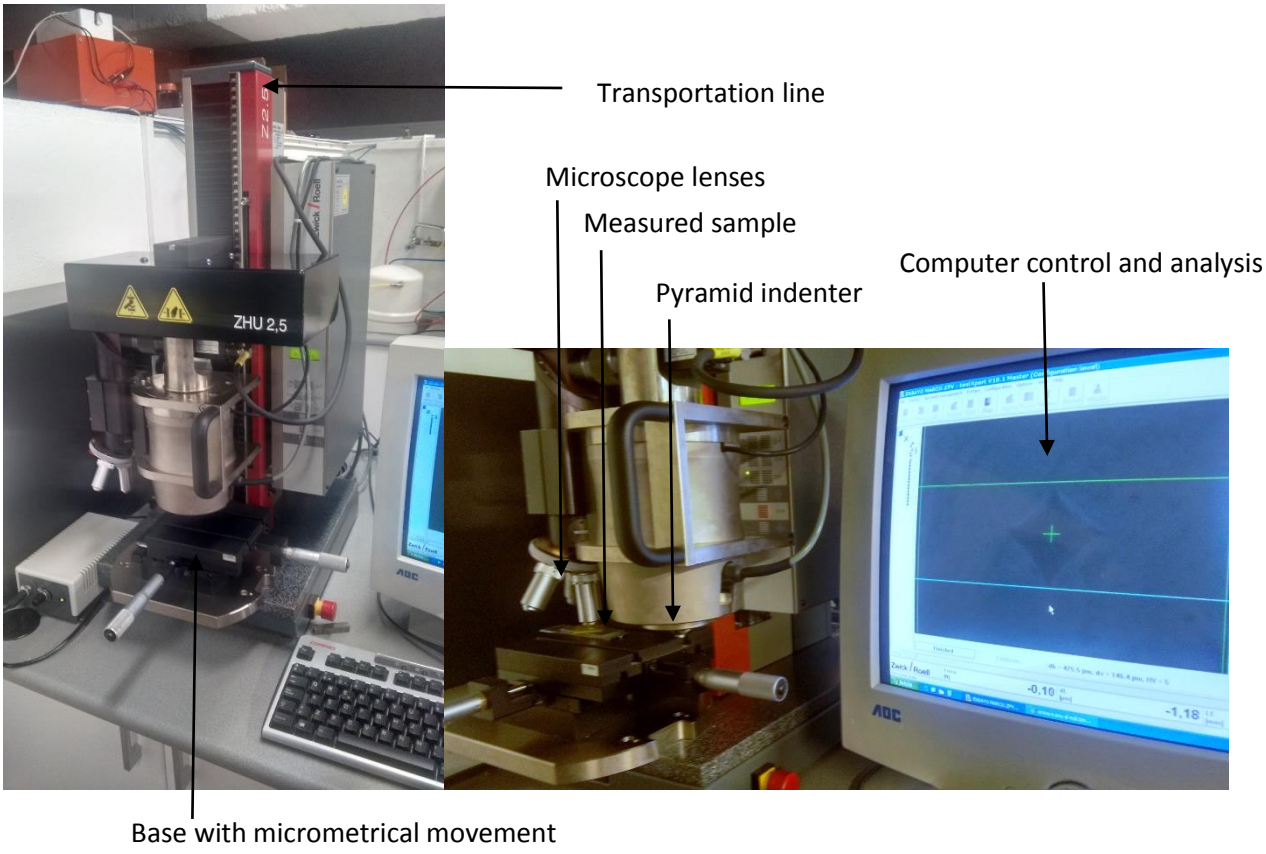

Figure 17. Zwick Roell BZ 2.5 during A) indentation and B) light microscope analysis.

2.2. Synthesis and characterization of nanocomposite precursors

2.2.1. Materials

2.2.1.1. Alumina Nanoparticles

Three types of γ-Al_2O_3 (Alumina) were used in the evaluation process to test different combinations and prove the absence of any contaminant. Two different Sigma-Aldrich dry alumina nanoparticles named **ANP1** and **ANP3**, with 50 nm nominal median size and 4 g·cm^{-3} density. Also, a suspension purchased from the same company with a 10 % weight concentration of Alumina in water, named **ANP2** was employed. Samples of every alumina were dried in an oven at 110°C for 3 hours and afterwards vacuum was pulled in to eliminate possible traces of non-desired moisture. Once dried, this bare Alumina was tested by TGA and FTIR. Specific surface area of alumina was measured by BET employing a Micromeritics Gemini VII (calculating 130 $m^2 \cdot g^{-1}$)

Calculus of OH in alumina surface

The Figure 19 shows the thermogram of the tree types of bare alumina (previously dried) used in this work. As previous studies affirm [120], bare alumina thermogram shows two regimes of weight loss; the weight lost in the first stage (100-400°C) is due to desorption of the physisorbed water; in the second one, beyond 400°C, dehydration occurs due to combination of adjacent OH groups to the surface.

The following reported expression [121] relates the number of OH present in alumina surface with the weight loss in this second regime:

$$n[OH \cdot nm^{-2}] = \left(\frac{2[WL(T_0) - WL(T_{final})]}{100 \cdot M_{H_2O}}\right)\left(\frac{N_A}{S_{BET}}\right)$$

Figure 18. Expression of OH in alumina surface.

Where $WL(T_0) - WL(T_{final})$ is the weight loss between $T_0 = 400^oC$ and $T_{final} = 900^oC$. M_{H_2O} is the molar mass of water (18 g·mol^{-1}), N_A is the Avogadro number (6,022×10^{23} mol^{-1}). S_{BET} is the specific surface area of γ-alumina calculated by BET (130 $m^2 \cdot g^{-1}$ or 1,30·10^{20} $nm^2 \cdot g^{-1}$).

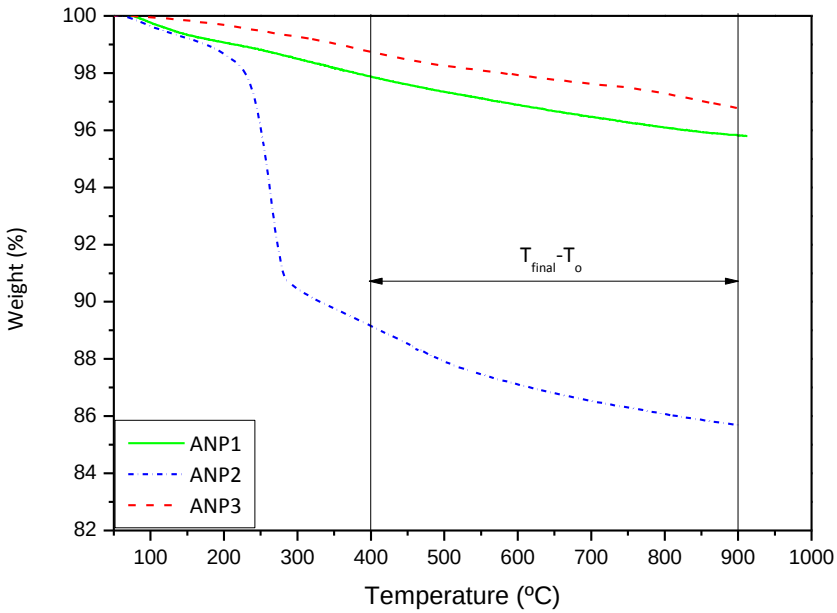

Figure 19. Thermograms of every bare alumina nanoparticle employed.

The molecules OH/nm^2 in every alumina are obtained applying the previous formula and presented in the Table 1. Abboud [120] calculated his n from 6 to 20 OH·nm-2, which comprehend the results obtained. Nevertheless it is higher than reported density from commercial alumina, this can be due to the TGA inability to distinguish from surface OH and OH groups inside the pores (which cannot be modified).

Table 1. Calculated values of the number of OH per surface unit

	$WL(T_0)$	$WL(T_{final})$	$n[OH \cdot nm^{-2}]$
ANP1	97.88	95.8226	10.58
ANP2	89.16	85.68962	17.86
ANP3	98.74	96.77322	9.751

ANP2 TGA reveals the existence of an undesired compound which carries an weight loss between 200 and 300ºC; the most plausible reason is the presence of a surfactant coated the surface nanoparticle ,to low the surface tension between liquid and solid, although it was not reported by Aldrich.

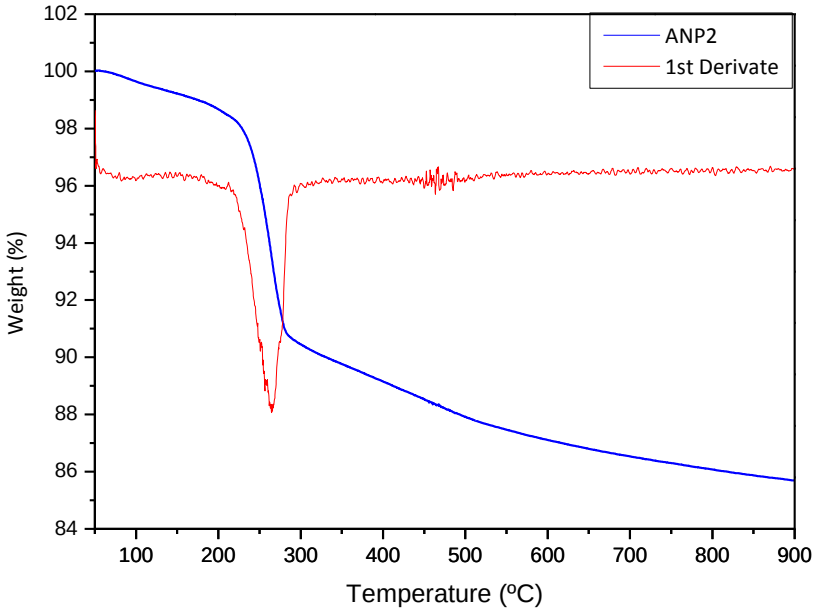

Figure 20. First derivate of ANP2.

Obtaining the first derivate of the weight loss function shown in Figure 20, a peak appears around 250°C, which indicates the presence of an organic cover, probably a kind of surfactant.

FTIR spectroscopy was used in order to determine and analyze the organic content after each functionalization. To compare, the FTIR spectra of bare alumina was also carried out. The Figure 21 shows the FTIR for the three alumina used.

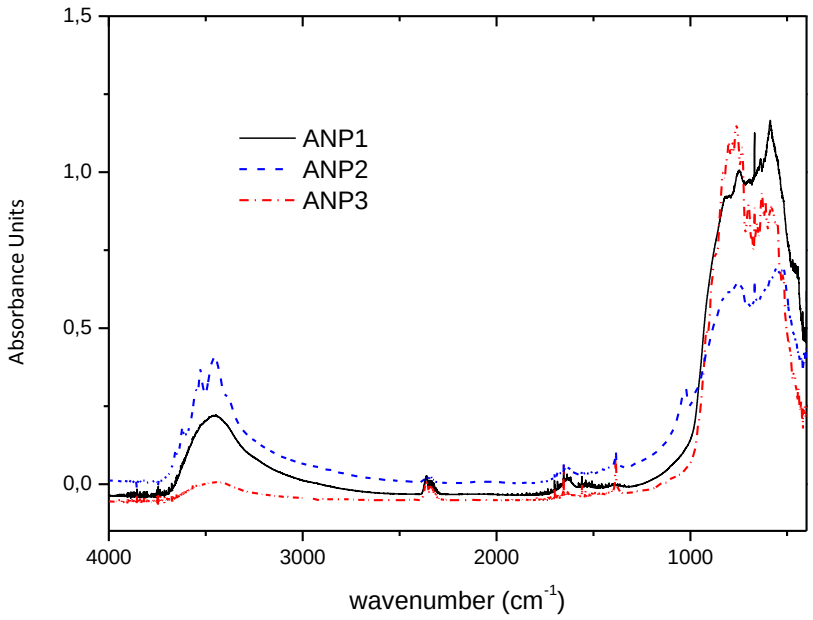

Figure 21. FTIR spectra of every bare alumina nanoparticle employed.

ANP1 and ANP3 showed a clean spectrum without organic compounds characteristic signals. Nevertheless, ANP2 clearly showed the characteristic absorption peaks of the organic compounds (3500 cm^{-1}).

ANP1 was evaluated by an X Ray Diffractometer, so as to obtain a value of the particle size. Results are shown in Figure 22 and subsequently evaluated.

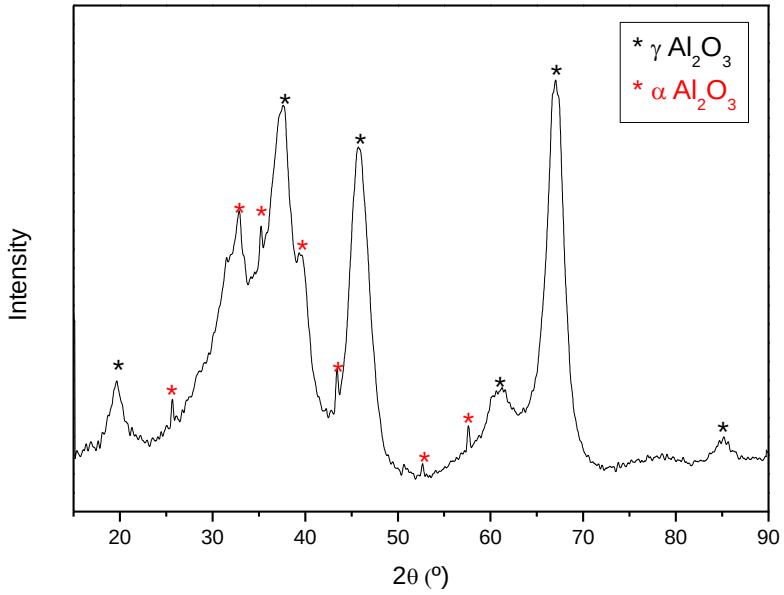

Figure 22. X Ray Diffraction of ANP1 nanoparticle.

It has been proved that the most of the peaks are asigned to γ-alumina (JCPDS standard cards no. 00-029-0063 and 00-002-1421), but small signals which matched α-alumina, also known as corundum, (JCPDS standard cards no. 01-074-1081 and 00-036-0149), both are considered crystals of anhydrous aluminum oxide. The formation of different crystalline structures depend on the temperature at which the previous material, bohemite, is kept at, if the temperature is above 800 K, it will acquire gamma-alumina structure (Face Centered Cube or FCC), but the temperature is above 1400 K, then corundum is obtained, whose structure is hexagonal compact (HC).

In order to calculate nanoparticles size, Scherrer method [122] was used, which supposes the material imperfections as negligible or inexistent and that the thickening of diffraction profiles is due exclusively to the crystalline size, this equation is applicable from 5 nm to up to 200 nm.

$$L = \frac{K\lambda}{\beta cos\theta}$$

Where L is the crystal size (Å), β the diffraction peak maximum thickness in radians; λ the incident wavelength radiation (1.54 Å); K the Scherrer constant, which depends on the particle morphology and θ Bragg's angle of the considered peak.

Given the signals overlapping it was necessary to deconvolve the peaks to calculate the peak thickness so as to obtain the most adjusted size. Normally the peak with 100% intensity is

the chosen but in this case it was overlapped, so the next one in intensity was chosen (2θ = 60^{o}). Finally, the obtained size was around 7.47 nm±0.07 nm.

2.2.1.2. Polysulfone

Polysulfone pellets employed were provided by Sigma Aldrich, with a molecular weight of Mn = 16.000 g/mol and Mw=32.000 g/mol. TGA, FTIR and DSC were employed to characterize the polymer, results are shown in Figure 24.

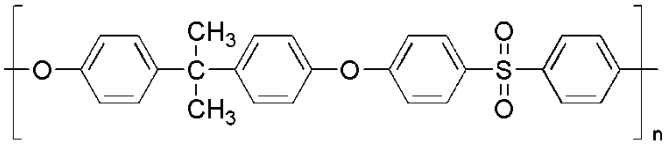

Figure 23. Polysulfone monomeric structure.

Sigma Aldrich polysulfone employed is terminated by OH groups in both of its sides. TGA DSC and FTIR were employed to characterize the polymer. The following figures show the respective TGA thermogram, DSC curve and FTIR:

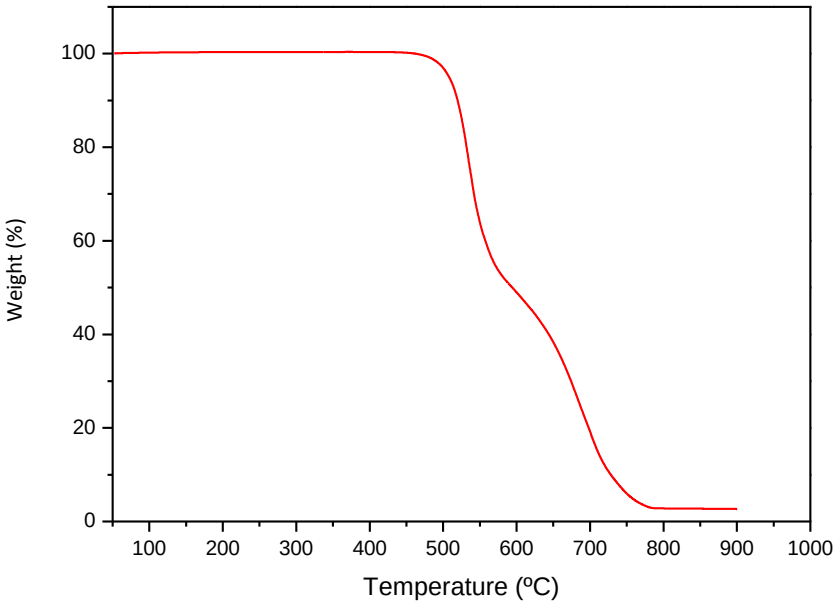
Weight (%)
100
80
60
40
20
0
100
200
300
400
500
600
700
800
900
1000
Temperature (ºC)

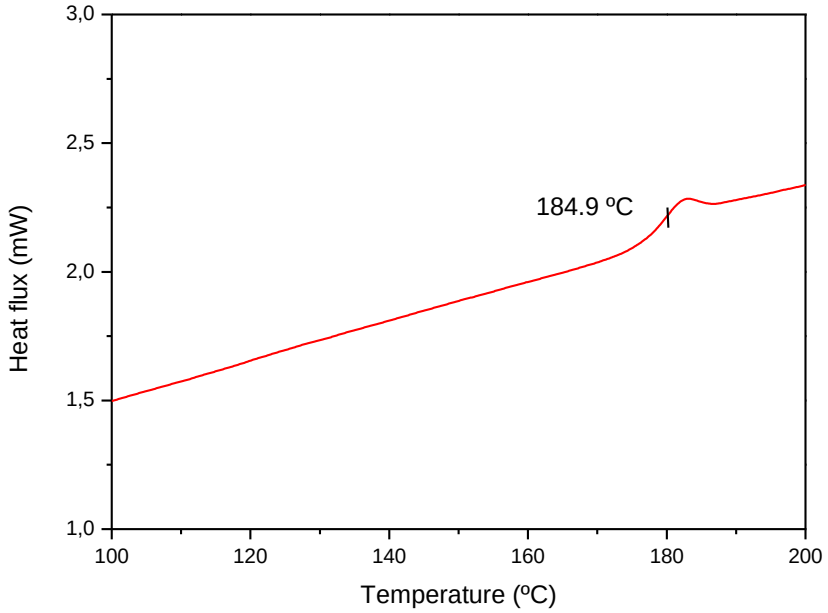
Heat flux (mW)
3,0
2,5
2,0
1,5
1,0
184.9 ºC
100
120
140
160
180
200
Temperature (ºC)

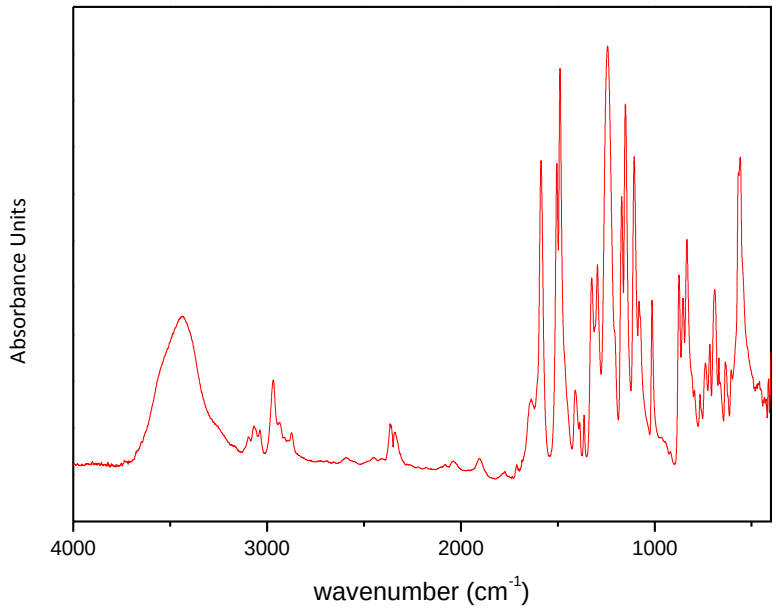

Figure 24. Characterization of commercial PSU: A) TGA thermogram, B) DSC curve and C) FTIR spectrum.

2.2.1.3. Other compounds

Other compounds employed during this work were (in order of appearance) 2-Cholorethyl isocyanate, N-Dimethyl formamide (DMF, Aldrich) and anhydrous DMF (Aldrich), methanol, distilled water, Sodium azida (NaN3, Aldrich), pentynoic acid (Aldrich), Tetrahydrofuran (THF, Aldrich), NaOH water solution 0.5 and 2 N, copper sulfate, sodium ascorbate, methylene dyphenil diisocyanate (MDI) and Dibutyltin dilaurate (DBTDL). No other compound outside this list was employed during the synthesis process.

Functionalization of nanoparticle surface

Two methods were used in this work to achieve two different graft densities:

- **Method A** (low graft density): "Click"-chemistry between alkyne functionalized alumina and azide-end PSU.

- **Method B** (high graft density): formation urethane bridge between diphenylmethane diisocyanate (MDI)-end PSU and OH groups of alumina surface.

2.2.2. Method A

2.2.2.1. Azidation of polysulfone

As previous step to the "grafting to" process, the objective of the azidation is to modify the polysulfone chain endings with azide groups by subsequent chloration and azidation processes [123].

Step 1-. Chloration of polysulfone

4g of Polysulfone were dissolved in 150 ml of anhydrous N-Dimethylformamide in a round bottom flask under magnetic stirring with nitrogen flux (the nitrogen atmosphere keeps the isocyanate group from hydrolization) at room temperature. Then 2-Cholorethyl isocyanate was added and the reaction was stirred for 24h at room temperature. The reaction is schematized in figure 25.

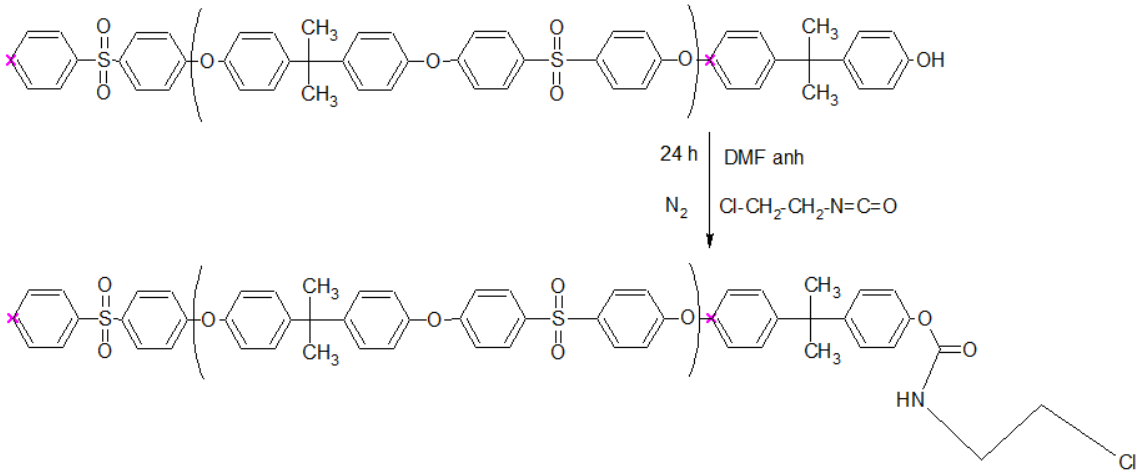

Figure 25. Schematic chloration process on a polysulfone chain.

This suspension was filtered by a Büchner funnel with two layers of paper as filter connected to a side-arm flask by means of a neoprene adapter, with a tube leading to a vacuum pump (fast water flow) to facilitate the filtering. It was afterwards washed by passing 2 l of water and 0.5 l of methanol through the filter, and was dried in vacuum for 5 hours and hold at 120ºC for 12 hours. Figure 25 shows the experimental setup for the reaction and subsequent washing of product. The product was weighed and used in Step 2 except for a sample saved for TGA and FTIR analysis (Figure 27).

Figure 26. A) Set-up for Chloration process and B) washing filtering set-up for both chloration and azidation of PSU.

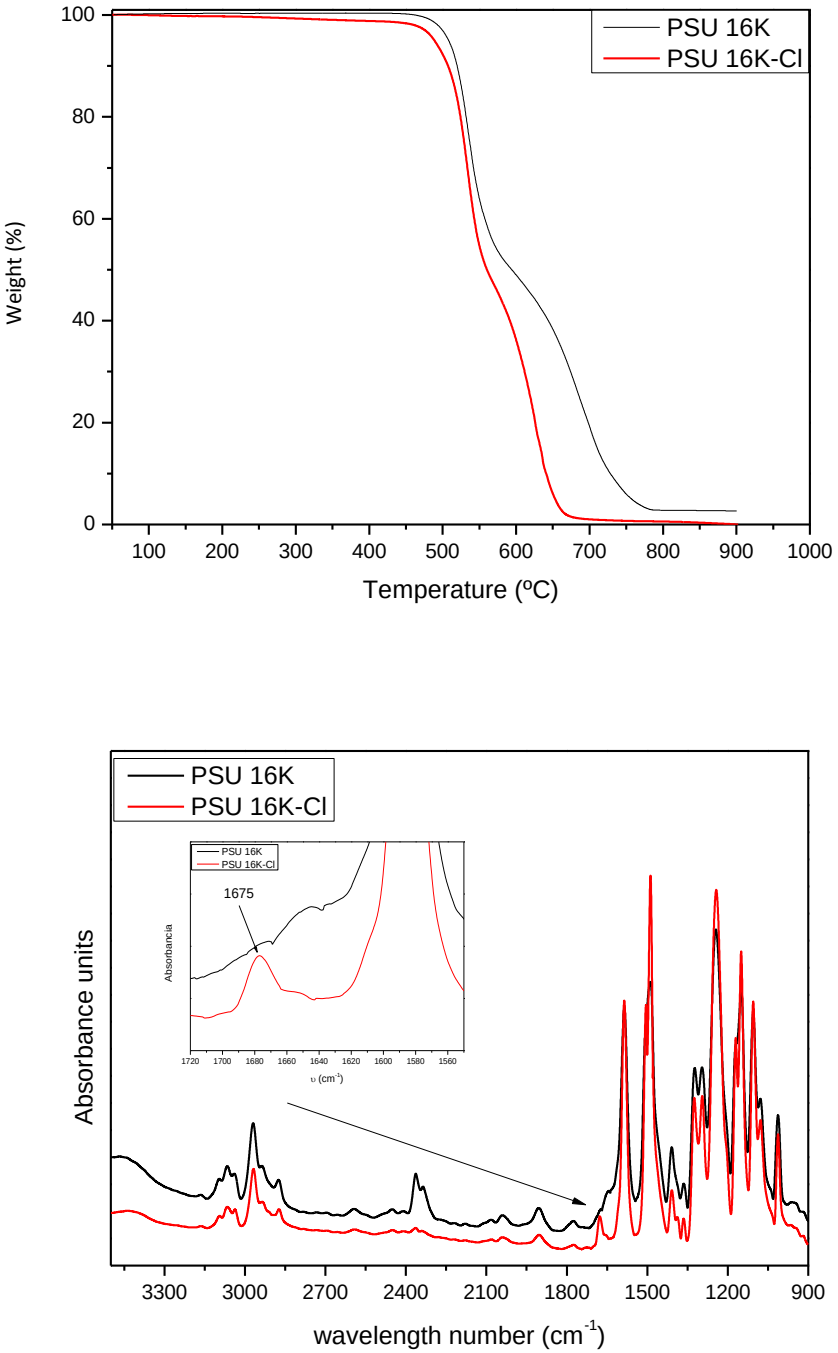

Figure 27. Characterization of chlorated PSU: A) TGA curve B) FTIR spectra.

Comparing both spectra, characteristic band of carbonilic carbon (C=0) from the formed urethane group is detected around 1700 cm^{-1}.

Step2-. Azidation of polysulfone

3.11 g of chlorated polysulfone were dissolved in 100 ml of DMF in a Schlenk magnetically stirred at 60ºC. 11.9 mg of sodium azide were added to the chlorated polysulfone solution and it was hold at the same temperature and stirred during 24h without nitrogen flux.

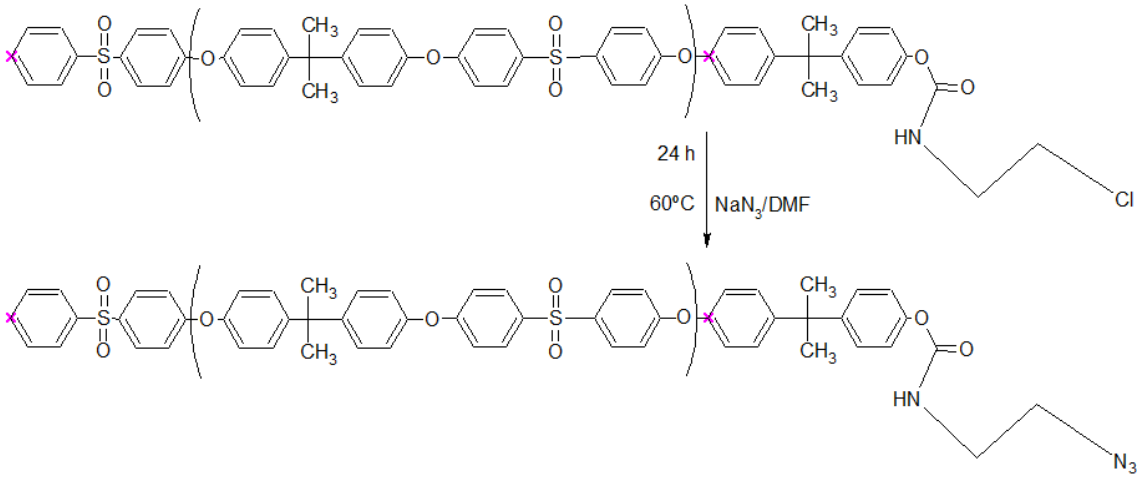

Figure 28. Schematic azidation process on a chlorated polysulfone chain.

Subsequently, 400 ml of methanol with 200 ml of water were cooled in a freezer, and magnetically stirred afterwards. The resulting azided polysulfone was introduced into this mix drop by drop, obtaining a whitened suspension of thin polysulfone fibers in methanol/water.

This suspension was filtered by a Büchner funnel connected to a side-arm flask by means of a neoprene adapter, with a tube leading to a vacuum pump (fast water flow) to facilitate the filtering. Once it was filtered, it was washed by flowing 3 l of water through the Büchner, to wash away non-reacted azida groups, and then with 0.5 liters of methanol so as to obtain a better drying. Subsequently the product was dried in a stove at 140ºC for X hours and vacuum was pulled afterwards under 140ºC heating,

Finally, it was evaluated by TGA and FTIR, whose results are shown in figure 29.

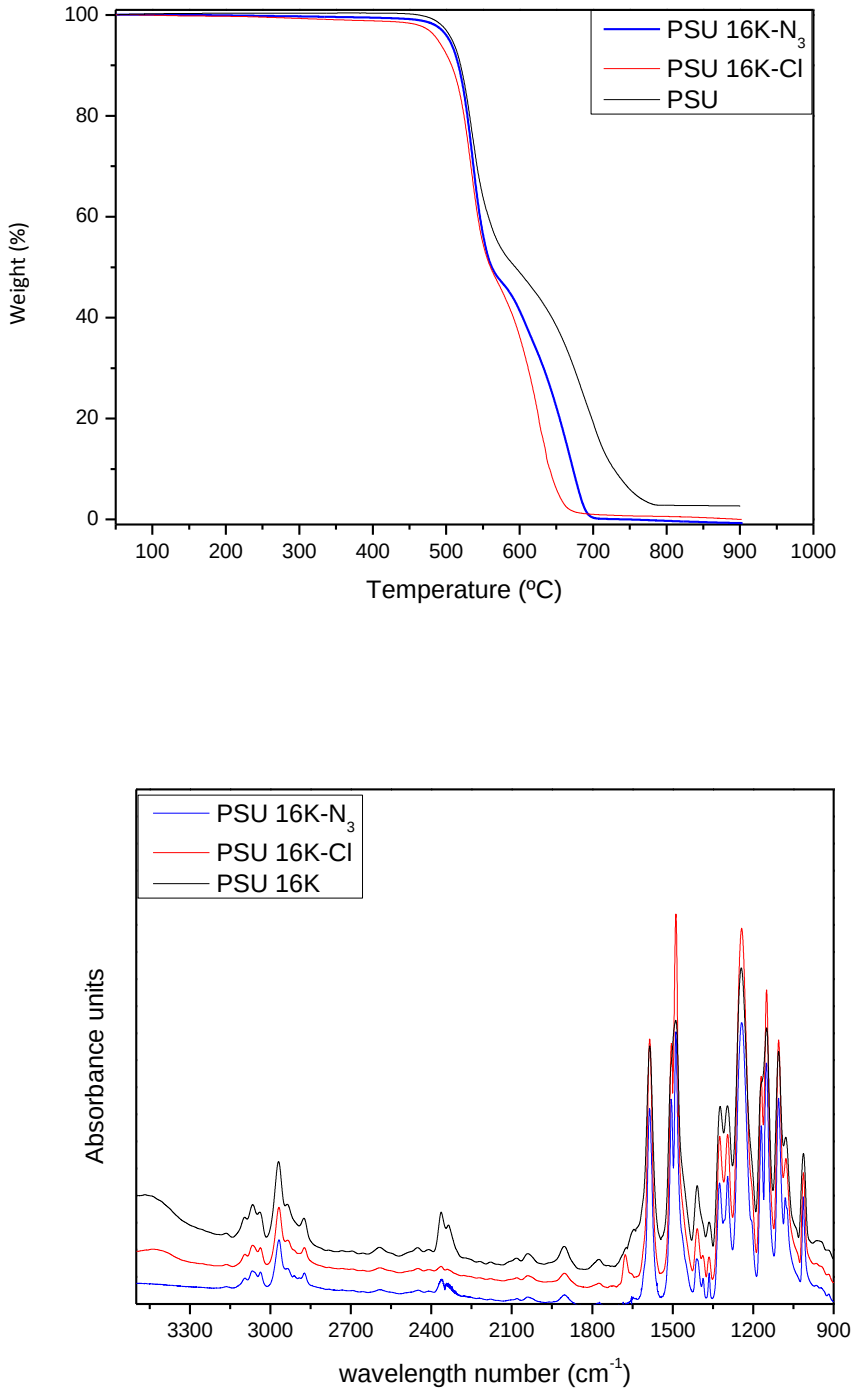

Figure 29. Characterization of azided polysulfone: A) TGA curve B) FTIR spectrum.

The FTIR spectrum does not shows any characteristic band of azida group (R-N_3) around 2100 cm^{-1}.These results confirm the low amount of azida group introduce on the polymeric chain. Although it is true that the molecular weight of the PSU used is very high and the maximum relative chain azide group (in mass) is very small: ~0,006.

2.2.2.2. Surface modification of alumina nanoparticles

These alumina particles were surface modified with Pentynoic acid in order to achieve a functionalized surface which facilitates the grafting of polysulfone chains to the alumina nanoparticles; the process is schematized in the following figure:

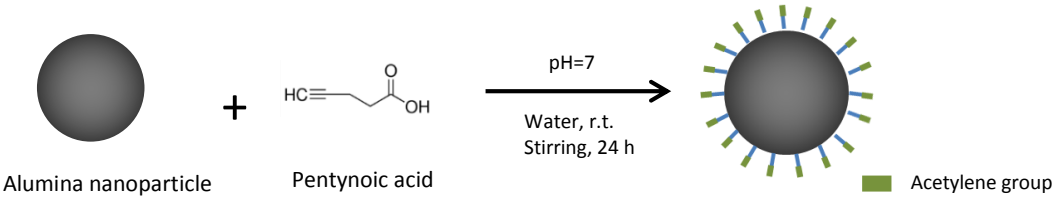

Figure 30. Surface functionalization of alumina nanoparticles with pentynoic acid.

Alumina nanoparticle was coated with pentynoic acid (pent-4-ynoic acid, P4yA, supplied by Aldrich) to incorporate "clickable" alkyne end groups on alumina surfaces. Eight different conditions, varying pH, temperature and other parameters were elaborated to select those with best results. The reaction conditions employed in this work were chosen according to the alumina isoelectric point (pzc) and the pentynoic acid pKa. Alumina nanoparticle has a point of zero charge (pzc) value between pH 8.0 and 9.0 [124]; hence, below pH 8.0, the alumina surface will be positively charged. For P4yA, pKa value is 4.4. Thus, above the pKa value, P4yA will be negatively charged. In figure 31 is shown a graph with the predominant species in pentynoic acid by pH (protoned and dissociated).

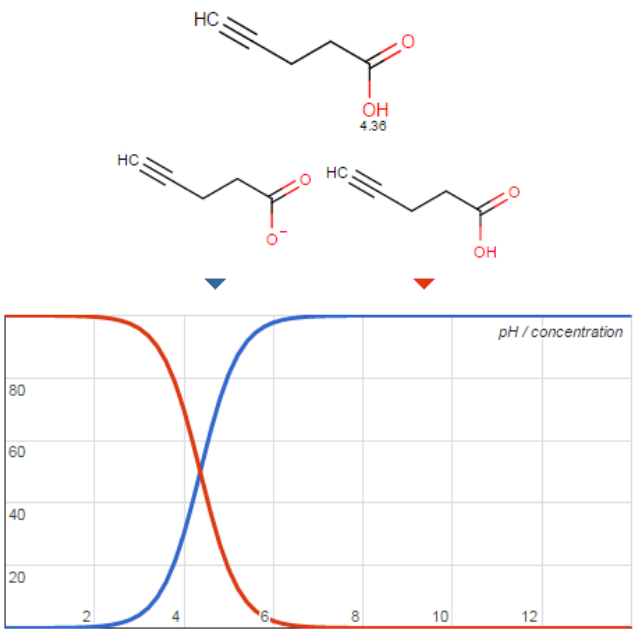

Figure 31. pH/concentration plot of pentynoic acid: Major species at pH=7 : pentynoic carboxylate (blue).

Table 2 shown below details the conditions employed for each one of the eight realized experiments.

Table 2. Conditions of alumina surface modification reactions.

	ALKYNE-MODIFIED NANOPARTICLES							
CONDITIONS	**R1**	**R2**	**R3**	**R4**	**R5**	**R6**	**R7**	**R8**
Alumina specie	ANP1	ANP1	ANP1	ANP2	ANP3	ANP1	ANP1	ANP1
Alumina (g)	2 g	3 g	3 g	3g	1 g	3 g	2 g	1 g
Pentynoic acid (g)	1.2 g	0.5 g	0.5 g	1 g	0,4 g	0.26 g	1 g	0,28 g
Solvent	Water	Water	Water	Water	Water	Water	THF	Water
Solvent volume (ml)	150 ml	100 ml	100 ml	150 ml	200 ml	110 ml	200 ml	200 ml
pH (before reaction)	7.43	4.58	4.60	10.00	11.00	9.00	6.00	11.00
Reaction temperature (ºC)	100ºC	120 ºC	80 ºC	25 ºC	85ºC	65 ºC	70 ºC	120 ºC
Reaction time (h)	14 h	14 h	14 h	14 h	5 h	24 h	24 h	1h*

The different reactions to modify alumina surface followed the same protocol with the indicated singularities in Table 2. As example, Reaction 1 will be described:

One carboxylate group P4yA can be adsorbed onto the alumina as shown in Scheme of Figure 29. In a typical preparation, 0.01 mol of P4yA was dissolved in 50 ml of water.

The pH of 150 ml of distilled water was adjusted to 9 by adding a 2 N solution of Sodium Hydroxide (NaOH) at room temperature under stirring conditions. Then 1.2 g of Pentynoic Acid was added under the same conditions, dropping the pH to 3. Searching for a pH above 7, more NaOH was added until reaching a pH of 7.43. Once the conditions were the desired ones, 2 g of Alumina (ANP1) were added to the solution and it was ultrasonicated for 1 minute (the ultrasonicator employed was a VCX750 processor)..

The reaction, where P4yA is dissociated and the alumina surface is positively charged, took place in a round bottom flask heated by silicone oil (high thermal stability) above 100°C over a heating plate which also stirred magnetically both the mix and the oil. The mixture was kept in reflux for the whole reaction time, and a Nitrogen flux was supplied during to avoid the influence of Oxygen in the reaction. The set-up is shown in Figure 32.A.

The process went on for 14 hours; after which the flask was removed from the set up and, after a few minutes, it cooled down and a clear layer of supernatant was observed, which was partially removed and saved separately, to make the further washing process easier. The pH of this “Zero” supernatant was evaluated.

Figure 32. A) Set-up for R1 and B) Rotofix 32A centrifuge machine

The remainder of the suspension was washed with distilled water a total of five times in a Rotofix 32A (shown in Figure 32.B) centrifuge machine in five periods of 15 minutes at 4000 rpm spinning with a previous ultrasonication. Supernatants pH was evaluated with a pHmeter and progressively drop each wash the results are shown in Table 3. This way, the surface-modified Alumina was washed from the remainder of Acid that did not react previously.

Subsequently, the resulting Alumina was dried to eliminate all the humidity it caught in permanent contact with water. It was introduced in an oven at 250°C for two hours, and placed into a vacuum heating plate over 100°C for four hours to erase possible traces of other compounds. The product was therefore characterized by TGA and FTIR.

Table 3. pH of supernatants during washing process. Second column of R6 represents x+5 supernatants.

	Supernatant's pH								
No. Supernatant	**R1**	**R2**	**R3**	**R4**	**R5**	**R6**		**R7**	**R8**
0	7.15	-	-	7.14	-	-	-		-
1	7.27	4.67	5.47	7.34	10.22	9.15	8.35	5.43	4.45
2	6.89	4.09	4.38	7.43	9.36	9.15	7.57	5.24	4.59
3	6.33	4.02	4.10	7.19	9.20	9.00	6.30	4.79	4.53
4	5.52	4.09	4.08	6.66	9.15	8.85	6.05	4.65	4.43
5	5.08	-	4.10	-	8.86	8.78	5.94	-	-

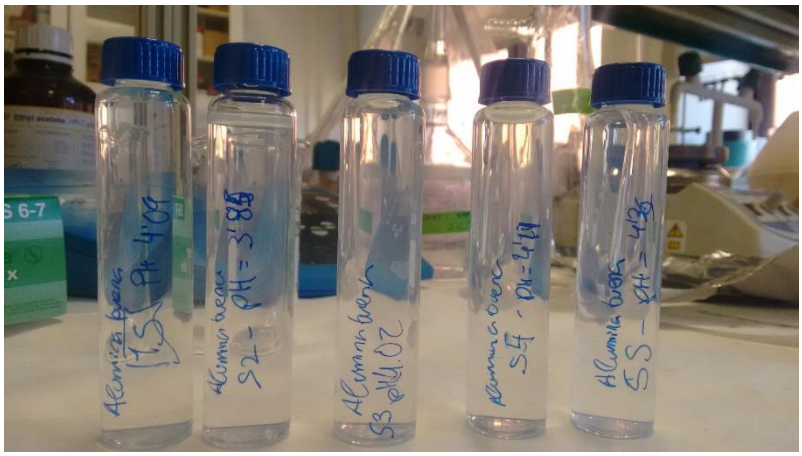

Figure 33. Example of saved supernatants from R5.

Hereby will be presented the TGA analysis and FTIR spectrum of every reaction accomplished. As well as any particularity or disconformity with the protocol previously explained:

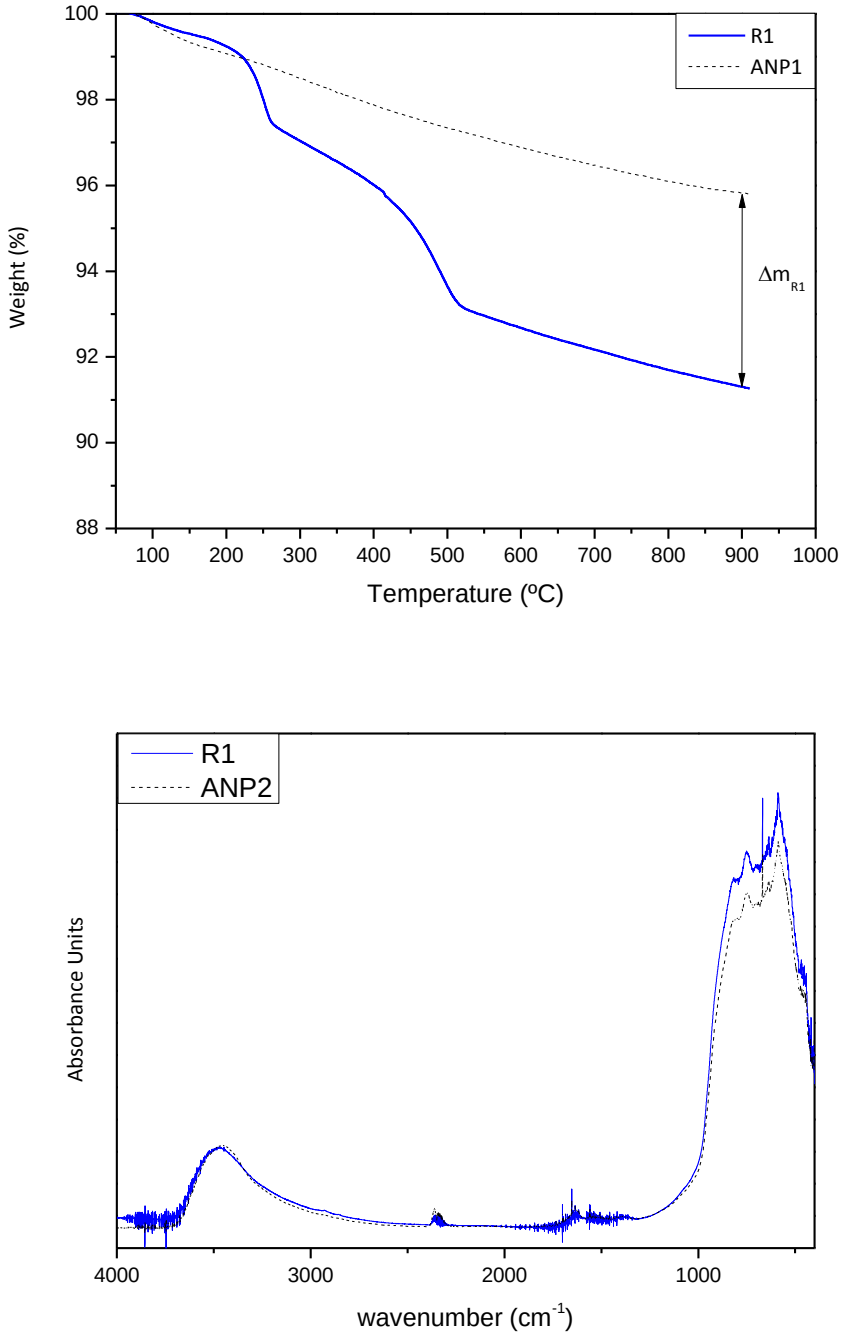

Figure 34. A) TGA Thermogram and B) FTIR spectrum from R1 compared to ANP employed.

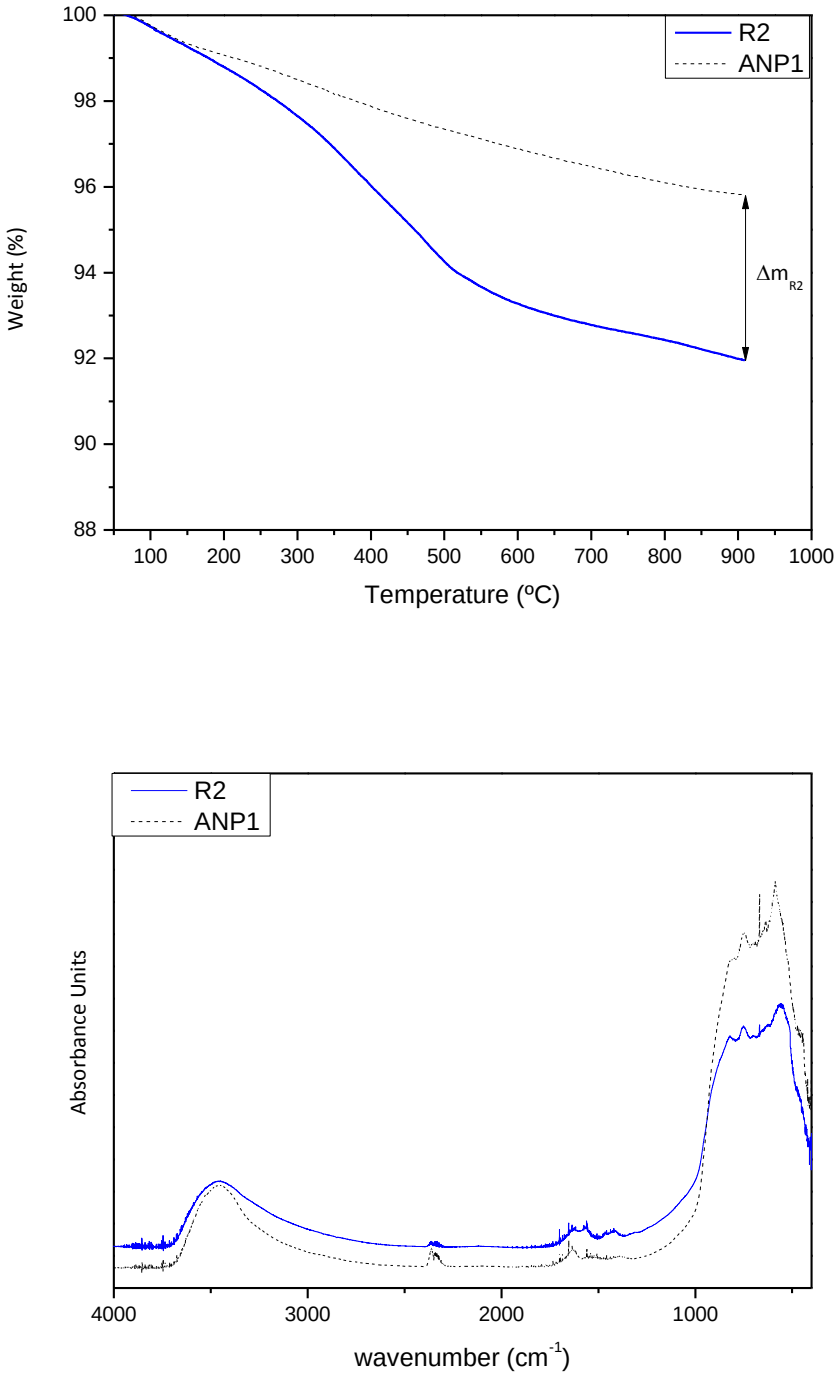

Figure 35. A) TGA Thermogram and B) FTIR spectrum from R2 compared to ANP employed.

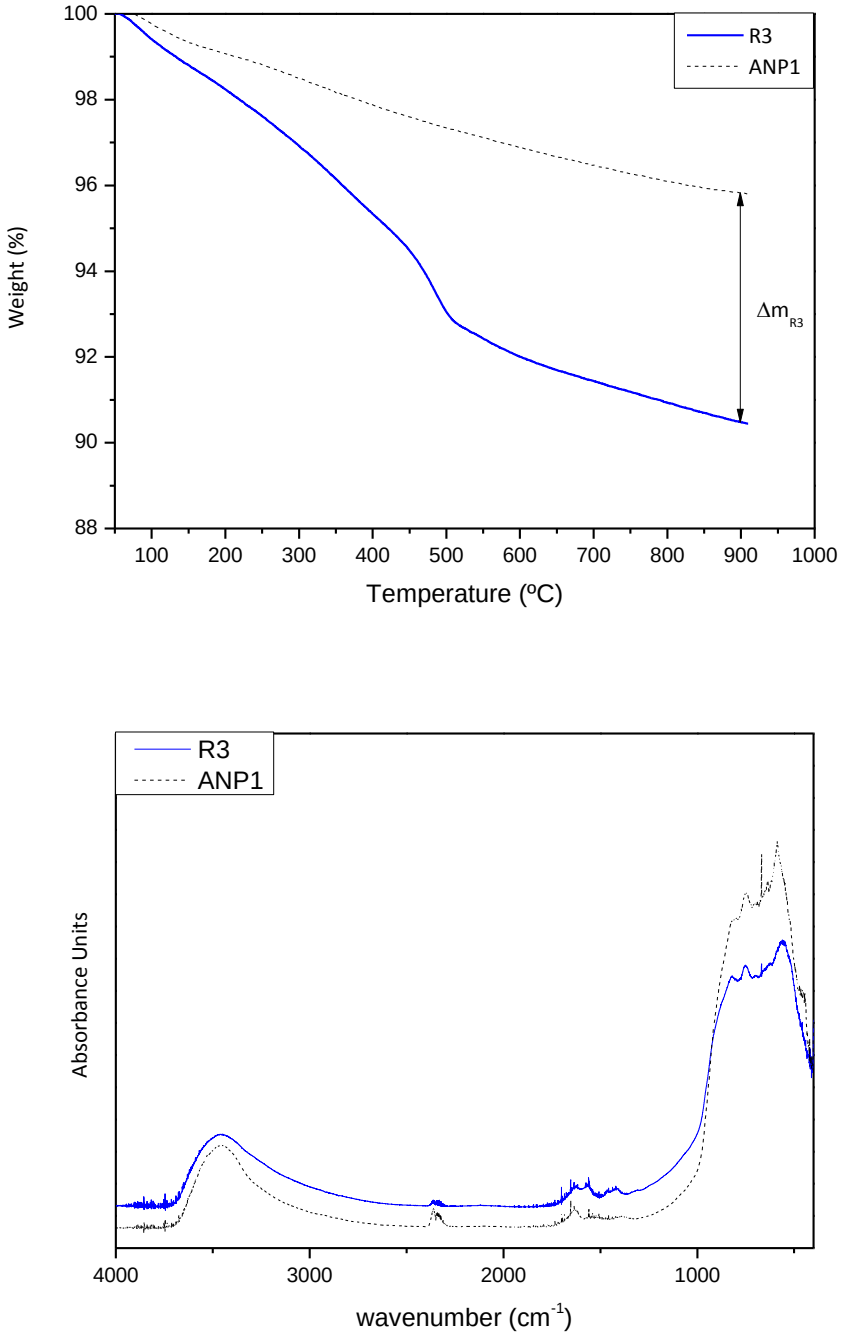

Figure 36. A) TGA Thermogram and B) FTIR spectrum from R3 compared to ANP employed.

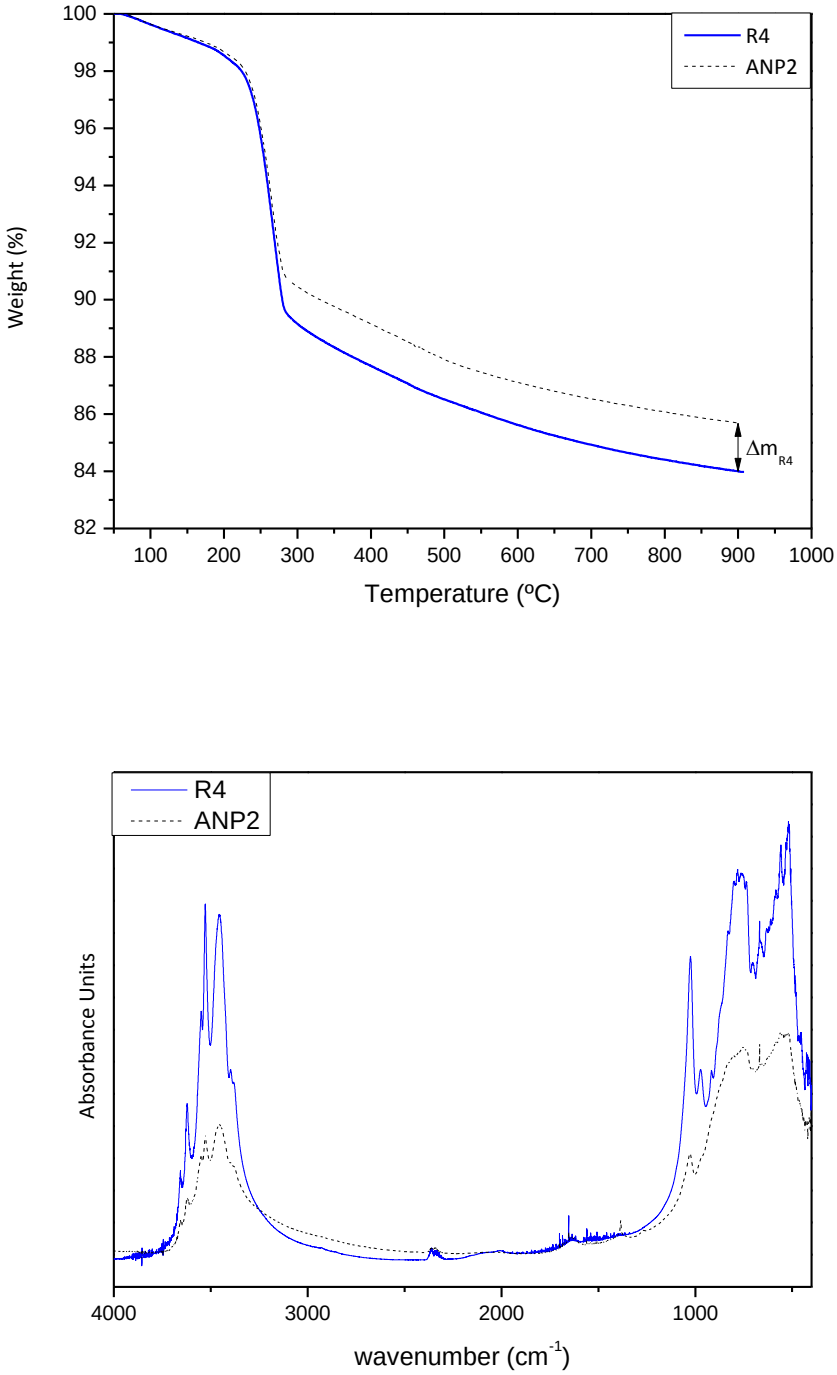

Figure 37. A) TGA Thermogram and B) FTIR spectrum from R4 compared to ANP employed.

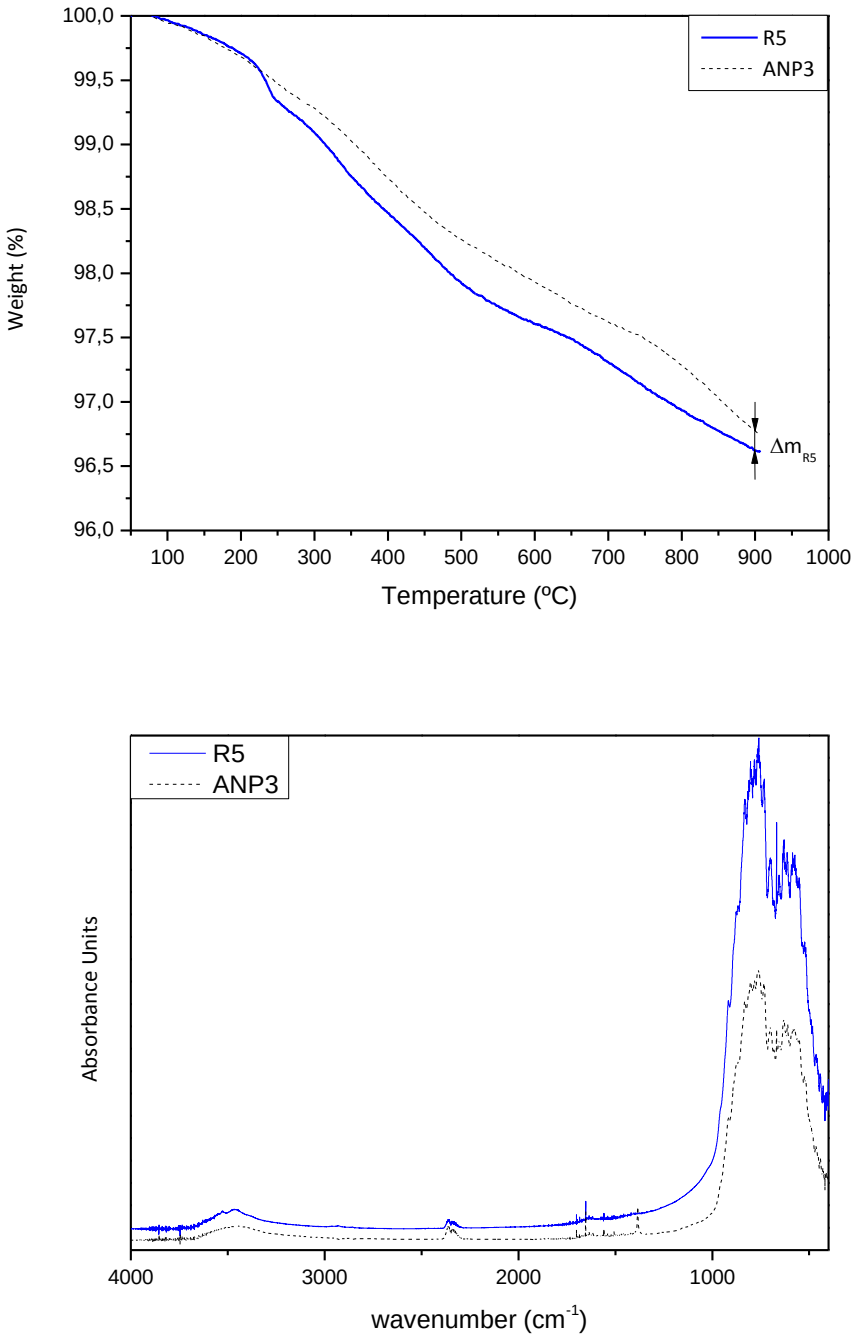

Figure 38. A) TGA Thermogram and B) FTIR spectrum from R5 compared to ANP employed.

As particularity, in R6, alumina was suspended in water and ultrasonicated for 30 minutes and strongly stirred for 60 minutes previously to mix it with a solution of pentynoic acid in water.

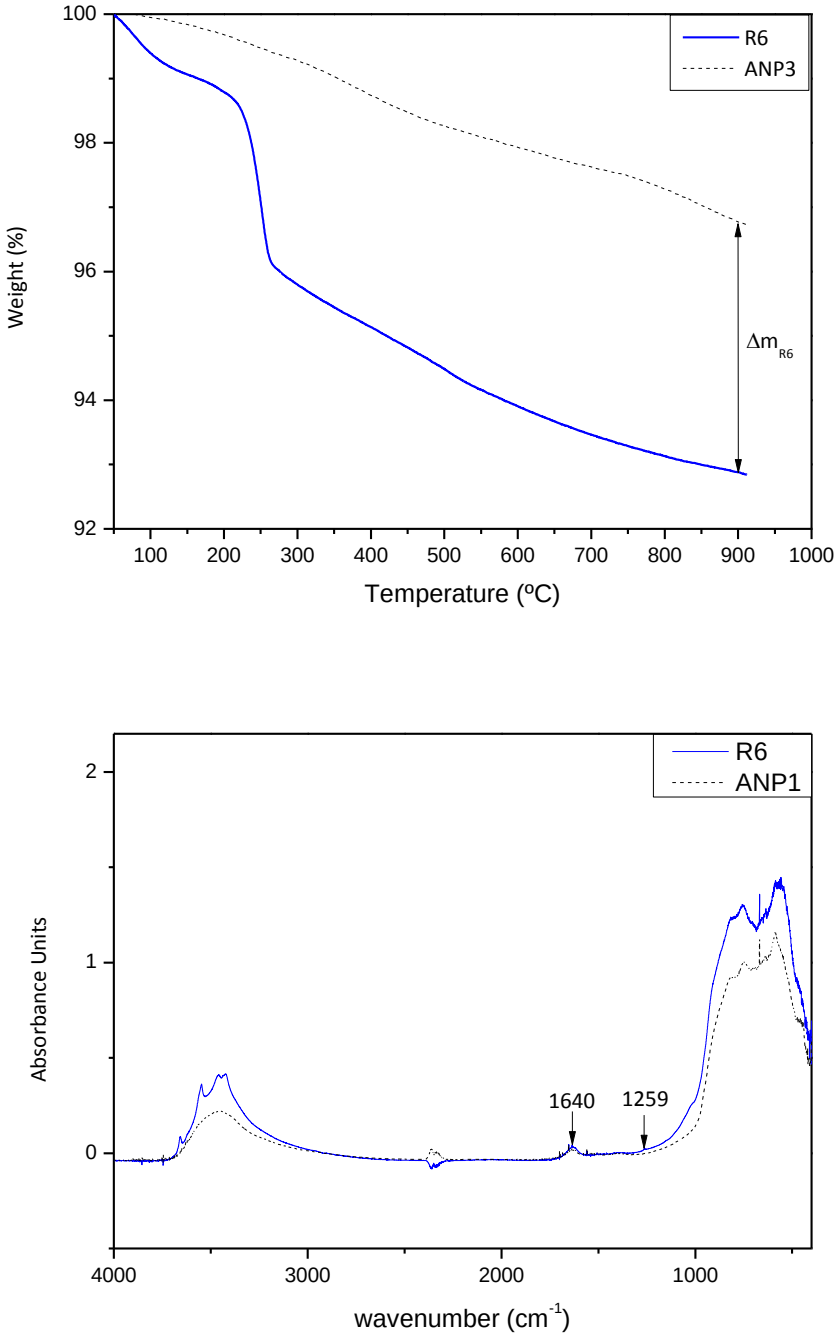

Figure 39. A) TGA Thermogram and B) FTIR spectrum from R6 compared to ANP employed.

The particularity for R7 was uniquely the washing in THF instead of water and the dry at a lower temperature (50 °C) and only 5 hours + 5 of vacuum due to it.

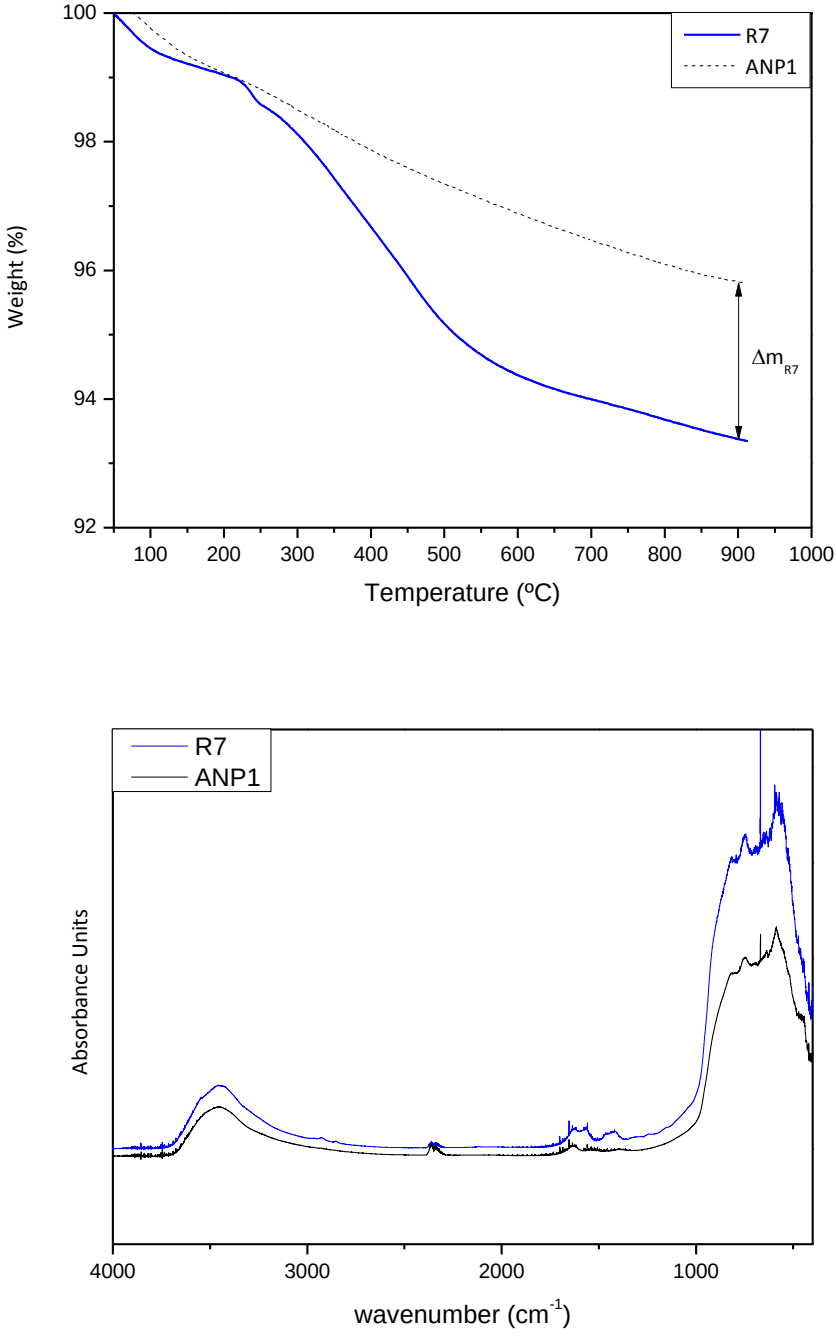

Figure 40. A) TGA Thermogram and B) FTIR spectrum from R7 compared to ANP employed.

The particularities of R8 are A) the initial step was not made at room temperature, but heated to 85°C; B) the reaction was done during 1 hour of ultrasonication; C) After the washing process, two more washes were effectuated, but with Acetone, whose pHs were 6.25 and 6.47 respectively. It can be remarked that the final compound was light grey colored instead of white, probably due to some carbon nanoparticles contamination.

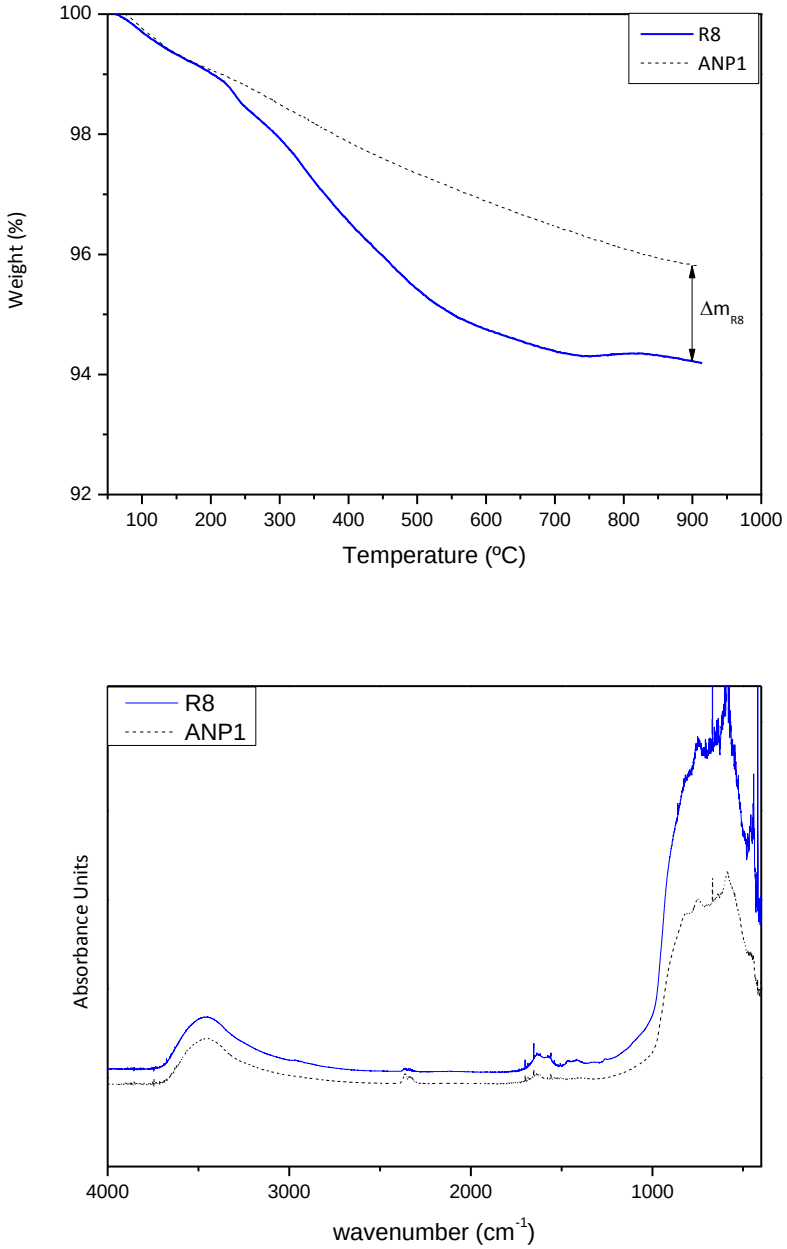

Figure 41. A) TGA Thermogram and B) FTIR spectrum from R8 compared to ANP employed.

Chemisorbed acid measurement

Every surface modified alumina presents triple bonds on its surface by its reaction with pentynoic acid; the density of this triple bonds over the surface will determine the capacity of the polysulfone to graft to alumina.

Calculation of the surface density σ (molecules/nm2) was done with the following expression:

$$\sigma_{graft} = \frac{\frac{\Delta m_{Ri}}{M_{pentynoic}} \cdot N_A}{(100 - \Delta m_{Ri}) \cdot S_{BET}}$$

Figure 42. Surface density of pentynoic acid on alumina surface.

Where $M_{pentynoic}$ is the molecular weight of pentynoic acid, NA the Avogadro number, S_{BET} is the specific surface area of γ-alumina calculated by BET (135 m2·g-1 or 1,35·1020 nm2·g-1).

From the TGAs for every reaction showed above, surface density was calculated, with the results shown in the following table:

Table 4. Surface density of pentynoic acid on alumina surface.

	R1/ANP1	**R2/ANP1**	**R3/ANP1**	**R4/ANP2**	**R5/ANP3**	**R6/ANP3**	**R7/ANP1**	**R8/ANP1**
WL_R	91,31	91,96	90,48	84	96,62	92,88	93,37	94,22
WL_{ANP}	95,81	95,81	95,81	85,69	96,77	96,77	95,81	95,81
Δm_{Ri}	4,5	3,85	5,33	1,69	0,15	3,89	2,44	1,59
σ_{graft}	**2,23**	**1,89**	**2,66**	**0,81**	**0,07**	**1,91**	**1,18**	**0,76**

In Figure 43. All the TGA curves are represented together for better comparison, the same study has been made for FTIR spectra in Figure 44.

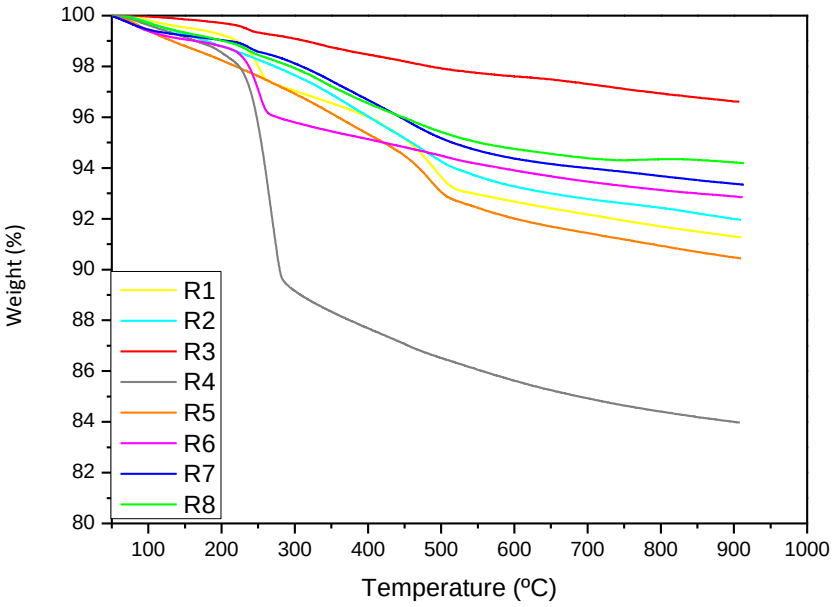

Figure 43. Comparison of all reactions weight loss during TGA analysis.

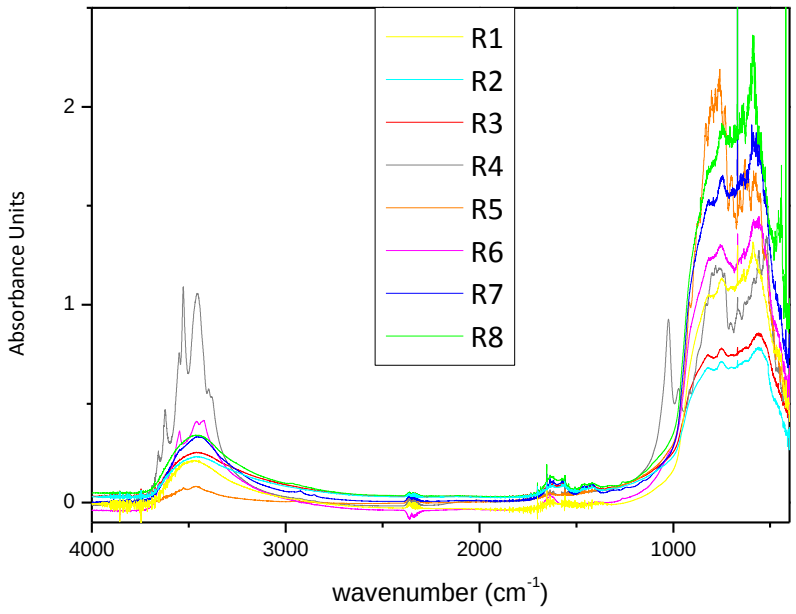

Figure 44. Comparison of all FTIR spectra.

Furthermore, the biggest pentynoic content of every reaction could also be predicted analyzing TGA. Pentynoic acid degrades above 250ºC [125], evaluating thermograms of every reaction, R6 presents the biggest weight loss in that temperature rank with a clean fall; since its calculated grafting density in Table 4 also ranks among the firsts, **R6 product was selected** as the functionalized alumina to continue with the click chemistry process. R6 alumina (from now on named functionalized/modified alumina) particle size was characterized by DLS (see Figure 45) and it was examined by TEM (shown in Figure 46).

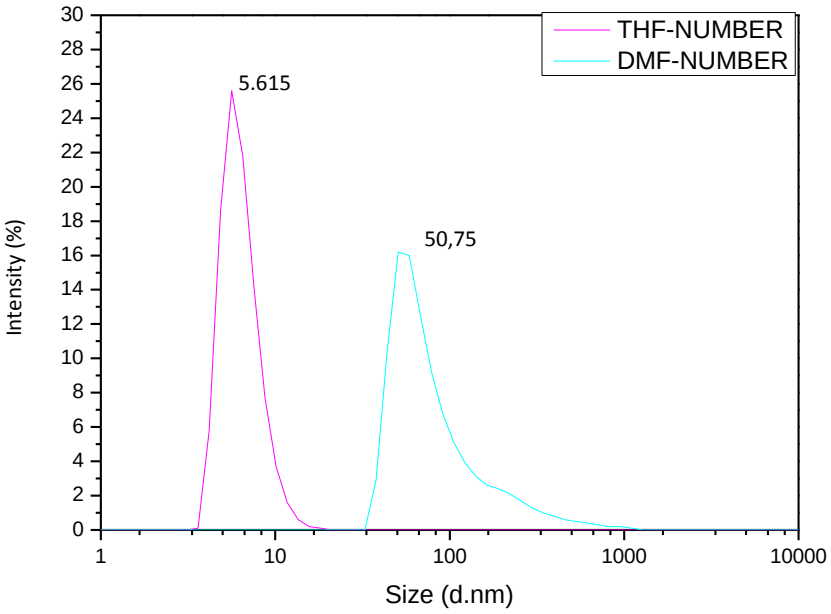

Figure 45. Characterization of NP size by Dynamic Light Scattering.

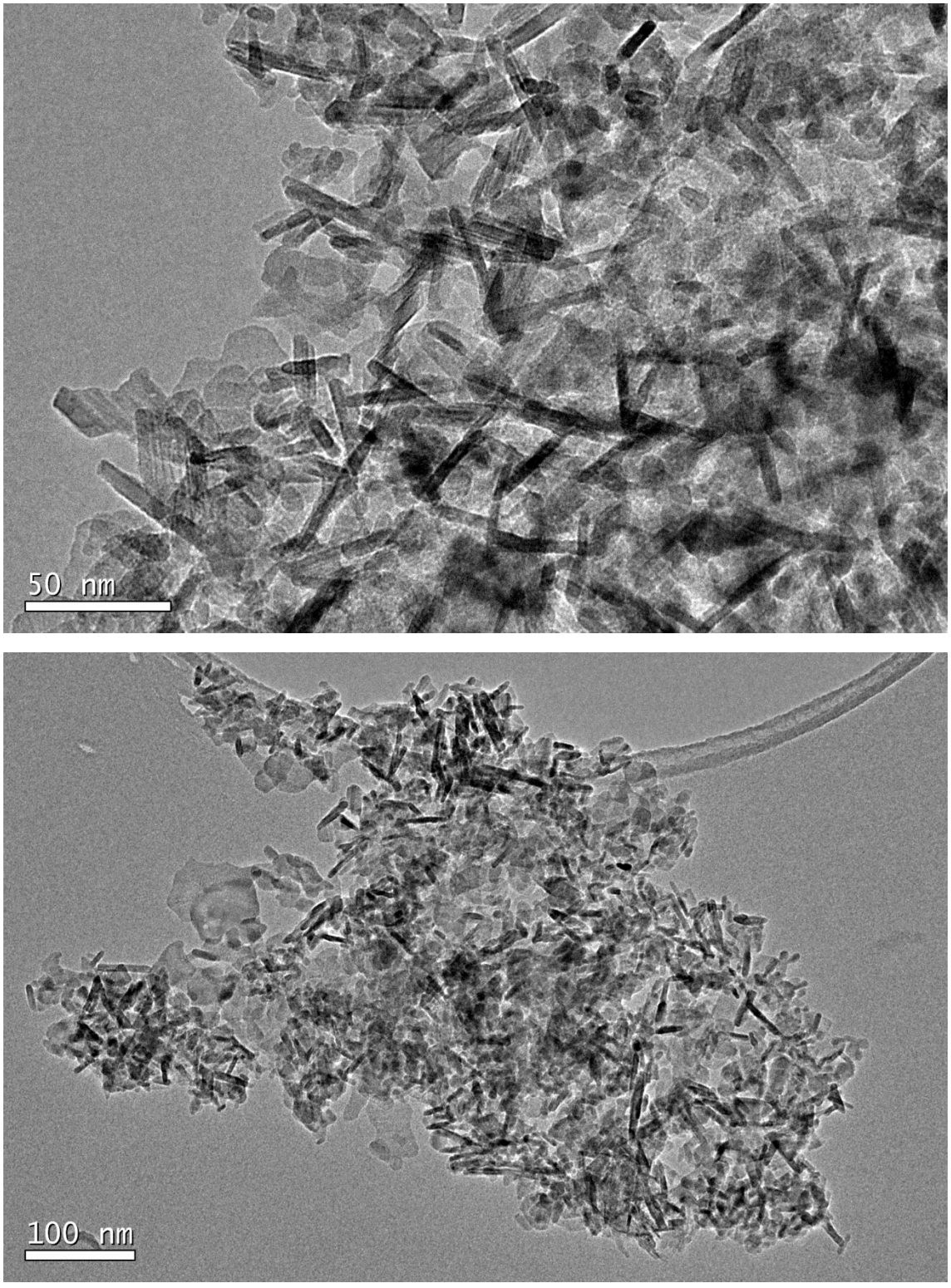

Figure 46.Pictures of Alkyne alumina product of R6 obtained by TEM.

In TEM micrography, nanoparticles aggregates are clearly observed as well as worm-like structures, which could be laminar structures on a side view, this is due in

part to the solution of the examined sample in acetone due to technical issues, which is not a good diluter of alumina.

2.2.2.3. Synthesis and Characterization of PSU-grafted-alumina nanoparticle

The remaining process was the grafting of azided polysulfone chains to functionalized alumina nanoparticles. Hereby the process employed will be described. The reaction is schematized in Figure 47.

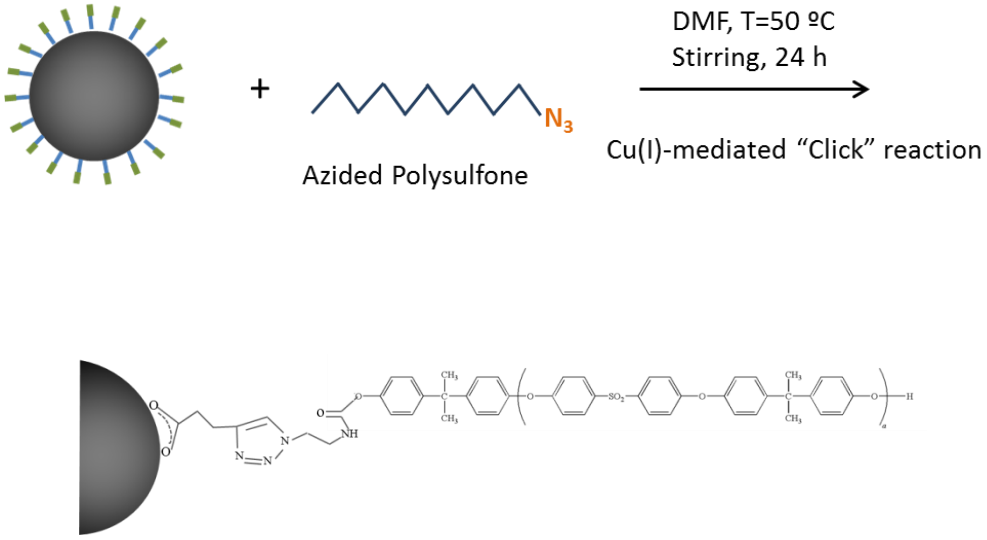

Figure 47. Schematic of general synthetic route to PSU-grafted-nanoparticle.

A 1:3 in mass Alumina-Polysulfone relation was calculated in order to graft Azided PSU to modified alumina surface. 2g of azided polysulfone were dissolved in 40 ml of anhydrous N-Dimethylformamide. Consequently a suspension of 0.66 g of alumina in 40 ml DMF was used.

The catalyst was prepared previously to the reaction of alumina and PSU. The chosen catalyst was Cu^{+} ion, obtained by the reaction of Copper sulfate (Cu^{2+}) ($CuSO_4 \cdot 5H2O$) with sodium ascorbate ($C_6H_7NaO_6$) in a 2:1 moles reaction by generation in situ process in which copper (II) is chemically reduced to copper (I) in a 2:1 DMF/water solution. 0.63 mg of copper sulfate and 1.65 mg of sodium ascorbate were calculated (thereafter it was decided to add sodium ascorbate in excess to ensure the

complete reaction of copper sulfate). The use of copper catalysts in organic synthesis is widely documented in a number of books and reviews [126].

At first, polysulfone dissolved in DMF was added to a Schlenk vase and stirred, thereafter functionalized alumina suspension in dimethylformamide was added. Finally, copper sulfate sodium ascorbate in DMF/water solution was added as catalyst. The schlenk was hold at 50°C by heating through silicone oil bath.

The product was filtered by a Büchner funnel connected to a side-arm with a tube leading to a vacuum pump. The resultant was recovered and dissolved in 40 ml of DMF, stirred until it got suspended and divided into four test tubes, subsequently introduced in a small centrifuge for 15 minutes (2000 rpm), and washed with more DMF three times; afterwards a 1:1 methanol water solution was used as washing liquid, water proposal was to carry the catalyst away, and methanol for better drying. The product was dried under vacuum and at 80 ° C. TGA, FTIR, DLS and TEM were used to characterize the sample, the results of these tests are shown in Figures 48 and 49.

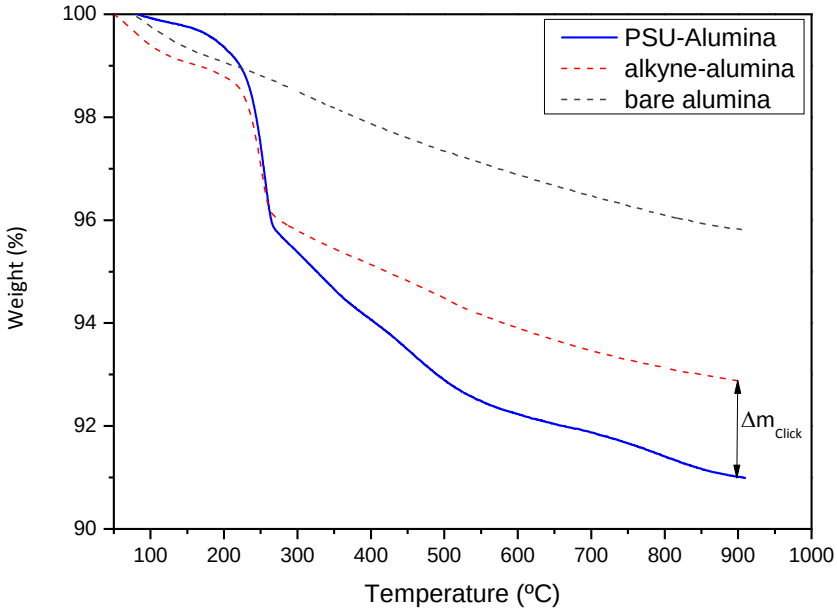

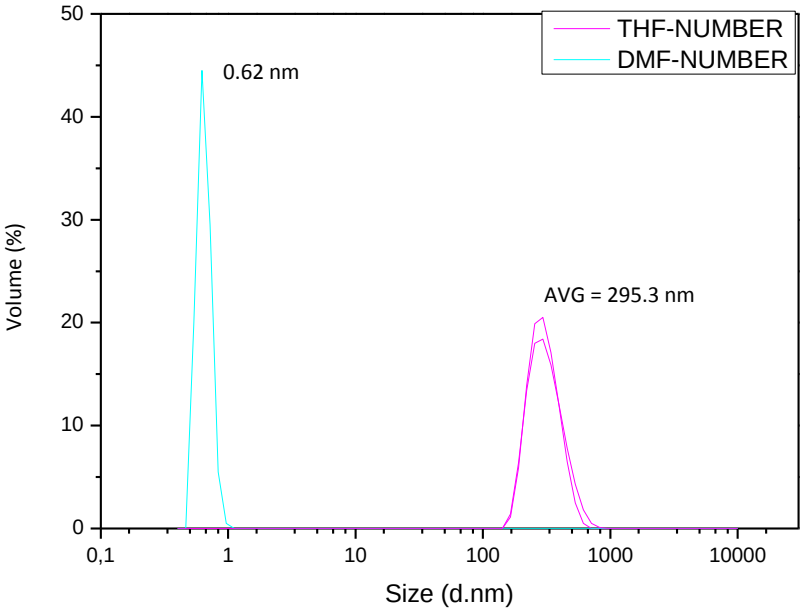

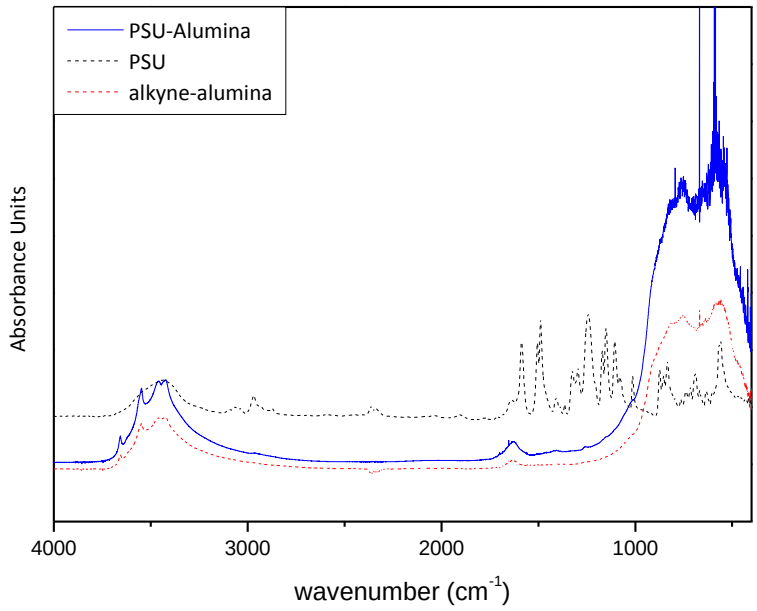

Figure 48. A) TGA B) DLS and C) FTIR of PSU-grafted-Alumina.

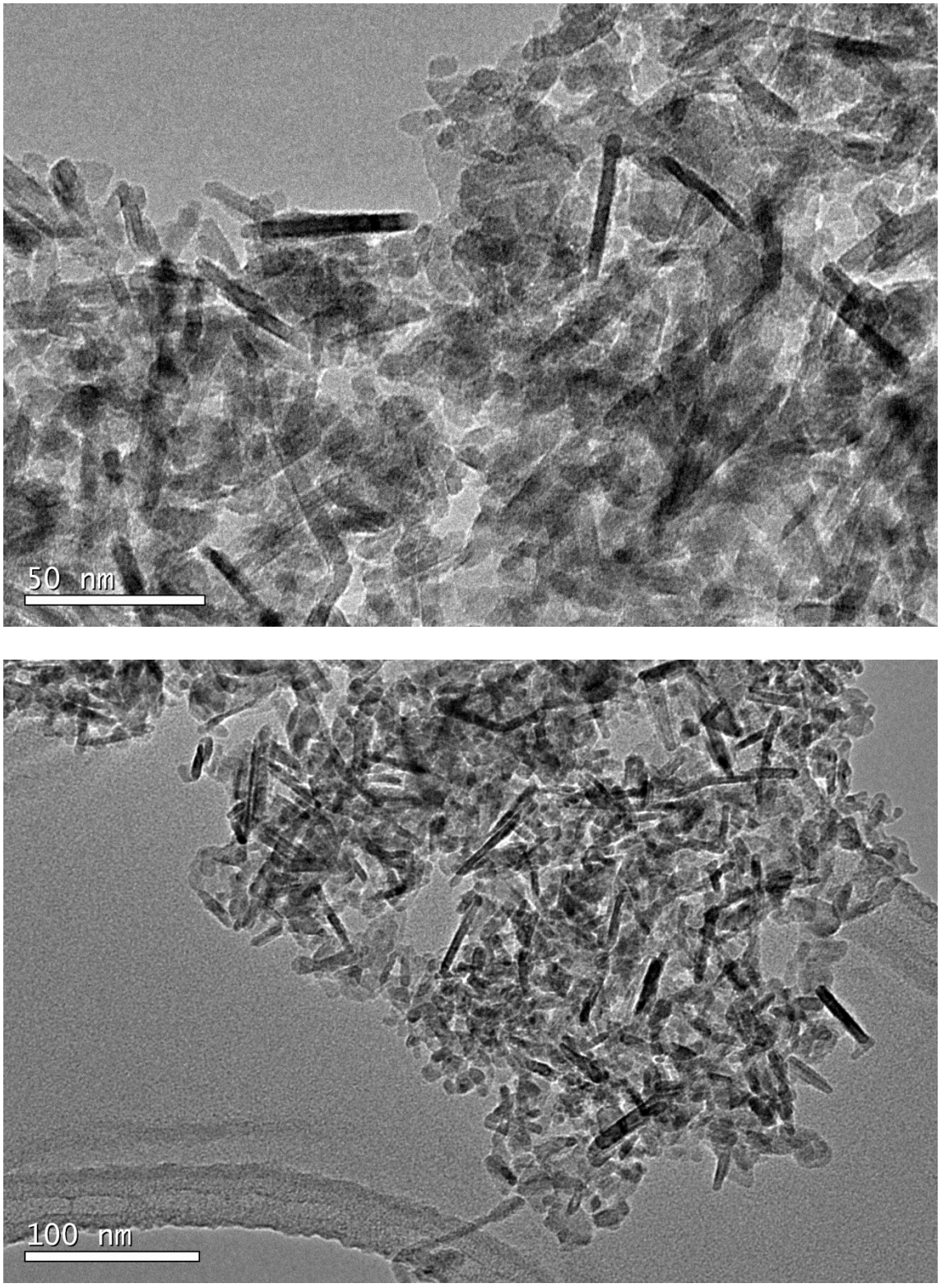

Figure 49. Pictures taken by TEM of PSU-grafted-Alumina by Method A.

Calculus of polymer grafting in alumina surface

The amount of polymer grafted to the nanoparticle is measured by the grafting density, which is obtained comparing degradation obtained by TGA of both the product of the click chemistry (Alumina-PSU) and the surface functionalized alumina employed (product of R6), applying the formula in Figure 50.

$$\sigma_{graft} = \frac{\frac{\Delta m_{click}}{M_{PSU}} \cdot N_A}{(100 - \Delta m_{click}) \cdot S_{BET}}$$

Figure 50. Surface density of pentynoic acid on alumina surface.

With M_{PSU}=16.000 g/mol and Δm_{click}=1.867, the amount of polysulfone grafted is σgraft = 0.0055 molecules/nm^2, approximately 10 times smaller than the results obtained with other polymers of similar molecular weight (other vynilic polymers as PS or PMMA), nevertheless, there is no report about PSU.

It was an expected result given the FTIR of azided PSU in which the characteristic band of azida group N_3 (Figure 29) did not appear (around 2100 cm^{-1}). Furthermore, click reaction result do not show characteristic bands from PSU, which reveals the low presence of polysulfone.

TEM does not reveal the presence of PSU grafted chains on polysulfone surface. This is due in part to the incomplete dispersion of nanoparticles, which difficults to detect the presence of PSU, in part to the low grafting density. The appearance, shape and aggregation of nanoparticles is similar to that shown In Figure 46.

2.2.3. Method B

Another method to obtain polysulfone brushes on alumina surface was examined. In this method isocyanate groups are expected to react with OH groups on the surface of the alumina. The chosen isocyanate was MDI (Methylene diphenyl diisocyanate), one ending of the DMI reacted with OH on the nanoparticle, and the other will remain free to react with OH end groups of polysulfone. Dibutyltin dilaurate (DBTDL) is an organotin compound and is used as a catalyst.

An isocyanate group is very active in chemical reaction which can easily react with compounds with –OH, –COOH, –NH2, etc. The compound is a kind of bifunctional-group organic chemical, which can be used as a coupling agent. It has been proved that –OH groups at the surface of nano-apatite have reactivity towards isocyanate groups [127]. Grafting MDI to alpha-alumina surface was investigated by Li [128] and Hongyan [129]. MDI was used as a grafting

agent to control the surface properties of alumina nanoparticles and at the same time react with the OH ends of polysulfone. This way, the process was carried out in two steps:

First step: functionalization of PSU with MDI:

Polysulfone OH endings reacted with MDI, statistically, a 50% of the polysulfone reacted by one of its ends, 25% reacted by both of them, and 25% did not react. 4 g of PSU were added to 150 ml of anhydrous DMF in a Schlenk vase immersed in silicone oil under stirring conditions and kept at 50ºC with a flux of N_2 to avoid the reaction of isocyanate groups with the exterior atmosphere, to assure this, a nitrogen trap and a gas bubbler were attached to the set-up. Then, 0.066 g of MDI were added. Finally, a drop of DBTDL was added as catalyst. The reaction is schematized in Figure 51.

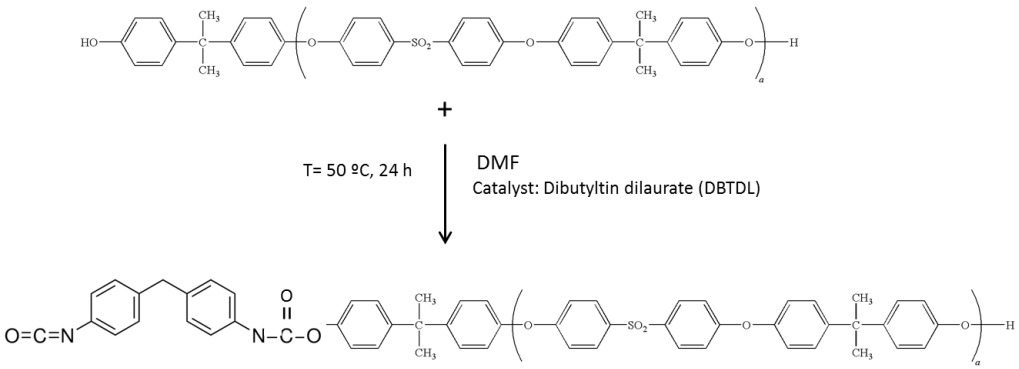

Figure 51. Functionalization of PSU with MDI.

Second step: Functionalization of alumina surface with MDI-PSU:

After the addition of the DBTDL, 1 g of Alumina (ANP1) was introduced in the Schlenk vase, and was kept under the same conditions than in the previous step for 24 hours, in which the free end of MDI reacted with alumina nanoparticles, a scheme of the reaction is shown in Figure 52. The set-up designed for this reaction is shown in Figure 53.

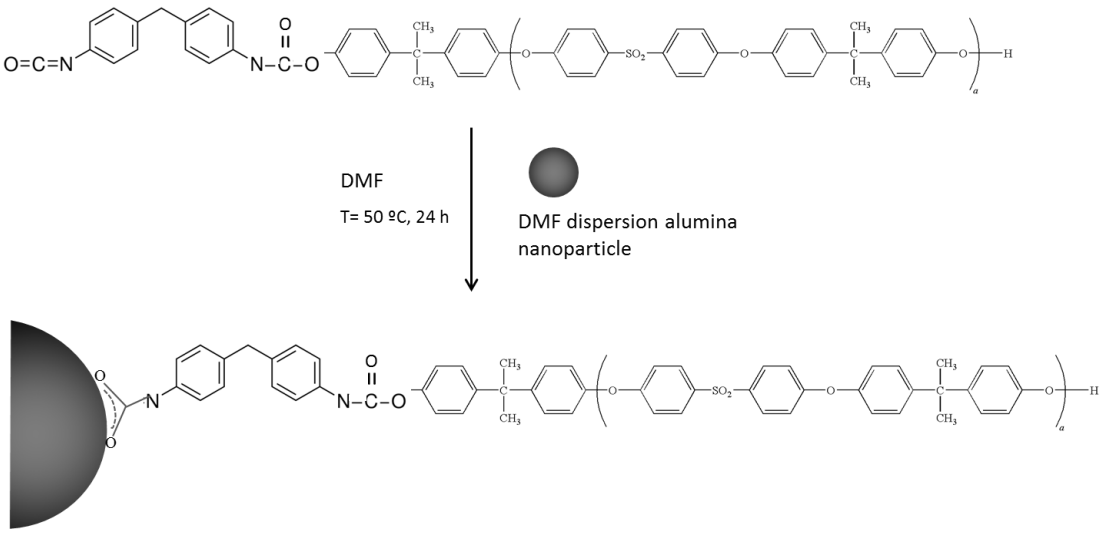

Figure 52. Functionalization of alumina surface with MDI-PSU.

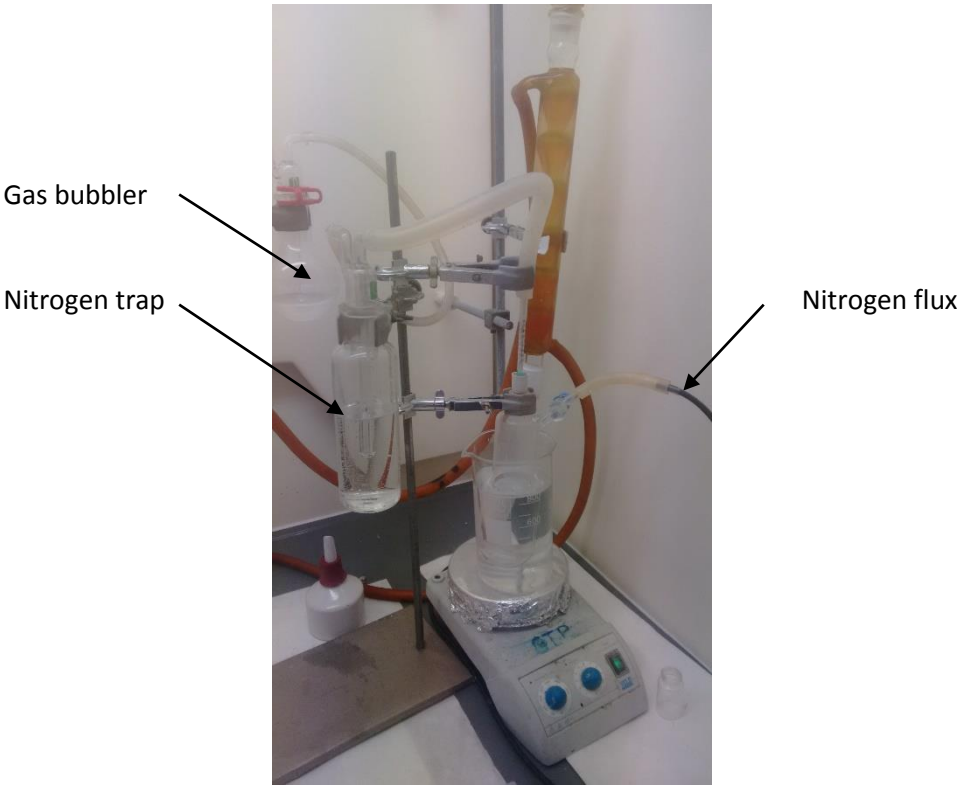

Figure 53. Set-up employed in Method B.

The product was precipitated in a 1:1 mix of methanol and distilled water stirred. Then this suspension was filtered by a Büchner funnel connected to a side-arm with a tube leading to a vacuum pump to eliminate non-reacted MDI traces by washing it with 600 ml of the same mix, after which was dried in vacuum at 110°C for 12 hours. This product was later named Unwashed Alumina-MDI-PSU, and 3.24 g were obtained. TGA was employed to analyze the material, the results are shown in Figure 54.

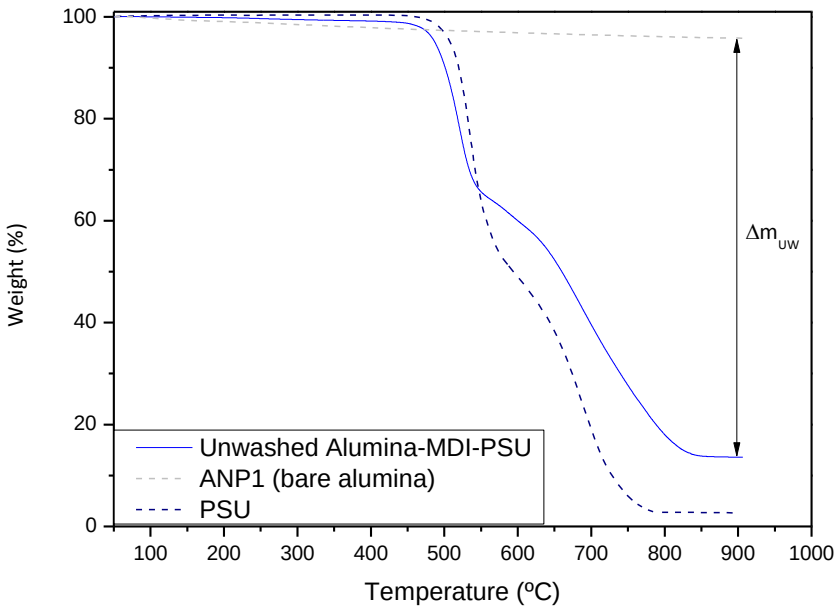

Figure 54. Characterization Unwashed Alumina-MDI-PSU: TGA curve.

The obtained fall of around 87% was not realistic, and it is explained by the presence of a large amount of non-reacted polysulfone, this fact is confirmed by FTIR, which shows a high absorbance in the characteristic band for PSU compounds. Nevertheless, the presence of unchained polysulfone might represent a benefit in terms of entanglement when introduced in the polysulfone matrix. In spite of this, the characterization to determine an effective number of polysulfone chains grafted to alumina surface was still needed.

1 g of Unwashed Alumina-MDI-PSU was separated, dissolved in 40 ml of DMF under stirring and divided into four test tubes, subsequently introduced in a small centrifuge for 15 minutes (2000 rpm), and washed with DMF three times, after which was dried in vacuum at 100°C for 12 hours. So as to characterize the product, TGA, DSC and FTIR techniques where employed, whose results are exposed in Figure 55, the material was also analyzed by TEM, two images are presented in figure 56.

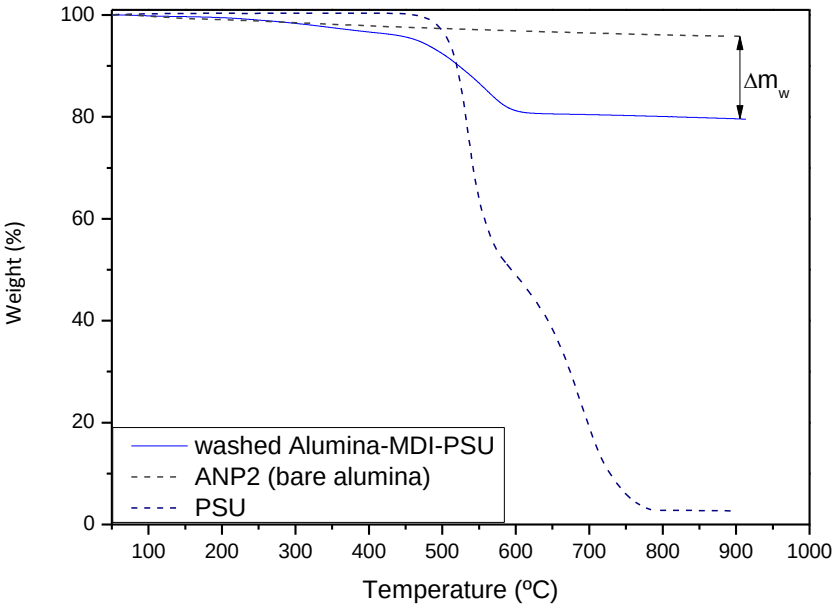
100
80
60
40
20
0
Weight (%)
Δm_w
washed Alumina-MDI-PSU
ANP2 (bare alumina)
PSU
100
200
300
400
500
600
700
800
900
1000
Temperature (ºC)

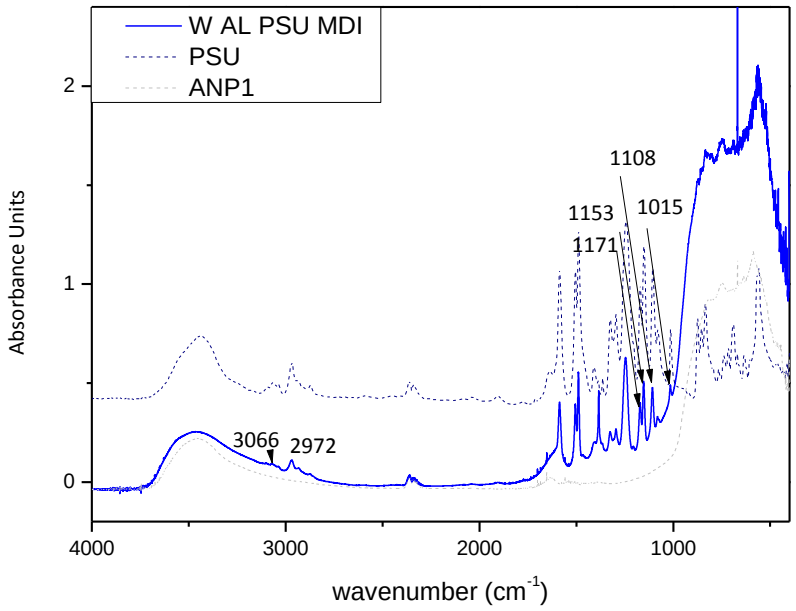
W AL PSU MDI
PSU
ANP1
2
1
0
Absorbance Units
1108
1153
1015
1171
3066
2972
4000
3000
2000
1000
wavenumber (cm-1)

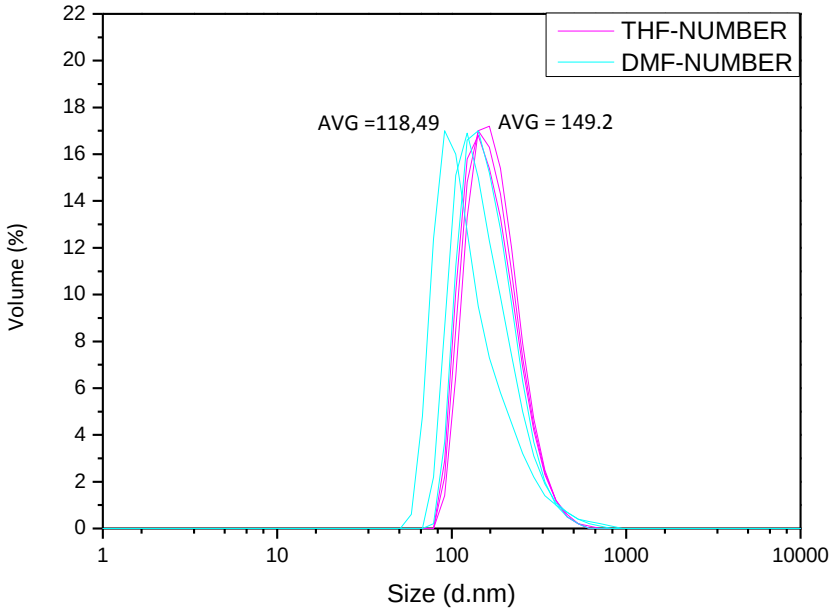

Figure 55. Characterization of Washed Alumina-MDI-PSU: A) TGA curve B) DLS analysis and C) FTIR spectra.

TGA now represents a more realistic weight loss, but still a very acceptable result. FTIR shows characteristic bands of both PSU and alumina in the spectra, which are analyzed in Table 5.

Table 5. Band assignation of Washed Alumina-MDI-PSU.

Absorbance (cm^{-1})	Assignation
3066	Stretching (C-H) bands of –C=C–H
2972	Symmetric stretching Aliphatic C-H bonds
1108	Asymmetric stretching C-O
1015	Planar deformation Aromatic-H

The molecular structure analyzed by TEM (Figure 56) shows the same state of aggregation due to its suspension in acetone for the analysis, which is not a good solute of Alumina or PSU. However, alumina nanoparticles present a layer of polysulfone grafted to its surface.

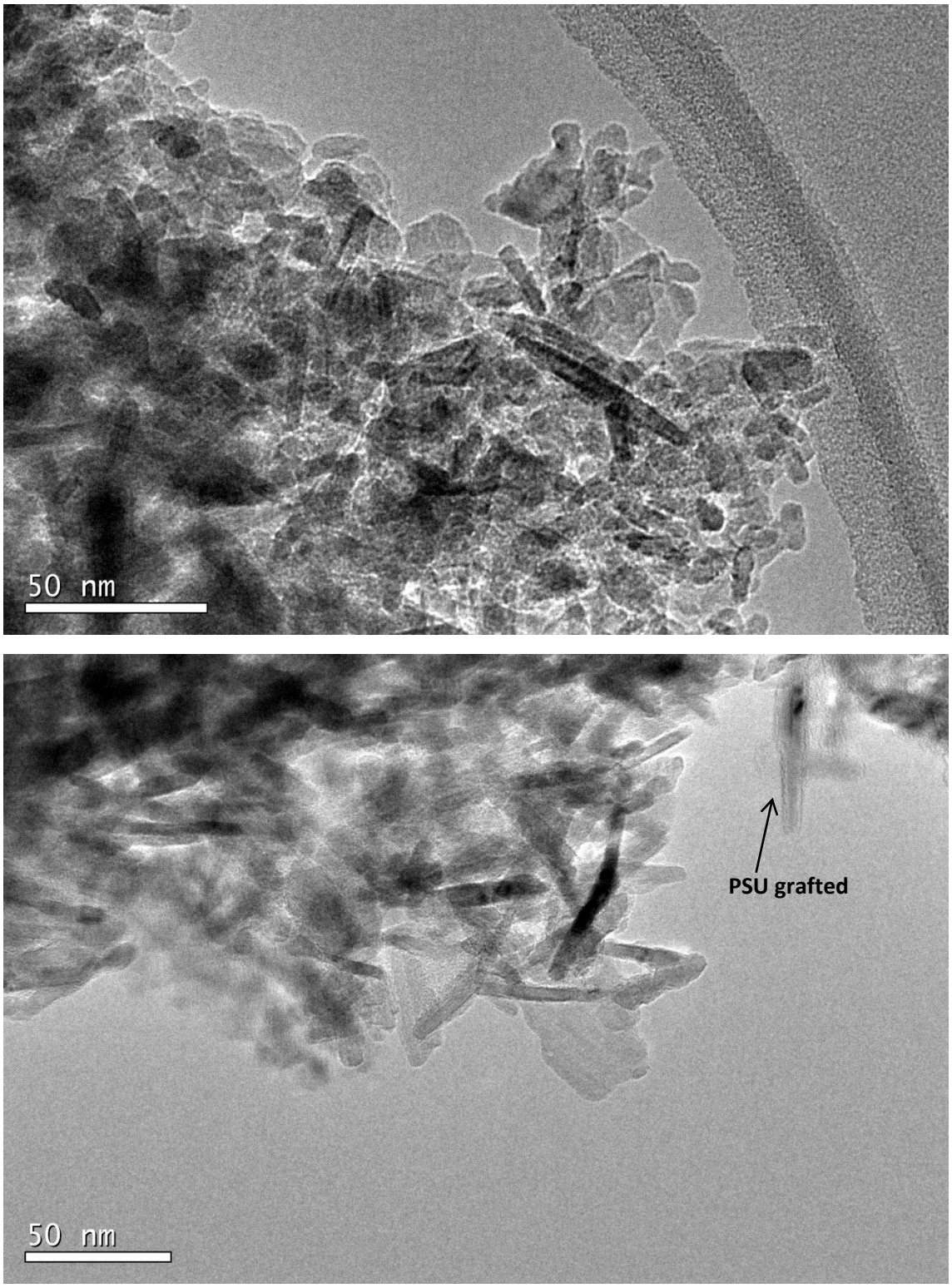

Figure 56. Pictures taken by TEM of PSU-grafted-Alumina by Method B.

Calculus of grafted polymer in alumina surface

The calculus of polysulfone grafted to alumina surface is done by grafting density (σ_{graft}) as in Method A. The weight loss is the calculated in washed Alumina-MDI-PSU, which represents a real percentage of PSU grafted to ANP. Grafting density is calculated by Figure 57.

$$\sigma_{graft} = \frac{\frac{\Delta m_W}{M_{W\,PSU}} \cdot N_A}{(100 - \Delta m_W) \cdot S_{BET}}$$

Figure 57. Grafting density formula for Washed Alumina-MDI-PSU.

With M_{PSU}=16.000 g/mol and Δm= 25,223, a grafting density σ_{graft}=0.056 molec/nm^2, a reasonable amount according to the reported in bibliography for other polymers as PS and PMMA.

As analysis, the comparison of both washed and unwashed Alumina-MDI-PSU TGA thermograms (Figure 58) gives the amount of non-reacted PSU, reacted PSU and Alumina present in Unwashed Alumina-MDI-PSU, calculated in Table 6, MDI mass was considered relatively insignificant.

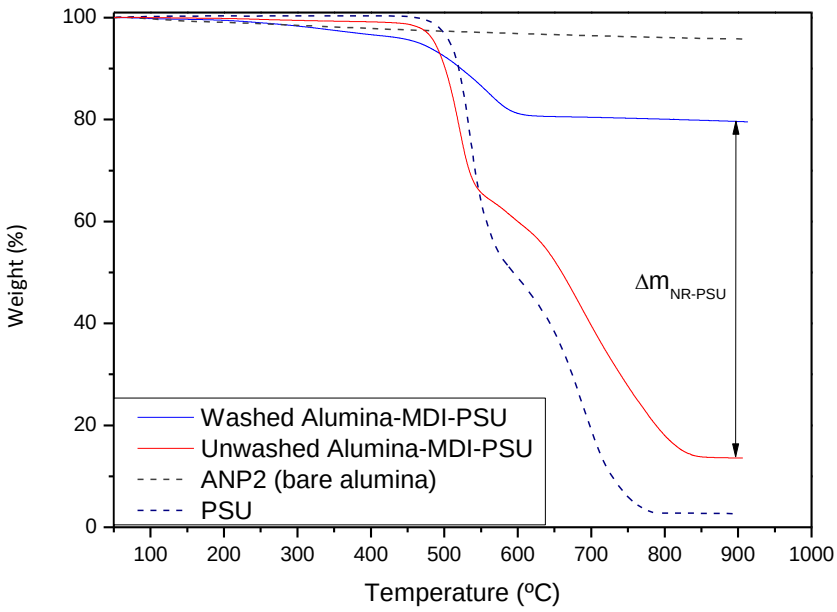

Figure 58. Comparison of TGA curves of Washed and Unwashed Alumina-MDI-PSU.

Table 6. Composition of Unwashed Alumina-MDI-PSU

	Weight (%)
Alumina	17.77
PSU	82.23
Grafted PSU	16.20
Non-grafted PSU	66.03

Grafting density is one of the most important parameter defining thermal and mechanical behavior of the composite, therefore, there appears the need of knowing the structure of grafted polymer hairs on alumina nanoparticle. Dukes reports that the grafted polymer chain structure not only depends on the grafting density, but also in the polymer chain length and the curvature of nanoparticles [90]. Therefore two extreme scenarios are presented, the formation of a mushroom structure, and in the other extreme, the existence of completely straightened polymer brushes (see Figure 3 and Figure 59).

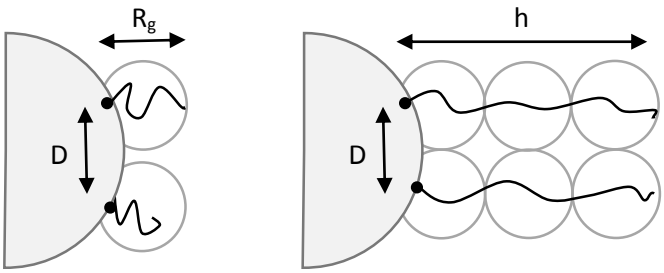

Figure 59. Theoretical behavior of polysulfone chains.

Supposing the existence of mushroom conformation (see figure 3), a new parameter is introduced, the radius of gyration of the chain (R_g), which will determine the height reached by the chain (h) by the next formula:

$$h \approx 2R_g$$

It is also assumed that in this regime:

$$R_g \approx l_o N^{1/2}$$

Where l_o is the monomer length (2.5 nm for polysulfone) and N is the polymerization degree (considering $M_{monomer}$= 442 g/mol $\phi_{nanoparticle}$=7.47 nm; 36 for PSU 16K). Then, the reached height h= 30 nm for the employed polysulfone. The next relation marks the limit to consider a grafted polysulfone as mushroom conformation structure:

$$\sigma < 1/R_g^2$$

Since grafting density calculated by TGA is **σ_{graft}=0.056 molec/nm²** and has to be less than 0.044 g to be considered **mushroom-like structure**, the formation of this structure **cannot be assumed**; therefore the rigidity of polysulfone must be critical and it affects more to its structure than grafting density. Then, the calculus are repeated based on the second scenario in which the grafted polymer is structured in straightened brushes, this calculus are based in the calculation of h in several reports [90][130][131], with which is obtained the same value for h, the expression used by de Genes has been employed:

$$h = \frac{N}{g_D} D$$

Where g_D is the number of monomers and it can be calculated as

$$g_D = \left(\frac{D}{l_o}\right)^{5/3}$$

Where D is the length between attachment points and a is the subunit length. Tchould [132] and Henn [133] reported an expression to calculate the average D

$$D = 1/\sqrt{\sigma}$$

The distance calculated for the grafted polymer is D= 4.23 nm. Iyer reported another expression for D [134], which results in a similar value D=4.77 nm, so the first one was the employed in further calculation.

$$D = \sqrt{4/\pi\sigma}$$

Therefore g_D= 2.4 monomers and h=63.38 nm. Table 7 shows every calculated parameter.

Table 7. Polysulfone 16K parameters

	Grafting Density	Molecular Weight	PDI	Degree of polymerization	Distance	R_g	$h_{mushroom}$	h_{brush}
	σ(molec/nm2)	Mn(g/mol)	(Mw/Mn)	N*	D(nm)	nm	nm	nm
PSU 16 K	0.056	16000	2.2	36	4.23	15	**30.00**	**63.38**

Based on the results, the chain length h and the grafting density are adequate for providing the nanoparticles of a good entanglement with the free PSU forming the matrix (in this work the length chain of grafted PSU (N) and free PSU (P) is the same).

2.3. Nanocomposite production

Nanocomposite was produced by the addition of the hairy alumina nanoparticles to polysulfone matrix (Aldrich) in pellets. Given the results in Method A and Method B, grafting density of PSU into alumina surface is ten time higher in Method B (σ_{graft}=0.056 molec/nm^2 vs σ_{graft}=0.0055 molecules/nm^2), therefore, **polysulfone-grafted-alumina from Method B was the employed** one in nanocomposite production. Particularly, non-washed alumina from method B was the employed in the synthesis of the nanocomposite.

This alumina presented the problematic of the creation of a tablet-like solid while the drying process due to the presence of non-reacted polysulfone. This eventuality posed a problem of heterogeneity in the material. This was solved by pressing the material in a hot plate press (Fontijne Grotnes / Fortune Presses LabPro Mod 50, shown in Figure 60) during 2 periods of 45 minutes at 310^{o}C with a 200 kN force. This way, pressed material was redistributed uniformly and ulterior mechanization processes were facilitated.

The pressed material was then cut with metal shears guillotines into pellets, favoring the mixing process with PSU pellets. Three different nanocomposites with different loads were planned, at 0.5, 1 and 2 % weight of grafted PSU alumina content. The weights of each component (Alumina-MDI-PSU and PSU commercial pellets) were calculated from Table 6 and the results are shown in Table 7. The components of each nanocomposite were mixed.

Figure 60. Hot plate press in pressing process for Alumina-MDI-PSU material.

Table 7. Weight loads and components of every nanocomposite.

Sample ANP weight load	Alumina-MDI-PSU (g)	PSU (g)
0.5 %	0.147	9.853
1 %	0.294	9.706
2 %	0.588	9.412

A Haake Minilab II micro compounder (from the company Eurortodoncias S.L.) was used to extrude the mixture of matrix and nanocomposite. The thermo scientific Haake Minilab II (shown in Figure 61) is a micro compounder with conical twin-screws, which offer a short and well defined dwell time. It is regularly used compounding expensive or small scale materials such as nanocomposites and the required amount 5 g or 7 cm3. The compounder temperature was 270^{o}C, screws were counter rotating and the time the material spent inside the twins was of 10 minutes each 5 g. The extruded materials result of this process were separately pelleted with metal shears guillotines.

Figure 61. Haake Minilab II micro compounder employed during extrusion.

These nanocomposite pellets were again pressed into rectangular shape by the hot plates press, for its use as specimen in different mechanical tests.

3. Results and discussion

The three different compositions were evaluated by different techniques. Bare PSU was also compounded-compressed for comparison (without the inclusion of ANP), for an accurate comparison between nanocomposite and bare material. The techniques employed were TGA, and DSC for thermal properties, and Microhardness test for mechanical properties.

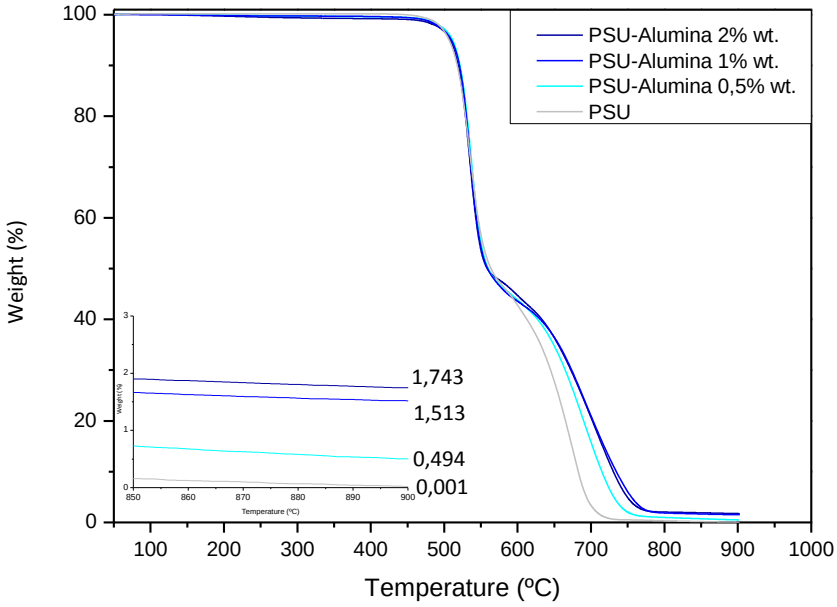

Figure 62. TGA Thermogram for every NP.

Figure 62 confirms the composition of the three materials in the total weight loss after TGA.

As shown in Figure 63 and Table 8, T_g has not improved, but polysulfone has exceptional properties and mechanical behavior and T_g improvement by nanoreinforcement addition is not usually reported. B. Serrano and J. Baselga reported [135] an improvement on PSU mechanical properties covered with fatty acids, obtaining improvements in Young modulus and resistance of 6 and 20% respectively with loads of up to 3% in weight of alumina explained by the formation of an ordered structure on nanoparticle surface by the eventual order of hydrocarbonated chains during the processing; nevertheless, T_g did not change. T_g is one of the most important properties

in polymer science, and a descent in glass transition temperature when adding nanoparticles into the matrix is a direct verification of the poor interaction interfacial matrix-nanoreinforcement. T_g does not suffer modifications by PSU alumina addition.

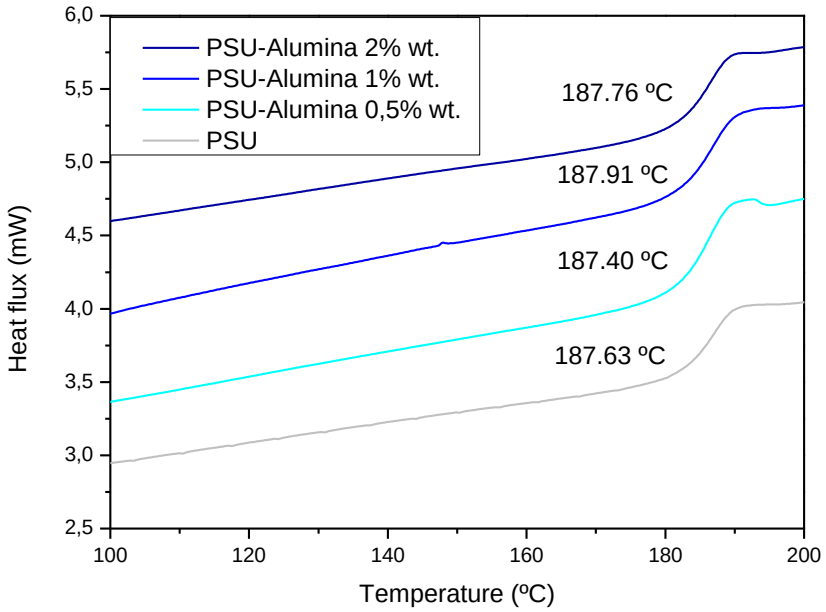

Figure 63. DSC Thermogram of every NC and their T_g.

Table 8. Glass transition Temperature obtained by DSC.

Material	T_g (ºC)
PSU	184.90ºC
Compounded PSU	187.63 ºC
PSU-Alumina 0.5 % wt.	187.40 ºC
PSU-Alumina 1 % wt.	187.91 ºC
PSU-Alumina 2 % wt.	187.76 ºC

Ten microhardness tests were carried out with Vickers indenter at 2 N maximum load on each material in order to analyze their mechanical properties. Results are statistically analyzed in Tables 9 and 10 and Figure 64.

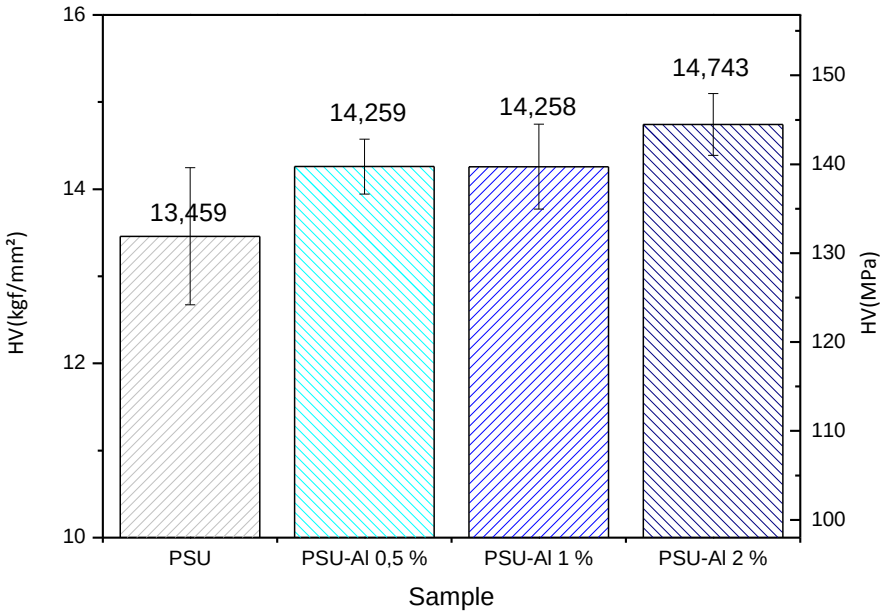

Figure 64. HV microhardness for every composite.

Table 9. HV microhardness values for every composite in kgf/mm².

kgf/mm²	PSU	PSU-Al 0.5 %	PSU-Al 1 %	PSU-Al 2 %
Average	**13,459**	**14,259**	**14,258**	**14,743**
Std. Deviation	0,787	0,315	0,487	0,355
Min	12,52	13,81	13,60	14,31
Median	13,39	14,28	14,32	14,71
Max	14,89	14,72	14,89	15,45

Table 10. HV microhardness values for every composite in MPa.

MPa	PSU	PSU-Al 0.5 %	PSU-Al 1 %	PSU-Al 2 %
Average	**131,98**	**139,82**	**139,81**	**144,57**
Std. Deviation	7,71	3,09	4,78	3,48
Min	122,77	135,42	133,36	140,32
Median	131,25	140,03	140,37	144,25
Max	146,01	144,34	146,01	151,50

Therefore, the inclusion of 2 % wt. ANP in PSU matrix enhances hardness implying an improvement of the resulting material hardness of around 9.5 %, which is positive given the medium load and the already good mechanical properties of bare PSU.

Finally, the homogeneity of the results along the tested specimens also reveals a good dispersion of ANP along the matrix.

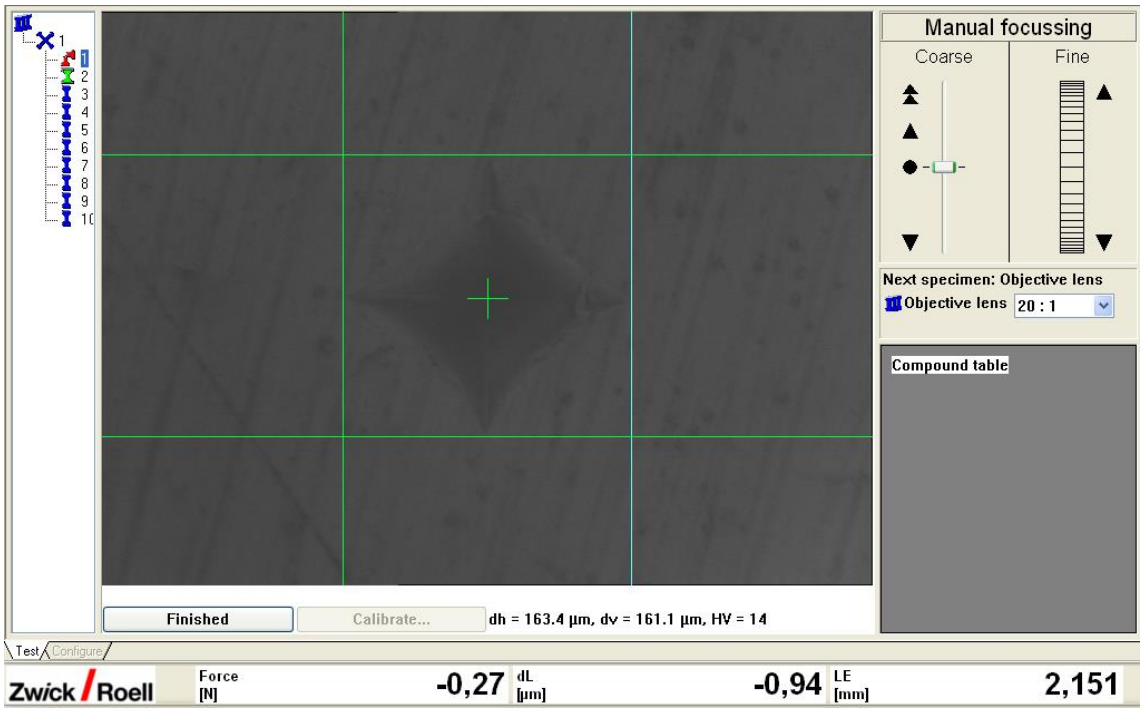

Figure 65. Indentation left on nanocomposite after test.

4. Conclusions

In this project, alumina nanoparticles functionalized with polysulfone hairs were synthetized by two different methods in different conditions and then used to prepare three different polysulfone matrix nanocomposites whose thermal and mechanical properties were tested later by different techniques.

In the project it has been established one grafting method (method B) which resulted in acceptable grafting density according with the “grafting to” methodology, on the other hand, method A presented a very low grafting density.

The nanocomposite showed better mechanical properties as a 10% increase in hardness for a 2 % weight alumina nanocomposite.

In conclusion, a high-performance polymer as polysulfone already presents very good mechanical and thermal properties that is difficult to obtain further improvements [136] as it has been shown in theoretical studies.

4.1. Possible applications

Most of the considered applications for the synthesized material are enclosed in the bioengineering field. As exposed before, polysulfone is used in dental applications such as implants or brackets, where the strength increase produced by alumina nanoparticles filling may reduce erosion induced by mastication and thus increase its service life.

Given the biocompatibility of the resulting material, its use as tissue replacement could be considered and investigated, other polysulfone based nanocomposites have been reported in this matter [137],.

Polysulfone has one of the highest service temperatures among all thermoplastics. Its resistance to high temperatures gives it a role of a flame retardant, without compromising its strength that usually results from addition of flame retardants, alumina can provide better mechanical properties in these applications.

Polysulfone is widely used in membranes manufacturing, which are used in applications as waste water recovery, hemodialysis, food and beverage processing, gas separation and car and electronic industries. The filter cartridges made of polysulfone membranes are sterilized with in-line stream in an autoclave, and usually they stand

up to 50 cycles, this number could be improved giving the filter cartridges an extended life by adding alumina nanoparticles.

Plastic lenses are starting to appear as a substitute of glass lenses in certain applications in optics (cameras, microscopes, telescopes and ophthalmic wear), since plastic lenses typically cost 1/100th of the price of similar glass lenses. These new lenses are made in polysulfone among other polymers as polystyrene and polycarbonate, which is modified by the addition of certain inorganic materials. Alumina nanoparticles represent an extended option for a PSU matrix, improving stability of the refractive index with respect to temperature [138], this nanocomposite could also present better impact resistance as higher mechanical properties.

4.2. Results improvement and future research

The research has been limited to the product scales, given the uncertainty of the synthesis procedure results and the sometimes-low performance of reactions and processes. The final obtaining of acceptable hairy nanoparticles has been conditioned to the amounts of the material, restricting certain synthesis strategies and compositions. Once this study has proven good grafting density methods for producing HNPs, this limitation should be eliminated in future researches.

Originated from the first problematic, the study has been enclosed to weight loads of up to 2% in weight alumina, although there have been reported better mechanical properties with 3-5% weight compositions, an increase of the alumina weight load would suppose an increase of material properties which should be determine in future studies.

The comparison with PSU-grafted-bare alumina nanoparticles has been based in reported studies, nevertheless, the different fabrication mechanisms could origin divergences in the properties by the procedure itself and not by the intrinsic properties of the material. Due to certain limitations, the production of several nanocomposites PSU-bare alumina has not been possible, nevertheless, the production under the same conditions is seen as very interesting to compare with the obtained nanocomposites and will be included in future research.

The employed polysulfone is a long chain polysulfone (M_w=16.000), nevertheless, it is known that short grafted polymer chains improves dispersion in a different way than long chain polymers and thus enhance certain properties, the employment and comparison of short PSU chains is aimed as future research.

Hardness is one of most important mechanical properties but not sufficient one to select correctly the material for a given application. A tensile test was planned but it turned out to be not possible due to technologic limitations, the impossibility of injecting the material for obtaining specimens adjusted to a norm or with the ideal

shape for this test. The employment of uniaxial or biaxial tensile test are presented as objective in further studies.

In the same line, the process of compounding-compression production process could vary the properties of the resulting composite in comparison with the originally planned compounding-injection. It could be interesting to quantify this divergence.

Finally, computer simulations are used to study static and dynamic properties of materials of down to nano-size range [139] [140] and so enhance the understanding of hierarchical structures and behaviors. This techniques could be applied in further investigation as parallel research with the laboratory work.

In general terms, nanocomposite materials are receiving a great attention among scientists, and it is found in a relatively young stage of development, so more effort is expected to be done in nanocomposite research in the future.

4.3. Economic issues

As a research project, the budget is not defined, and it results into a difficult quantification, since a lot of variables take place in its cost, from employed materials and compounds to electricity, water, nitrogen and air fluxes cost, researchers involved, general measurement equipment and devices, third parties devices, shared installations, among others. All of them charged to different entities, and which in its bigger part remains unknown to the author.

The importance of nanocomposites research is of incalculable value for development has been showed along the last few decades. Therefore the investigation cost is not as relevant as it could be for projects in other fields more oriented towards economics.

5. Acknowledgements

The author would like to thank Universidad Carlos III de Madrid for the used installations, equipment and devices employed, as well as the funding for the investigation. Especially to the Department of Materials Science and Chemical Engineering, where most of the work was developed and for how the author was integrated in their team; with special attention to prof. Juan Carlos Cabanelas for his help in the use of certain equipment.

Also to show gratitude to Eurortodoncias SL. for the use of their installations and their micro compounder for the fulfilment of this study as for the help received from their staff. The same acknowledgement for Universidad Complutense de Madrid Department of Microscopy within the Faculty of Chemistry for the use of their TEM microscope for measurements done in order to characterize different compositions included in this study.

Finally, the author would like to express his more sincere gratitude to the tutor, prof. Berna Serrano, and cotutor, phd. student Amaia Llorente, for all the help they offered with dedication and patience, without their knowledge and help, the fulfillment of this project would have never been possible.

6. Nomenclature

2D	2 Dimensions
ANP	Alumina nanoparticles
ATRP	AtomTransfer Radical Polymerization
BET	Brunauer–Emmett–Teller Theory
CMNC	Ceramic Matrix Nanocomposite
CNT	Carbon Nanotubes
CPB	concentrated polymer brush
CRP	Controlled Radical Polymerization
CS	Chitosan
DBTDL	Dibutyltin dilaurate
DLS	Dynamic Light Scattering
DMF	N-Dimethyl formamide
DSC	Differential Scanning Calorimetry
DTA	Differential Thermal Analysis
FTIR	Fourier transformed Infrared spectroscopy
GR	Graphene
HNP	Hairy Nanoparticle
HVEM	High Voltage Electron Microscope
HVT	Hardness Vickers Test
LED	Light Emitting Diode
MDI	methylene dyphenil diisocyanate
MMC	Metal Matrix Composite
MMNC	Metal Matrix Nanocomposite
MRI	Magnetic Resonance Imaging
MWCNT	Multi Wallled Carbon Nanotubes
NP	Nanoparticle
P4yA	Pentynoic Acid
PAAc	Poly(acrylic acid)
PAM	Polyacrylamide
PANI	Polyaniline
PDMS	Poly (dimethyl siloxane)
PdNPs	Pallladium nanoparticles
PEG	Polyethylene Glycol
PEGMA	Poly(poly(ethylene glycol) monomethacrylate)
PEI	polyethylenimine
PGMA	Poly(glycidylmethacrylate)
PHEA	Polyhydroethyl acrylate
PMAA	Poly methyl Acrylic Acid
PMMA	Polymethylmethacrylate
PMNC	Polymer Matrix Nanocomposite
PNC	Polymer Nanocomposite
poly (MPC)	Polymethacryloyloxyethyl Phosphorylcholin
PPEG	Phosphonated-Polyethylene Glycol
PS	Polystyrene
PSU	Polysulfone
PVA	Poly (vinyl alcohol)
QELS	Quasi-Electric Light Scatterin
RAFT	Reversible Addition Fragmentation chain Transfer
SDPB	semidilute polymer brush
SWCNT	Single Walled Carbon Nanotubes
TEM	Transmission electron Microscopy
TGA	Thermogravimetric Analysis
THF	Tetrahydrofuran
UTS	Ultimate Tensile Strength
UV	Ultra Violet
XRD	X-ray Diffraction

7. References

[1] Robert M. Jones (1999). Mechanics of Composite Materials (2nd ed.). Taylor & Francis. ISBN 9781560327127.

[2] Hussain, F., Hojjati, M., Okamoto, M., & Gorga, R. E. (2006). Review article: polymer-matrix nanocomposites, processing, manufacturing, and application: an overview. Journal of composite materials, 40(17), 1511-1575.

[3] Ajayan, P. M., Schadler, L. S., & Braun, P. V. (2006). Nanocomposite science and technology. John Wiley & Sons.

[4] Oriakhi, C.O. (1998). Nano Sandwiches, Chem. Br., 34: 59–62.

[5] Chiari, G., Giustetto, R., & Ricchiardi, G. (2003). Crystal structure refinements of palygorskite and Maya Blue from molecular modelling and powder synchrotron diffraction. European Journal of Mineralogy, 15(1), 21-33.

[6] Littmann, E. R. (1980). Maya Blue. A New Perspective. American Antiquity, 87-100.

[7] Kruis, F. E., Fissan, H., & Peled, A. (1998). Synthesis of nanoparticles in the gas phase for electronic, optical and magnetic applications—a review. Journal of Aerosol Science, 29(5), 511-535.

[8] Low, I. M. (Ed.). (2014). Advances in ceramic matrix composites. Woodhead Publishing.

[9] Meyyappan, M. (2005) Introduction to Nanotechnology. In Nanotechnology Aerospace Applications (pp. I-1 – I-2). Educational Notes RTO-EN-AVT-129

[10] Nicolais, L., & Carotenuto, G. (Eds.). (2004). Metal-polymer nanocomposites. John Wiley & Sons.

[11] Casati, R., & Vedani, M. (2014). Metal matrix composites reinforced by nano-particles—a review. Metals, 4(1), 65-83.

[12] Dash, M. P., Tripathy, M., Sasmal, A., Mohanty, G. C., & Nayak, P. L. (2010). Poly (anthranilic acid)/multi-walled carbon nanotube composites: spectral, morphological, and electrical properties. Journal of materials science, 45(14), 3858-3865

[13] Hussain, F., Hojjati, M., Okamoto, M., & Gorga, R. E. (2006). Review article: polymer-matrix nanocomposites, processing, manufacturing, and application: an overview. Journal of composite materials, 40(17), 1511-1575.

[14] Francis, R., Joy, N., Aparna, E. P., & Vijayan, R. (2014). Polymer grafted inorganic nanoparticles, preparation, properties, and applications: a review. Polymer Reviews, 54(2), 268-347.

[15] Hanemann, T., & Szabó, D. V. (2010). Polymer-nanoparticle composites: from synthesis to modern applications. Materials, 3(6), 3468-3517.

[16] Zuiderduin, W. C. J., Westzaan, C., Huetink, J., & Gaymans, R. J. (2003). Toughening of polypropylene with calcium carbonate particles. Polymer, 44(1), 261-275.

[17] Wu, D., Wang, X., Song, Y., & Jin, R. (2004). Nanocomposites of poly (vinyl chloride) and nanometric calcium carbonate particles: Effects of chlorinated polyethylene on mechanical properties, morphology, and rheology. Journal of Applied Polymer Science, 92(4), 2714-2723.

[18] Guo, Z., Kim, T. Y., Lei, K., Pereira, T., Sugar, J. G., & Hahn, H. T. (2008). Strengthening and thermal stabilization of polyurethane nanocomposites with silicon carbide nanoparticles by a surface-initiated-polymerization approach. Composites Science and Technology, 68(1), 164-170.

[19] Ajayan, P. M., & Zhou, O. Z. (2001). Applications of carbon nanotubes. In Carbon nanotubes (pp. 391-425). Springer Berlin Heidelberg.

[20] Iijima, S. (1991). Helical microtubules of graphitic carbon. Nature, 354(6348), 56-58.

[21] Yu, A., Ramesh, P., Itkis, M. E., Bekyarova, E., & Haddon, R. C. (2007). Graphite nanoplatelet-epoxy composite thermal interface materials. The Journal of Physical Chemistry C, 111(21), 7565-7569.

[22] Li, B., & Zhong, W. H. (2011). Review on polymer/graphite nanoplatelet nanocomposites. Journal of materials science, 46(17), 5595-5614.

[23] Ye, C., Bando, Y., Shen, G., & Golberg, D. (2006). Thickness-dependent photocatalytic performance of ZnO nanoplatelets. The Journal of Physical Chemistry B, 110(31), 15146-15151.

[24] Rehab, A. and Salahuddin, N. (2005). Nanocomposite Materials Based on Polyurethane Intercalated into Montmorillonite Clay, Materials Science and Engineering A, 399: 368–376.

[25] Yokoyama, R., Suzuki, S., Shirai, K., Yamauchi, T., Tsubokawa, N., & Tsuchimochi, M. (2006). Preparation and properties of biocompatible polymer-grafted silica nanoparticle. European polymer journal, 42(12), 3221-3229.

[26] Maurice, V., Slostowski, C., Herlin-Boime, N., & Carrot, G. (2012). Polymer-Grafted Silicon Nanoparticles Obtained Either via Peptide Bonding or Click Chemistry. Macromolecular Chemistry and Physics, 213(23), 2498-2503.

[27] Li, Z. F., & Ruckenstein, E. (2004). Water-soluble poly (acrylic acid) grafted luminescent silicon nanoparticles and their use as fluorescent biological staining labels. Nano Letters, 4(8), 1463-1467.

[28] Chowdhury, P., Saha, S. K., Guha, A., & Saha, S. K. (2012). Chemical and biochemical activities of sonochemically synthesized poly (N-isopropyl acrylamide)/silica nanocomposite. Applied Surface Science, 261, 598-604.

[29] Yuan, Q., Venkatasubramanian, R., Hein, S., & Misra, R. D. K. (2008). A stimulus-responsive magnetic nanoparticle drug carrier: Magnetite encapsulated by chitosan-grafted-copolymer. Acta Biomaterialia, 4(4), 1024-1037.

[30] Rutnakornpituk, M., Puangsin, N., Theamdee, P., Rutnakornpituk, B., & Wichai, U. (2011). Poly (acrylic acid)-grafted magnetic nanoparticle for conjugation with folic acid. Polymer, 52(4), 987-995.

[31] Wang, Y. X. J., Hussain, S. M., & Krestin, G. P. (2001). Superparamagnetic iron oxide contrast agents: physicochemical characteristics and applications in MR imaging. European radiology, 11(11), 2319-2331.

[32] Demir, M. M., Memesa, M., Castignolles, P., & Wegner, G. (2006). PMMA/Zinc Oxide Nanocomposites Prepared by In-Situ Bulk Polymerization. Macromolecular Rapid Communications, 27(10), 763-770.

[33] Çevik, E., Şenel, M., Baykal, A., & Abasıyanık, M. F. (2012). A novel amperometric phenol biosensor based on immobilized HRP on poly (glycidylmethacrylate)-grafted iron oxide nanoparticles for the determination of phenol derivatives. Sensors and Actuators B: Chemical, 173, 396-405.

[34] Khaled, S. M., Sui, R., Charpentier, P. A., & Rizkalla, A. S. (2007). Synthesis of TiO2-PMMA nanocomposite: using methacrylic acid as a coupling agent. Langmuir, 23(7), 3988-3995.

[35] Matsuno, R., Yamamoto, K., Otsuka, H., & Takahara, A. (2004). Polystyrene-and poly (3-vinylpyridine)-grafted magnetite nanoparticles prepared through surface-initiated nitroxide-mediated radical polymerization. Macromolecules, 37(6), 2203-2209.

[36] Tang, E., Liu, H., Sun, L., Zheng, E., & Cheng, G. (2007). Fabrication of zinc oxide/poly (styrene) grafted nanocomposite latex and its dispersion. European Polymer Journal, 43(10), 4210-4218.

[37] Liu, P., & Wang, T. (2008). Poly (hydroethyl acrylate) grafted from ZnO nanoparticles via surface-initiated atom transfer radical polymerization. Current Applied Physics, 8(1), 66-7.

[38] Auerkari, P. (1996). Mechanical and physical properties of engineering alumina ceramics (pp. 6-24). Finland: Technical Research Centre of Finland.

[39] Gupta, S., Ramamurthy, P. C., & Madras, G. (2011). Covalent grafting of polydimethylsiloxane over surface-modified alumina nanoparticles. Industrial & Engineering Chemistry Research, 50(11), 6585-6593.

[40] Jung, C. H., Choi, J. H., Lim, Y. M., Jeun, J. P., Kang, P. H., & Nho, Y. C. (2006). Preparation and characterization of polypropylene nanocomposites containing polystyrene-grafted alumina nanoparticles. J. Ind. Eng. Chem, 12(6), 900-904.

[41] Rothon, R. N., & Hornsby, P. R. (1996). Flame retardant effects of magnesium hydroxide. *Polymer Degradation and Stability*, *54*(2), 383-385.

[42] Liu, P., & Guo, J. (2007). Organo-modified magnesium hydroxide nano-needle and its polystyrene nanocomposite. Journal of Nanoparticle Research, 9(4), 669-673.

[43] Panigrahi, S., Basu, S., Praharaj, S., Pande, S., Jana, S., Pal, A., ... & Pal, T. (2007). Synthesis and size-selective catalysis by supported gold nanoparticles: study on heterogeneous and homogeneous catalytic process. The Journal of Physical Chemistry C, 111(12), 4596-4605. 347.

[44] Liu, Y., Shipton, M. K., Ryan, J., Kaufman, E. D., Franzen, S., & Feldheim, D. L. (2007). Synthesis, stability, and cellular internalization of gold nanoparticles containing mixed peptide-poly (ethylene glycol) monolayers. Analytical chemistry, 79(6), 2221-2229.

[45] Gam-Derouich, S., Mahouche-Chergui, S., Truong, S., Hassen-Chehimi, D. B., & Chehimi, M. M. (2011). Design of molecularly imprinted polymer grafts with embedded gold nanoparticles through the interfacial chemistry of aryl diazonium salts. Polymer, 52(20), 4463-4470.

[46] Zhang, D., Chen, L., Zang, C., Chen, Y., & Lin, H. (2013). Antibacterial cotton fabric grafted with silver nanoparticles and its excellent laundering durability. Carbohydrate polymers, 92(2), 2088-2094.

[47] Betancourt-Galindo, R., Cabrera Miranda, C., Puente Urbina, B. A., Castañeda-Facio, A., Sánchez-Valdés, S., Mata Padilla, J., ... & Rodríguez-Fernández, O. S. (2012). Encapsulation of Silver Nanoparticles in a Polystyrene Matrix by Miniemulsion Polymerization and Its Antimicrobial Activity. ISRN Nanotechnology, 2012.

[48] Bridot, J. L., Faure, A. C., Laurent, S., Riviere, C., Billotey, C., Hiba, B., ... & Tillement, O. Hybrid Gadolinium Oxide Nanoparticles: Multimodal Contrast Agents for in vivo imaging. J. Am. Chem. Soc. 2007, 9, 129; 16, 5076–5084.

[49] Guay-Bégin, A. A., Chevallier, P., Faucher, L., Turgeon, S., & Fortin, M. A. (2011). Surface modification of gadolinium oxide thin films and nanoparticles using poly (ethylene glycol)-phosphate. Langmuir, 28(1), 774-782.

[50] Chen, L., Sun, L. J., Luan, F., Liang, Y., Li, Y., & Liu, X. X. (2010). Synthesis and pseudocapacitive studies of composite films of polyaniline and manganese oxide nanoparticles. Journal of Power Sources, 195(11), 3742-3747.

[51] Bae, K. H., Lee, K., Kim, C., & Park, T. G. (2011). Surface functionalized hollow manganese oxide nanoparticles for cancer targeted siRNA delivery and magnetic resonance imaging. Biomaterials, 32(1), 176-184.

[52] (2014) Ohji, T., Colombo, P., Naito, M., Garay, J.E. Lin, H-T. Innovative Processing and Manufacturing of Advanced Ceramics and Composites II: Ceramic Transactions, Volume 243. ISBN: 978-1-118-77150-1

[53] Parlak, O., & Demir, M. M. (2011). Toward transparent nanocomposites based on polystyrene matrix and PMMA-grafted CeO2 nanoparticles. ACS applied materials & interfaces, 3(11), 4306-4314.

[54] Zhang, D., Fu, H., Shi, L., Pan, C., Li, Q., Chu, Y., & Yu, W. (2007). Synthesis of CeO2 nanorods via ultrasonication assisted by polyethylene glycol. Inorganic chemistry, 46(7), 2446-2451.

[55] Wei, Q. B., Luo, Y. L., Zhang, C. H., Fan, L. H., & Chen, Y. S. (2008). Assembly of Cu nanoparticles in a polyacrylamide grafted poly (vinyl alcohol) copolymer matrix and vapor-induced response. Sensors and Actuators B: Chemical, 134(1), 49-56.

[56] Zhang, X., Crespilho, F. N., Zucolotto, V., Manohar, S. K., Mattoso, L. H. C., & Bergamaski, K. (2009). Polypyrrole and platinum nanocomposite for fuel cell applications. In ABSTRACTS OF PAPERS OF THE AMERICAN CHEMICAL SOCIETY (Vol. 237). 1155 16TH ST, NW, WASHINGTON, DC 20036 USA: AMER CHEMICAL SOC.

[57] Carrot, G., Gal, F., Cremona, C., Vinas, J., & Perez, H. (2008). Polymer-grafted-platinum nanoparticles: From three-dimensional small-angle neutron scattering study to tunable two-dimensional array formation. Langmuir, 25(1), 471-478.

[58] Zeng, Q., Cheng, J. S., Liu, X. F., Bai, H. T., & Jiang, J. H. (2011). Palladium nanoparticle/chitosan-grafted graphene nanocomposites for construction of a glucose biosensor. Biosensors and Bioelectronics, 26(8), 3456-3463.

[59] Lin, H., Yang, J., Liu, J., Huang, Y., Xiao, J., & Zhang, X. (2013). Properties of Pd nanoparticles-embedded polyaniline multilayer film and its electrocatalytic activity for hydrazine oxidation. Electrochimica Acta, 90, 382-392.

[60] Ajayan, P. M., Schadler, L. S., & Braun, P. V. (2006). Nanocomposite science and technology. John Wiley & Sons.

[61] Xu, C., Ohno, K., Ladmiral, V., & Composto, R. J. (2008). Dispersion of polymer-grafted magnetic nanoparticles in homopolymers and block copolymers. Polymer, 49(16), 3568-3577.

[62] Capozzi, C. J., & Gerhardt, R. A. (2007). Novel percolation mechanism in PMMA matrix composites containing segregated ITO nanowire networks.Advanced Functional Materials, 17(14), 2515-2521.

[63] Luo, Y. S., Yang, J. P., Dai, X. J., Yang, Y., & Fu, S. Y. (2009). Preparation and optical properties of novel transparent Al-doped-ZnO/epoxy nanocomposites. The Journal of Physical Chemistry C, 113(21), 9406-9411.

[64] Decher, G., & Schlenoff, J. B. (Eds.). (2006). Multilayer thin films: sequential assembly of nanocomposite materials. John Wiley & Sons.

[65] Colver, P. J., Colard, C. A., & Bon, S. A. (2008). Multilayered nanocomposite polymer colloids using emulsion polymerization stabilized by solid particles.Journal of the American Chemical Society, 130(50), 16850-16851.

[66] Cheng, L., & Cox, J. A. (2001). Preparation of multilayered nanocomposites of polyoxometalates and poly (amidoamine) dendrimers. Electrochemistry communications, 3(6), 285-289.

[67] Vaia, R. A., & Maguire, J. F. (2007). Polymer nanocomposites with prescribed morphology: going beyond nanoparticle-filled polymers. Chemistry of Materials, 19(11), 2736-2751.

[68] Chevigny, C., Dalmas, F., Di Cola, E., Gigmes, D., Bertin, D., Boué, F., & Jestin, J. (2010). Polymer-grafted-nanoparticles nanocomposites: dispersion, grafted chain conformation, and rheological behavior. Macromolecules, 44(1), 122-133.

[69] Green, P. F. (2011). The structure of chain end-grafted nanoparticle/homopolymer nanocomposites. Soft Matter, 7(18), 7914-7926.

[70] Borukhov, I., & Leibler, L. (2002). Enthalpic stabilization of brush-coated particles in a polymer melt. Macromolecules, 35(13), 5171-5182.

[71] Daou, T. J., Greneche, J. M., Pourroy, G., Buathong, S., Derory, A., Ulhaq-Bouillet, C., ... & Begin-Colin, S. (2008). Coupling agent effect on magnetic properties of functionalized magnetite-based nanoparticles. Chemistry of Materials, 20(18), 5869-5875.

[72] Bagwe, R. P., Hilliard, L. R., & Tan, W. (2006). Surface modification of silica nanoparticles to reduce aggregation and nonspecific binding. Langmuir, 22(9), 4357-4362.

[73] Bansal, A., Yang, H., Li, C., Benicewicz, B. C., Kumar, S. K., & Schadler, L. S. (2006). Controlling the thermomechanical properties of polymer nanocomposites by tailoring the polymer–particle interface. Journal of Polymer Science Part B: Polymer Physics, 44(20), 2944-2950.

[74] Rungta, A., Natarajan, B., Neely, T., Dukes, D., Schadler, L. S., & Benicewicz, B. C. (2012). Grafting bimodal polymer brushes on nanoparticles using controlled radical polymerization. Macromolecules, 45(23), 9303-9311.

[75] Gao, J., Li, J., Benicewicz, B. C., Zhao, S., Hillborg, H., & Schadler, L. S. (2012). The mechanical properties of epoxy composites filled with rubbery copolymer grafted SiO2. Polymers, 4(1), 187-210.

[76] Akcora, P., Kumar, S. K., García Sakai, V., Li, Y., Benicewicz, B. C., & Schadler, L. S. (2010). Segmental dynamics in PMMA-grafted nanoparticle composites. Macromolecules, 43(19), 8275-8281.

[77] Corbierre, M. K., Cameron, N. S., Sutton, M., Laaziri, K., & Lennox, R. B. (2005). Gold nanoparticle/polymer nanocomposites: dispersion of nanoparticles as a function of capping agent molecular weight and grafting density. Langmuir,21(13), 6063-6072.

[78] Lan, Q., Francis, L. F., & Bates, F. S. (2007). Silica nanoparticle dispersions in homopolymer versus block copolymer. Journal of Polymer Science Part B: Polymer Physics, 45(16), 2284-2299.

[79] Yokoyama, R., Suzuki, S., Shirai, K., Yamauchi, T., Tsubokawa, N., & Tsuchimochi, M. (2006). Preparation and properties of biocompatible polymer-grafted silica nanoparticle. European polymer journal, 42(12), 3221-3229.

[80] Grest, G. S. (1996). Grafted polymer brushes in polymeric matrices. The Journal of chemical physics, 105(13), 5532-5541.

[81] Edmondson, S., Osborne, V. L., & Huck, W. T. (2004). Polymer brushes via surface-initiated polymerizations. Chemical society reviews, 33(1), 14-22.

[82] Li, C., & Benicewicz, B. C. (2005). Synthesis of well-defined polymer brushes grafted onto silica nanoparticles via surface reversible addition-fragmentation chain transfer polymerization. Macromolecules, 38(14), 5929-5936.

[83] Li, Y., & Benicewicz, B. C. (2008). Functionalization of silica nanoparticles via the combination of surface-initiated RAFT polymerization and click reactions.Macromolecules, 41(21), 7986-7992.

[84] Corbierre, M. K., Cameron, N. S., & Lennox, R. B. (2004). Polymer-stabilized gold nanoparticles with high grafting densities. Langmuir, 20(7), 2867-2873.

[85] Kolb, H. C., Finn, M. G., & Sharpless, K. B. (2001). Click chemistry: diverse chemical function from a few good reactions. Angewandte Chemie International Edition, 40(11), 2004-2021.

[86] Edgecombe, S. R., Gardiner, J. M., & Matsen, M. W. (2002). Suppressing autophobic dewetting by using a bimodal brush. Macromolecules, 35(16), 6475-6477.

[87] Green, D. L., & Mewis, J. (2006). Connecting the wetting and rheological behaviors of poly (dimethylsiloxane)-grafted silica spheres in poly (dimethylsiloxane) melts. Langmuir, 22(23), 9546-9553.

[88] Yezek, L., Schärtl, W., Chen, Y., Gohr, K., & Schmidt, M. (2003). Influence of hair density and hair length on interparticle interactions of spherical polymer brushes in a homopolymer matrix. Macromolecules, 36(11), 4226-4235.

[89] Matsen, M. W., & Gardiner, J. M. (2001). Autophobic dewetting of homopolymer on a brush and entropic attraction between opposing brushes in a homopolymer matrix. The Journal of Chemical Physics, 115(6), 2794-2804.

[90] Dukes, D., Li, Y., Lewis, S., Benicewicz, B., Schadler, L., & Kumar, S. K. (2010). Conformational transitions of spherical polymer brushes: synthesis, characterization, and theory. Macromolecules, 43(3), 1564-1570.

[91] Green, P. F. (2011). The structure of chain end-grafted nanoparticle/homopolymer nanocomposites. Soft Matter, 7(18), 7914-7926.

[92] Wenz, L. M., Merritt, K., Brown, S. A., Moet, A., & Steffee, A. D. (1990). In vitro biocompatibility of polyetheretherketone and polysulfone composites. Journal of biomedical materials research, 24(2), 207-215.

[93] Mark, H. F. (2013). Encyclopedia of polymer science and technology, concise. John Wiley & Sons.

[94] Ash, B. J., Siegel, R. W., & Schadler, L. S. (2004). Mechanical behavior of alumina/poly (methyl methacrylate) nanocomposites. Macromolecules, 37(4), 1358-1369.

[95] Hakimelahi, H. R., Hu, L., Rupp, B. B., & Coleman, M. R. (2010). Synthesis and characterization of transparent alumina reinforced polycarbonate nanocomposite. Polymer, 51(12), 2494-2502.

[96] Sawyer, W. G., Freudenberg, K. D., Bhimaraj, P., & Schadler, L. S. (2003). A study on the friction and wear behavior of PTFE filled with alumina nanoparticles. Wear, 254(5), 573-580.

[97] Guo, Z., Pereira, T., Choi, O., Wang, Y., & Hahn, H. T. (2006). Surface functionalized alumina nanoparticle filled polymeric nanocomposites with enhanced mechanical properties. Journal of Materials Chemistry, 16(27), 2800-2808.

[98] Thamaraiselvi, T., & Rajeswari, S. (2004). Biological evaluation of bioceramic materials-a review. Carbon, 24(31), 172.

[99] Christel, P. S. (1992). Biocompatibility of surgical-grade dense polycrystalline alumina. Clinical orthopaedics and related research, 282, 10-18.

[100] Coats, A. W.; Redfern, J. P. (1963). Thermogravimetric Analysis: A Review. Analyst 88: 906–924

[101] Gilbert, J. B.; Kipling, J. J.; McEnaney, B.; Sherwood, J. N. (1962). Carbonization of Polymers I - Thermogravimetric Analysis. Polymer 3: 1–10

[102] Griffiths, P. R., & De Haseth, J. A. (2007). Fourier transform infrared spectrometry (Vol. 171). John Wiley & Sons.

[103] Banwell, C. N., & McCash, E. M. (1983). Fundamentals of molecular spectroscopy (pp. 77-80). London: McGraw-Hill.

[104] Smith, B. C. (2011). Fundamentals of Fourier transform infrared spectroscopy. CRC press.

[105] Höhne, G., Hemminger, W., & Flammersheim, H. J. (2003). Differential scanning calorimetry. Springer Science & Business Media.

[106] Gill, P., Sauerbrunn, S., & Reading, M. (1993). Modulated differential scanning calorimetry. Journal of Thermal Analysis and Calorimetry, 40(3), 931-939.

[107] Fillon, B., Wittmann, J. C., Lotz, B., & Thierry, A. (1993). Self-nucleation and recrystallization of isotactic polypropylene (α phase) investigated by differential scanning calorimetry. Journal of Polymer Science Part B: Polymer Physics,31(10), 1383-1393.

[108] Gaur, U., & Wunderlich, B. (1980). Study of microphase separation in block copolymers of styrene and α-methylstyrene in the glass transition region using quantitative thermal analysis. Macromolecules, 13(6), 1618-1625.

[109] Pecora, R. (2000). Dynamic light scattering measurement of nanometer particles in liquids. Journal of nanoparticle research, 2(2), 123-131.

[110] Berne, B. J., & Pecora, R. (2000). Dynamic light scattering: with applications to chemistry, biology, and physics. Courier Corporation.

[111] Amis, E. J., & Han, C. C. (1982). Cooperative and self-diffusion of polymers in semidilute solutions by dynamic light scattering. Polymer, 23(10), 1403-1406.

[112] Manual, Z. N. S. U. (2003). Malvern Instruments Ltd. Manual Version IM, 100, 1-23.

[113] Kohl, H. (2008). Transmission Electron Microscopy: Physics If Image Formation. Springer.

[114] Williams, D. B., & Carter, C. B. (1996). The transmission electron microscope (pp. 3-17). Springer Us.

[115] Reimer, L. (2013). Transmission electron microscopy: physics of image formation and microanalysis (Vol. 36). Springer.

[116] Warren, B. E. (1969). X-ray Diffraction. Courier Corporation.

[117] Klug, H. P., & Alexander, L. E. (1954). X-ray diffraction procedures.

[118] Bragg, W. L. (1913, February). The diffraction of short electromagnetic waves by a crystal. In Proceedings of the Cambridge Philosophical Society (Vol. 17, No. 43, p. 4).

[119] Farges, G., & Degout, D. (1989). Interpretation of the indentation size effect in vickers microhardness measurements-absolute hardness of materials. Thin Solid Films, 181(1), 365-374.

[120] Abboud, M., Turner, M., Duguet, E., & Fontanille, M. (1997). PMMA-based composite materials with reactive ceramic fillers. Part 1.—Chemical modification and characterisation of ceramic particles. Journal of Materials Chemistry, 7(8), 1527-1532.

[121] Kujawa, J., Cerneaux, S., & Kujawski, W. (2014). Characterization of the surface modification process of Al 2 O 3, TiO 2 and ZrO 2 powders by PFAS molecules. Colloids and Surfaces A: Physicochemical and Engineering Aspects, 447, 14-22.

[122] Patterson, A. L. (1939). The Scherrer formula for X-ray particle size determination. Physical review, 56(10), 978.

[123] Yilmaz, G., Toiserkani, H., Demirkol, D. O., Sakarya, S., Timur, S., Yagci, Y., & Torun, L. (2011). Modification of polysulfones by click chemistry: amphiphilic graft copolymers and their protein adsorption and cell adhesion properties. Journal of Polymer Science Part A: Polymer Chemistry, 49(1), 110-117.

[124] Reymond, J. P., & Kolenda, F. (1999). Estimation of the point of zero charge of simple and mixed oxides by mass titration. Powder technology, 103(1), 30-36.

[125] Hoskins, J. N., & Grayson, S. M. (2009). Synthesis and degradation behavior of cyclic poly (ε-caprolactone). Macromolecules, 42(17), 6406-6413.

[126] Li, N., & Binder, W. H. (2011). Click-chemistry for nanoparticle-modification. Journal of Materials Chemistry, 21(42), 16717-16734.

[127] Liu, Q., de Wijn, J. R., de Groot, K., & van Blitterswijk, C. A. (1998). Surface modification of nano-apatite by grafting organic polymer. Biomaterials, 19(11), 1067-1072.

[128] Li, H., Yan, Y., Liu, B., Chen, W., & Chen, S. (2007). Studies of surface functional modification of nanosized α-alumina. Powder Technology, 178(3), 203-207.

[129] Hongyan, L., Shufan, N., Bin, L., Wei, C., & Shoutian, C. (2006). Surface Functional Modification of Nanosized α-Alumina and Its Characterisation [J]. Journal of Xi'an Jiaotong University, 2, 025.

[130] De Gennes, P. G. (1987). Polymers at an interface; a simplified view.Advances in Colloid and Interface Science, 27(3), 189-209.

[131] Yamamoto, S., Ejaz, M., Tsujii, Y., & Fukuda, T. (2000). Surface interaction forces of well-defined, high-density polymer brushes studied by atomic force microscopy. 2. Effect of graft density. Macromolecules, 33(15), 5608-5612.

[132] Tchoul, M. N., Fillery, S. P., Koerner, H., Drummy, L. F., Oyerokun, F. T., Mirau, P. A., ... & Vaia, R. A. (2010). Assemblies of titanium dioxide-polystyrene hybrid nanoparticles for dielectric applications. Chemistry of Materials, 22(5), 1749-1759.

[133] Henn, G., Bucknall, D. G., Stamm, M., Vanhoorne, P., & Jérôme, R. (1996). Chain end effects and dewetting in thin polymer films. *Macromolecules*, *29*(12), 4305-4313.

[134] Iyer, K. S., & Luzinov, I. (2004). Effect of macromolecular anchoring layer thickness and molecular weight on polymer grafting. Macromolecules, 37(25), 9538-9545.

[135] Anaya, S., Serrano, B., Herrero, B., Cervera, A., & Baselga, J. (2014). γ-Alumina Modification with Long Chain Carboxylic Acid Surface Nanocrystals for Biocompatible Polysulfone Nanocomposites. ACS applied materials & interfaces, 6(16), 14460-14468.

[136] Sur, G. S., Sun, H. L., Lyu, S. G., & Mark, J. E. (2001). Synthesis, structure, mechanical properties, and thermal stability of some polysulfone/organoclay nanocomposites. Polymer, 42(24), 9783-9789.

[137] Wang, M., Yue, C. Y., & Chua, B. (2001). Production and evaluation of hydroxyapatite reinforced polysulfone for tissue replacement. Journal of Materials Science: Materials in Medicine, 12(9), 821-826.

[138] Border, J., & McGovern, M. R. (2002). U.S. Patent No. 6,441,077. Washington, DC: U.S. Patent and Trademark Office.

[139] Hackett, E., Manias, E., & Giannelis, E. P. (2000). Computer simulation studies of PEO/layer silicate nanocomposites. Chemistry of Materials, 12(8), 2161-2167.

[140] Zeng, Q. H., Yu, A. B., & Lu, G. Q. (2008). Multiscale modeling and simulation of polymer nanocomposites. Progress in Polymer Science, 33(2), 191-269.